UNIVERSITY OF OSLO
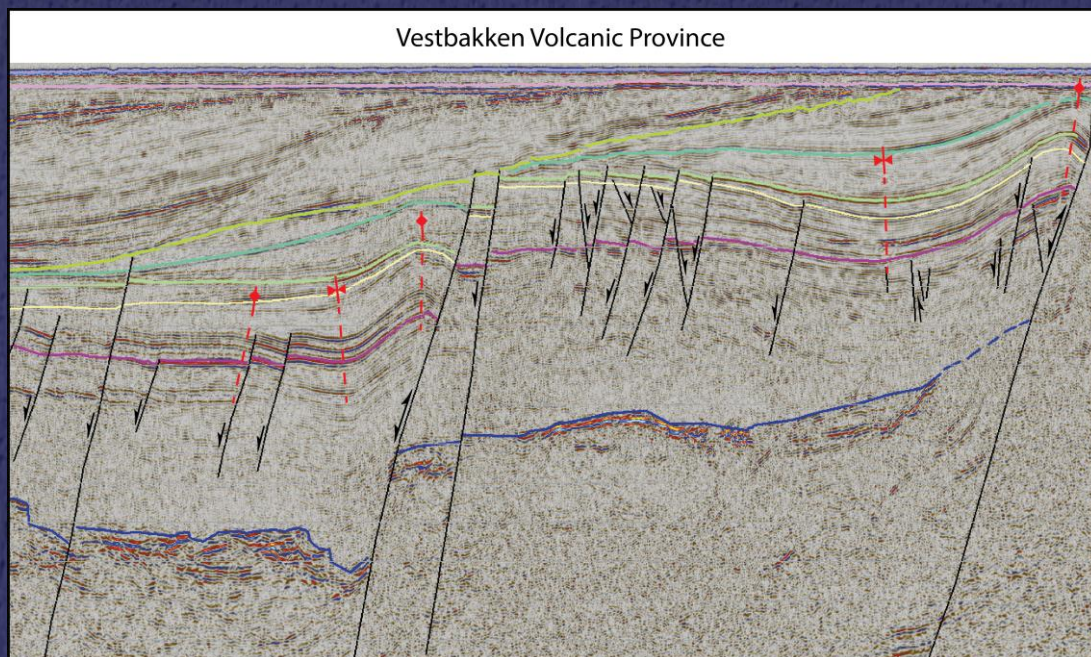
FACULTY OF MATHEMATICS AND NATURAL SCIENCES

DEPARTMENT OF GEOSCIENCES

Master Thesis in Geosciences

Vestbakken Volcanic Province

"The Structural Development of the Vestbakken Volcanic Province, Western Barents Sea. Relation Between Faults and Folds"

By Panagiotis Athanasios Giannenas

The Structural Development of the Vestbakken Volcanic Province, Western Barents Sea. Relation Between Faults and Folds

Panagiotis Athanasios Giannenas

Master Thesis in Geosciences

Discipline: Petroleum Geology and Petroleum Geophysics

30 credits

Department of Geosciences

Faculty of Mathematics and Natural Sciences

UNIVERSITY OF OSLO

June 2018

© **Giannenas Panagiotis Athanasios, 2018**

Title: "The Structural Development of the Vestbakken Volcanic Province, Western Barents Sea. Relation Between Faults and Folds"

Tutor(s): **Kjetil Indrevær, Roy H. Gabrielsen, Jan Inge Faleide, UiO**

This work is published digitally through DUO – Digitale Utgivelser ved UiO

http://www.duo.uio.no

Preface

This master thesis completes the two year master program in Petroleum Geology and Petroleum Geophysics undertaken at the Department of Geosciences, University of Oslo. This master thesis has been supervised by the postdoctoral researcher Kjetil Indrevær, Prof. Roy Helge Gabrielsen and Prof. Jan Inge Faleide.

Acknowledgements

Giannenas Panagiotis Athanasios, 2018

Abstract

An eastward (releasing) bend in the Eocene dextral Barents Shear Margin gave rise to the formation of the Vestbakken Volcanic Province. The area has been affected by complex tectonics and both extensional and contractional structures are observed. This thesis focuses on the analysis of structural styles in this area and their relation to the regional tectonic setting. Faults and folds are interpreted from 2D seismic reflection data calibrated by well data. The structural analysis is based on interpreted key seismic profiles and constructed structural maps, time maps and special maps which focus on the geometric and spatial relations of faults and folds. The area is divided into structurally homogenous subareas. Two half-grabens, two domal areas, a gently dipping slope area and an uplifted footwall block area have been defined. The study reveals the existence of two partially inverted master faults, several branch faults with anastomosing character and many isolated secondary faults, a few reverse faults and thrust faults and 18 folds. The dominant strike of structural features in the Vestbakken Volcanic Province is NE-SW. Exceptions include the N-S striking eastern boundary fault, which defines the boundary between Vestbakken Volcanic Province and Stappen High to the east. Faults primarily dip towards NW. Structural analysis of faults revealed chiefly planar fault plane geometries that locally are interpreted to be slightly modified through later deformation. Three extensional events have been identified: (i) a late Paleocene-early Eocene event which is related to the continental break-up in the Norwegian-Greenland Sea, (ii) an early Oligocene event attributed to the plate reorganization (34 Ma) affecting mainly NW-SE striking faults and (iii) an extensional Pliocene event. Evidence of volcanic activity is observed in the 2D seismic data accompanying the first two events. Analysis of folds revealed specific structural styles: (a) upright to steeply inclined close to open anticlines with snakehead (head on) geometries buttressed against pre-existing normal faults and (b) upright or steeply inclined gentle to open synclines that are interpreted as partly inverted synclinal depocenters. Folds are principally observed to be fault-related, where regionally expressed anticlines are developed in the upper stratigraphic sections, in the hanging wall fault blocks of pre-existing extensional master faults, typically affecting middle Eocene – lower Miocene strata. The folds trend parallel to, and are focused along these faults. Folds are mainly interpreted as buckle folds and deformation was controlled by the geometry of the faults, which acted as buttresses accommodating shortening. Fault-bend folds and fault propagation folds are observed locally. Onlap configuration and pinch-out geometries reveal that the phase of tectonic inversion (which caused folding, reverse faulting and reverse reactivation of extensional faults) commenced in early Miocene times under top-to-SE contraction prior to the onset of Pliocene. The event is suggested to be primarily related to the development of the Knipovich Ridge in the NW which caused SE-directed stress through ridge-push. A SE-directed tectonic transport direction is consistent with geometric observations such as slightly steeper forelimbs compared to backlimbs, axial plane inclinations, strike and dip of fault planes that have undergone flexural rotation, thrust faults that ramp-up to the SE and forethrusting. Apart from ridge-push other processes involved may include lithospheric thinning, gravitational stresses by the elevated Iceland margin and plume-enhanced spreading.

Contents

Chapter 1

1   Introduction

Geographically, the Barents Sea covers an area of approximately 1.3 million km^2 (Worsley, 2008) and comprises the shelf area which refers to the area north of the Scandinavian and western Russian Arctic mainland (**Fig. 1.1**), (Henriksen et al., 2011). To the west the basin borders the oceanic Norwegian Sea (**Fig. 1.1**) with a passive shear margin that started to develop in the Paleocene (Faleide et al., 1993). The eastern boundary is generally defined by Novaya Zemlya but references are also made to the Kara Sea and the west Siberian Basin (Henriksen et al., 2011). To the north, it is bounded by the Svalbard archipelago (NW) and the Franz Joseph Land (NE).
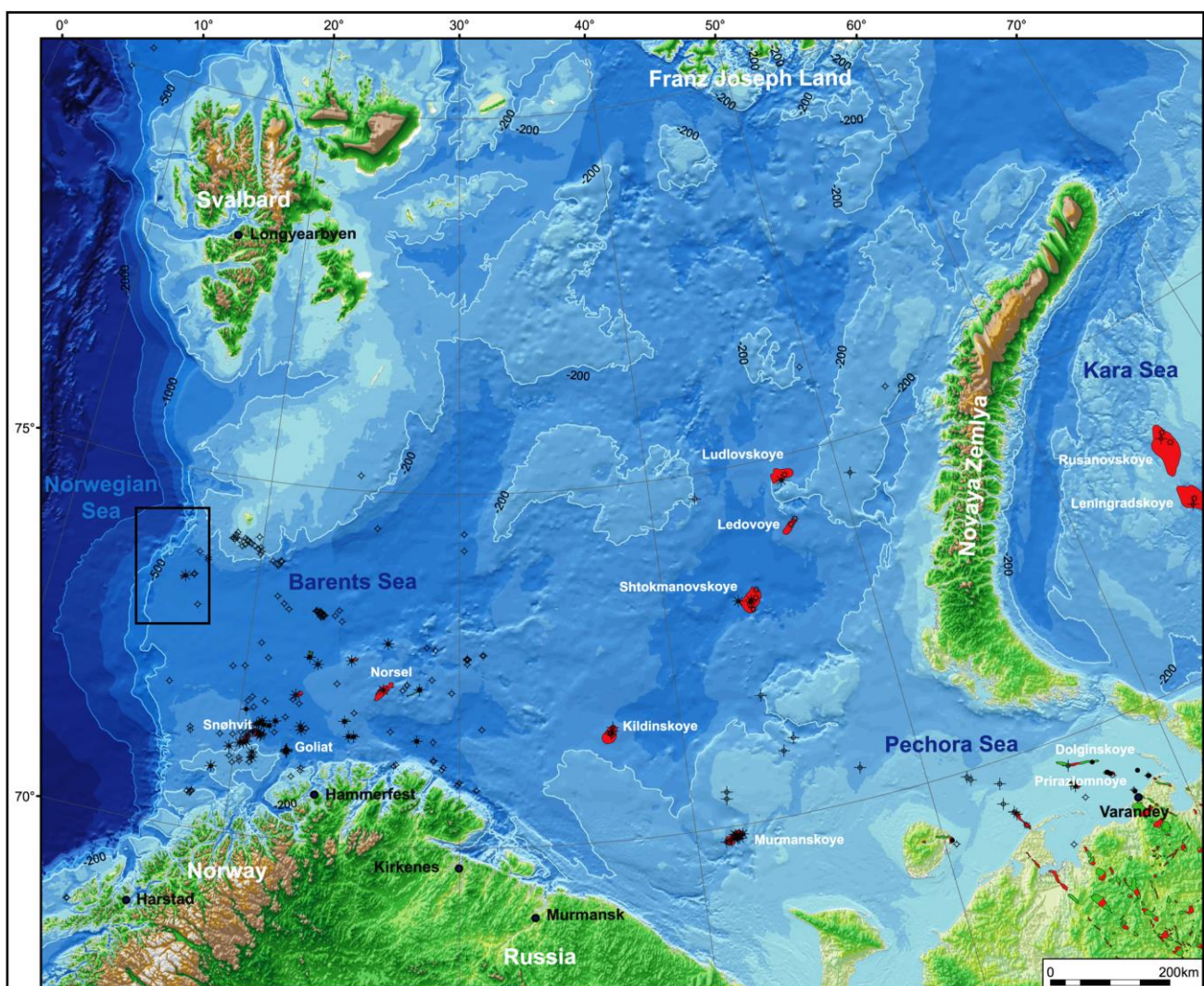
Fig. 1.1: *Bathymetric map of the Barents Sea with depth contours in meters (modified from Henriksen et al., 2011). Study area is located within the Vestbakken Volcanic Province marked with black rectangle.*

Geologically, the Barents Sea region overlies an intracratonic basin which has been affected by several phases of tectonism since the Caledonian orogenetic movements terminated in Late Devonian times (with the Svalbardian event), (Harland, 1969; Gabrielsen et al., 1990). It consists of a series of structural elements with the western geological province displaying a more complex mosaic pattern which includes several basins and sub-basins, highs, platforms, (Henriksen et al., 2011) and long lived fault complexes (see **Fig. 2.2A**), (Gabrielsen, 1984). This thesis concerns the geological province known as the Vestbakken Volcanic Province which is a Cenozoic volcanic rift segment of the western Barents Sea Margin, the tectonic evolution of which is primarily a consequence of the North Atlantic-Arctic breakup of Pangea and spreading of the Norwegian-Greenland Sea.

The main objectives of this thesis include: detailed mapping and structural analysis of folds and faults in the Vestbakken Volcanic Province in the western Barents Sea margin and research on the association of observed structural styles to the regional tectonic setting. Emphasis is given on timing of folding, fold genesis, folding mechanisms, fault kinematics, reverse/normal fault reactivations and inversion. Finally, a well-studied ongoing tectonically similar system is introduced for making comparisons with the study area and help on improving the understanding on its tectonic evolution.

This study is based on 2D seismic lines and well data processed in Schlumberger's Petrel E&P Software Platform 2016. Seismic well tie and paper based calibration was performed before the detailed seismic interpretation. Interpreted key seismic profiles, time-structure maps, structural maps and special maps with respect to faults and folds that provide key information have been generated and processed. These are described in Chapter 4 (Results) and have provided the basis for the discussion in Chapter 5.

Chapter 2

2   Geological framework

2.1   Regional Setting

Geologically, the Barents Sea can be divided into two major geological provinces, the east province and the west structurally more complicated mosaic-like province (Worsley, 2008).

After the Paleozoic Caledonian Orogeny which caused uplift to the west, a series of events occurred and affected the area regionally: a rift phase at Late Devonian? – middle Carboniferous, a Late Carboniferous – Mesozoic Uralide Orogeny which included uplift to the east while a series of rift events affected the west with possibly three Late Paleozoic – Early Mesozoic rift episodes, a Middle Jurassic – Early Cretaceous rifting phase affecting mainly the west province, an early Tertiary rift episode acting similarly to the west and finally, crustal break-up in the western Barents Sea margin (see Gabrielsen et al., 1984; Henriksen et al., 2011; Faleide et al., 2010; Faleide et al., 2008; Doré et al., 1999; Skogseid et al., 2000; Worsley, 2008; Tsikalas et al., 2012; Ziegler, 1988).

Structurally, the Barents Shelf is dominated by ENE–WSW to NE–SW and NNE–SSW to NNW–SSE trends with local influence of WNW–ESE striking elements as shown in **Fig. 2.2B** and **Fig. 2.3**. N–S trends prevail to the west and northwest (Gabrielsen et al., 1990). The most tectonically active part throughout Mesozoic and Cenozoic times was the western part of the Barents Sea. The eastern and northeastern parts have acted as stable platforms with less tectonic influence at the same period (Gabrielsen et al., 1990).

The lithostratigraphy of the Barents Sea includes a thick sedimentary succession of Paleozoic to Cenozoic strata (Faleide et al., 2010) exhibiting lateral and vertical variations in terms of thickness and facies as shown in **Fig. 2.1**. Typically, rocks and sediments of Upper Paleozoic include mixed carbonates, evaporites and clastics which rest beneath Mesozoic-Cenozoic clastic sedimentary rocks (Faleide et al., 2010).
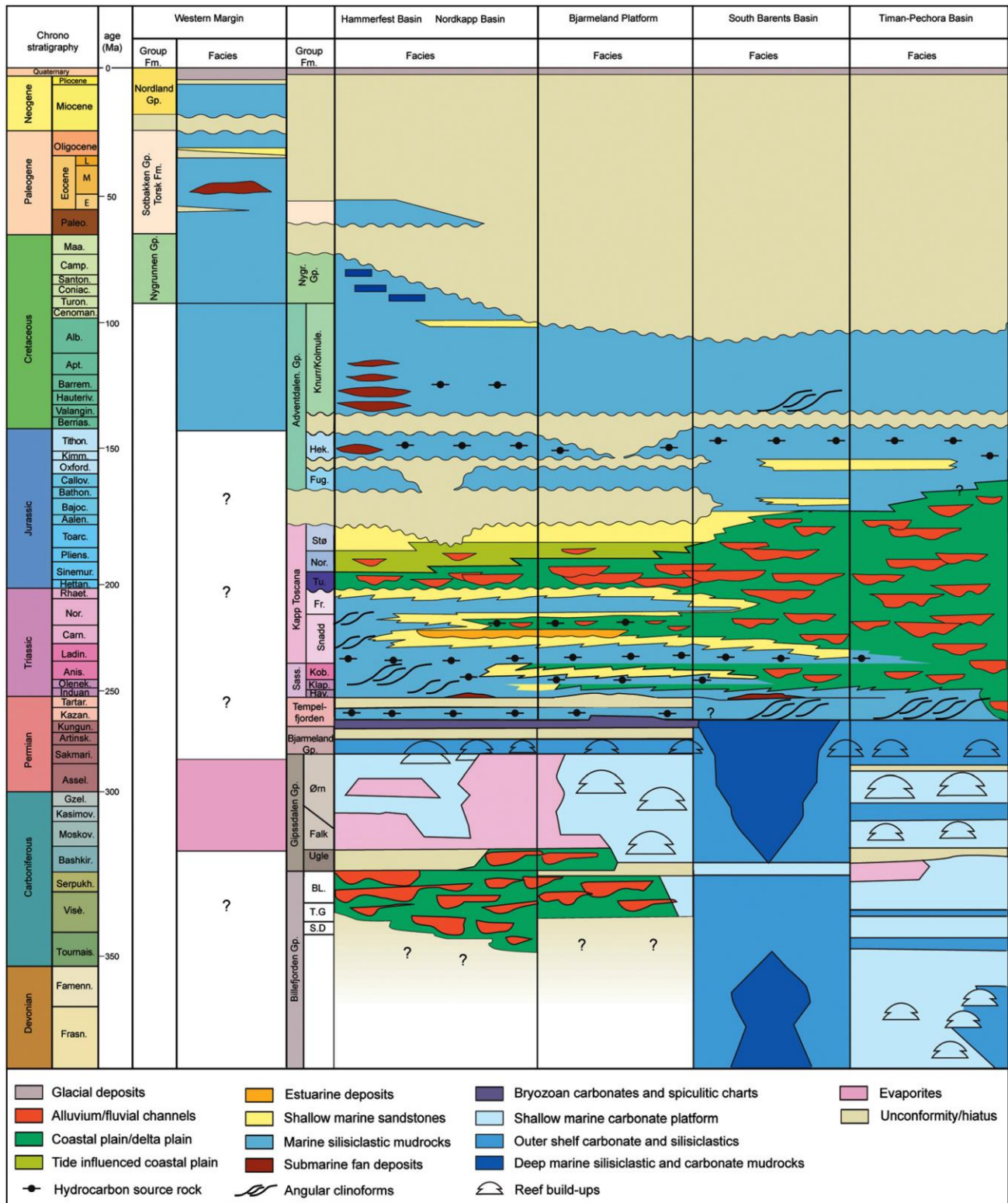
Fig. 2.1: *Summary of Chronostratigraphy and facies of the greater Barents Sea (modified from Henriksen et al., 2011; lithostratigraphy based on Dalland et al., 1988; Dallmann, 1999 and Larssen et al., 2005).*

2.2 Main Geological Provinces

As previously mentioned, according to Worsley (2008), the greater Barents Sea can be divided into the east and the west provinces. The western Barents Sea province (**Fig. 2.2A** and **Fig. 2.2B**, black rectangles) overlies a thick succession of Upper Paleozoic to Cenozoic rocks and sediments and can be further subdivided into three regions (Faleide et al., 2010):

- The Svalbard Platform which seems to be covered by a succession of Upper Paleozoic and Mesozoic sediments (Faleide et al., 2010).

- A basin province between the Svalbard Platform (or Edgeøya Platform together with Hopen High after their mergence, Anell et al., 2016) and the Norwegian coast which is characterized by a number of sub-basins and highs. Sediments of Jurassic to Cretaceous age are preserved in basins to the eastern part of this province whereas, sediments of Paleocene to Eocene age can be found in the basins to the west (Faleide et al., 2010).

- The continental Barents Sea margin consists of three main structural segments: the Senja Fracture Zone; The Vestbakken Volcanic Province and the Hornsund Fault Zone (see **Fig. 2.2A** and **Fig. 2.3**, marked as SFZ, VVP, and HFZ, accordingly), (Faleide et al., 2001, 2008, 2010; Tsikalas et al., 2012).

The structural segments and the tectonic evolution of the western Barents Sea margin are discussed in great detail in the next paragraphs since their development and evolution is directly related to the study area in the Vestbakken Volcanic Province.
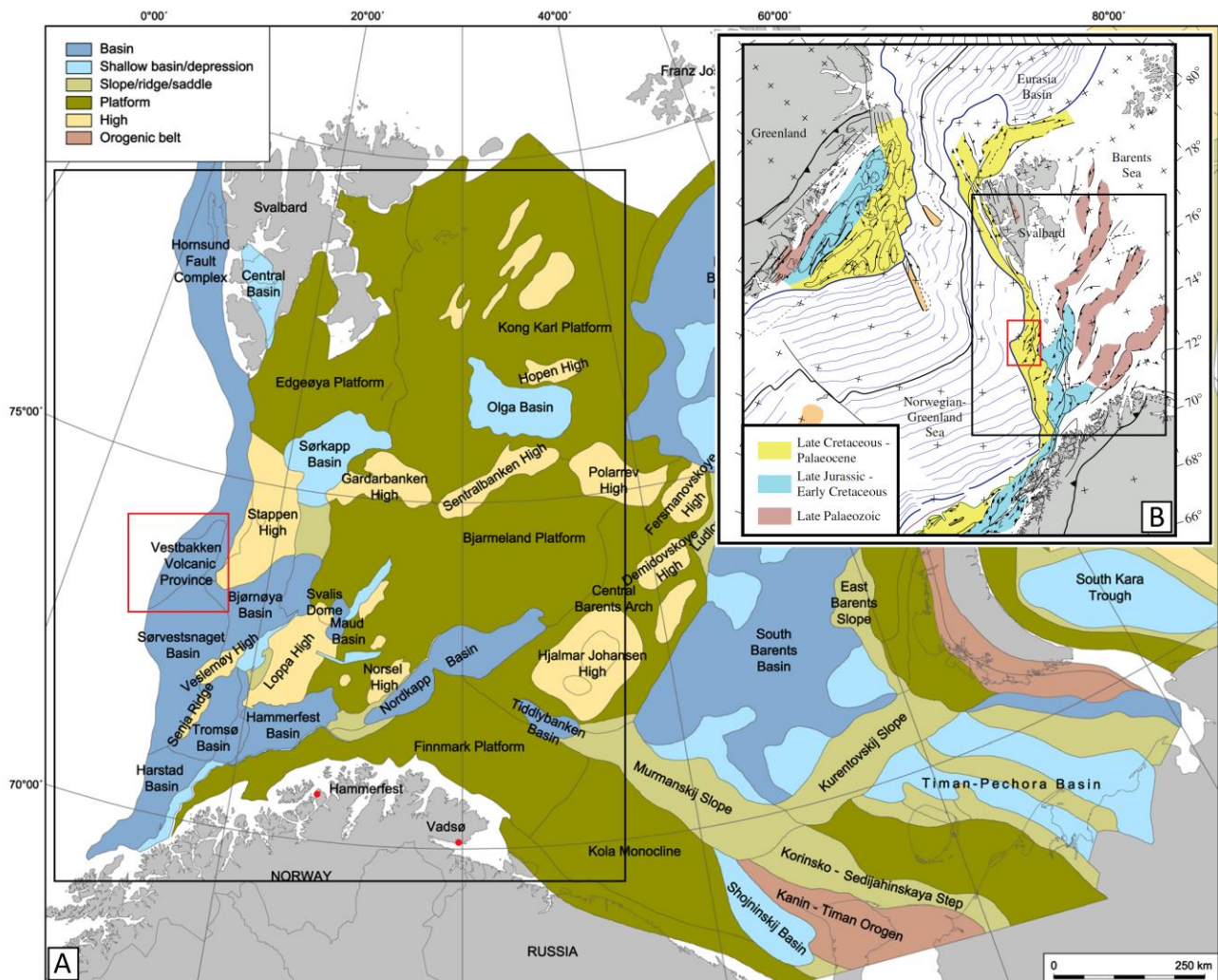
Fig. 2.2: **(A)** *Main structural elements of the greater Barents Sea (modified from Henriksen et al., 2011); **(B)** Northeast Atlantic region and western Barents Sea tectonic setting, structural elements and related rift phases (modified from Faleide et al., 2010). Black rectangles mark the western Barents Sea province and red rectangles mark the study area in the Vestbakken Volcanic Province.*

2.3   Main structural segments in the western Barents Sea margin

The present continental margin of the western Barents Sea and Svalbard extends about 1000 km in a broadly NNW direction (**Fig. 2.2** and **Fig. 2.3**). It comprises three major structural segments as previously mentioned: a southern, sheared margin along the Senja Fracture Zone (SFZ) characterized by a sharp continent-ocean transition (COT), a central volcanic rift segment (Vestbakken Volcanic Province) with an obscure and partly masked by volcanics continent-ocean transition (COT), and a northern, initially sheared and later rifted margin along the Hornsund Fault Zone (HFZ) (see Faleide et al., 2008; Ryseth et al., 2003; Gabrielsen et al., 1990) and Svalbard margin characterized by a rapid thinning of continental crust (**Fig. 2.3**). Note that these elements are commonly referred as part of the De Geer Zone (firstly by Harland, 1969), a mega shear system

linking the North Atlantic to the Arctic prior to breakup. Each segment is characterized by distinct crustal properties, structural and magmatic styles and history of vertical motion, mainly as a result of three controlling parameters (1) the pre-breakup structure, (2) the geometry of the plate boundary at opening and (3) the direction of relative plate motion (Faleide et al., 1991, 2008).
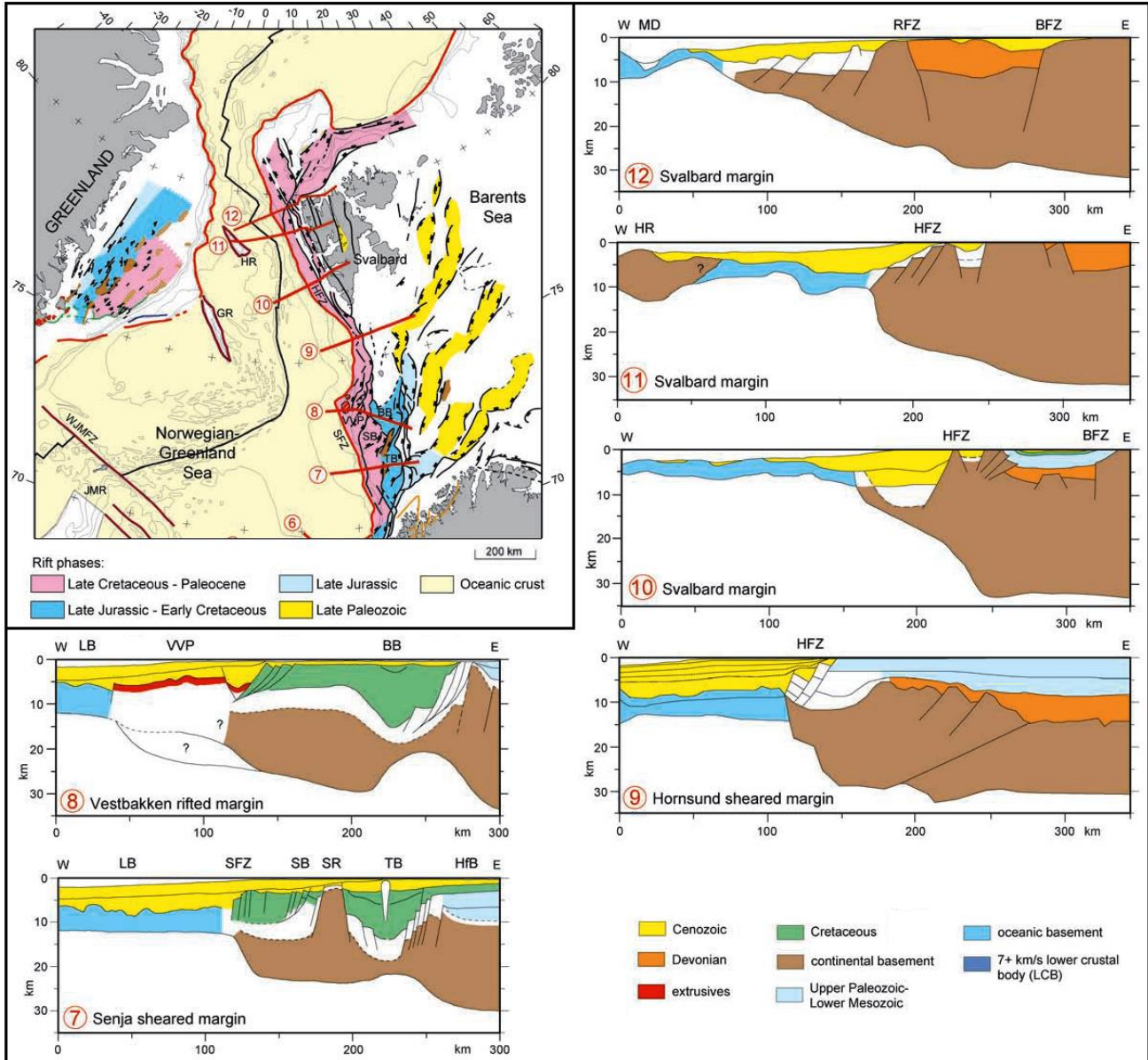
Fig. 2.3: *Top left side picture represents a regional structural map showing structural elements related to different rift phases affecting the NE Atlantic region-western Barents Sea margin. Location of margin crustal transects are also shown. BB: Bjørnøya Basin, GR: Greenland Ridge, HFZ: Hornsund Fault Zone, HR: Hovgård Ridge, JMR: Jan Mayen Ridge, MB: Møre Basin, SB: Sørvestsnaget Basin, SFZ: Senja Fracture Zone, TB: Tromsø Basin, TP: Trøndelag Platform, VVP: Vestbakken Volcanic Province, WJMFZ: West Jan Mayen Fracture Zone. From 7 to 12, crustal transects across the mainly sheared western Barents Sea-Svalbard margin can be seen. BFZ: Billefjorden Fault Zone, LB: Lofoten Basin, MD: Molloy Deep, RFZ: Raudfjorden Fault Zone, SR: Senja Ridge, HfB: Hammerfest Basin (modified from Faleide et al., 2008).*

2.3.1   Sheared margin along the Senja Fracture Zone (SFZ)

The Senja Fracture Zone (marked SFZ in **Fig. 2.3**), or Senja Shear Margin is the southernmost of these segments and developed during the Eocene opening of the Norwegian-Greenland Sea (**Fig. 2.4**), first by continent-continent shear between the Laurentia and Baltica plates followed by continent ocean shear and has been passive since earliest Oligocene time (Faleide et al., 2008).

2.3.2   Central volcanic rift segment – Vestbakken Volcanic Province (VVP)

The Vestbakken volcanic province is located south and west of Bjørnøya (**Fig. 2.3** as VVP, **Fig. 2.2A** and **Fig. 2.2B**, as red rectangles). It was named after Vestbakken which is a bathymetrical slope west of Bjørnøya. The province is defined seismically by a highly reflective level which can be interpreted as lava covering older sediments. The age of lavas was interpreted as early Eocene by Faleide et al. (1988) and after drilling and core sampling the interpretation was proven valid. Within the province, there are a few intrusions which might be linked to the volcanic activity and are interpreted as younger than the lavas (Faleide et al., 1988). The Vestbakken Volcanic Province was structured after the formation of the lavas and now represents a structurally homogeneous area (Gabrielsen et al., 1990).

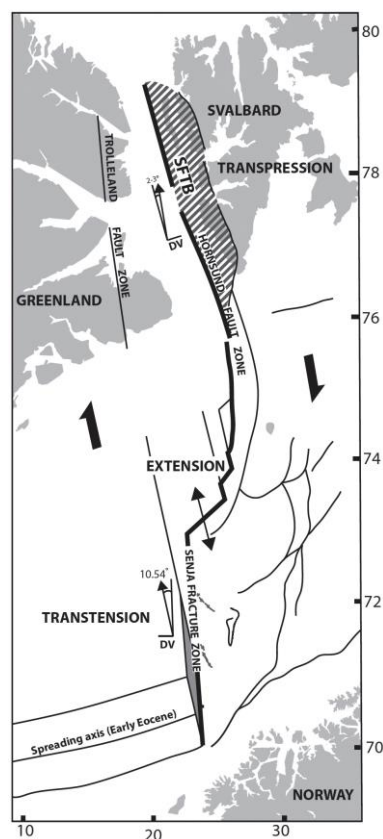***Fig. 2.4****: Structural setting of the western Barents Sea margin in early Eocene shortly after continental break-up. Transtension is shown in the Senja Fracture Zone, extension in the Vestbakken Volcanic Province and northern Sørvestsnaget Basin and transpression in the Hornsund Fault Zone under an overall dextral shear setting (modified from Kristensen et al., 2017 after Faleide et al., 1988).*

An east-stepping of the Eocene dextral shear margin (releasing bend) gave rise to basin formation in a pull-apart setting (**Fig. 2.4**, area marked with extension). The structures in the Vestbakken Volcanic Province are mainly extensional, but transpressional structures are observed locally. The main extensional deformation took place through two stages: (i) early Eocene break-up related rifting and (ii) Oligocene renewed extensional faulting related to change in relative plate motion (Faleide et al., 1993, Tsikalas et al., 2012). The Cenozoic evolution of the NE Norwegian-Greenland Sea was complex due to repeated tectonic activity and this is now imprinted in the complicated pull-apart setting within the Vestbakken Volcanic Province. Eight tectonic and three volcanic events have been identified in this province (Jebsen and Faleide, 1998).

2.3.3 Sheared-rifted margin along the Hornsund Fault Zone (HFZ)

The Hornsund Fault Zone (**Fig. 2.3** and **Fig. 2.4**) consists of the fault and dome structures defined by the Tertiary sequences west of the Stappen High and the Sørkapp-Hornsund High. It is bounded by the Vestbakken Volcanic Province to the south but to the north is not clearly defined. It can be divided into southern part striking N-S and northern part striking NW–SE. The Hornund fault complex is associated with the opening of the Norwegian-Greenland Sea and it was initiated in earliest Tertiary to Oligocene times (Gabrielsen et al., 1990). The largest fault of this complex is commonly described as the Knølegga Fault.

Coeval to the shear along the Senja Fracture Zone and basin formation in the Sørvestsnaget Basin transpression along the Hornsund Fault Zone led to orogenesis along the western part of Svalbard creating the west Spitsbergen Fold Belt (**Fig. 2.3** and **Fig. 2.4**). The orogenesis along western Svalbard led to Paleocene-Eocene basin formation in the Spitsbergen Central Basin. The Svalbard Fold and Thrust Belt orogenesis is characterized by a partitioning of strain between strike slip faults and broad zones of convergent strain during overall transpression (Leever et al., 2011; Kristensen et al., 2017).

2.4 Tectonic evolution of the margin from Middle Jurassic to present day

The tectonic evolution of the western Barents Sea margin since Middle Jurassic time consists of two main phases as previously mentioned: the Late Mesozoic rifting and basin formation and Early Tertiary rifting and opening of the Norwegian-Greenland Sea (**Fig. 2.5**, **Fig. 2.6** and **Fig. 2.7**). However, in relation to the major plate tectonic movements in the North Atlantic-Arctic region one can summarize many different events as follows:

Middle-Late Jurassic rifting: The Middle-Late Jurassic phase rifted the Barents Sea through the Hammerfest and Bjørnøya basins (**Fig. 2.5A**, for location of basins see **Fig. 2.2A**) along the pre-existing tectonic grain, causing block faulting along east and north-east trends (Faleide et al., 1993).

Early Cretaceous rifting: The northward propagation of the North Atlantic rifting was accompanied by crustal extension and thinning that led to the development of major Cretaceous basins acting as main depocentres (**Fig. 2.5B** at 75Ma, rift zone marked with blue color). Rifting and decoupling of the Harstad, Tromsø, Sørvestsnaget and Bjørnøya Basins (see **Fig. 2.2A** for location of basins) from the basins and highs farther east took place. These basins underwent rapid differential subsidence and segmentation into sub-basins and highs. Regional uplift in the north gave rise to southward sediment progradation in the Barents Sea (Faleide et al., 2008).

Late Cretaceous-Paleocene rifting: Faulting took place in the Harstad and Sørvestsnaget Basins. On Spitsbergen, a foreland basin was sourced from uplifted parts of the fold-and thrust belt in the west during latest Paleocene-Eocene times (**Fig. 2.3**. transect 10) (Faleide et al., 2008). **Fig. 2.6A** represents the structural setting of the margin at the end of this event (Late Paleocene-Early Eocene).
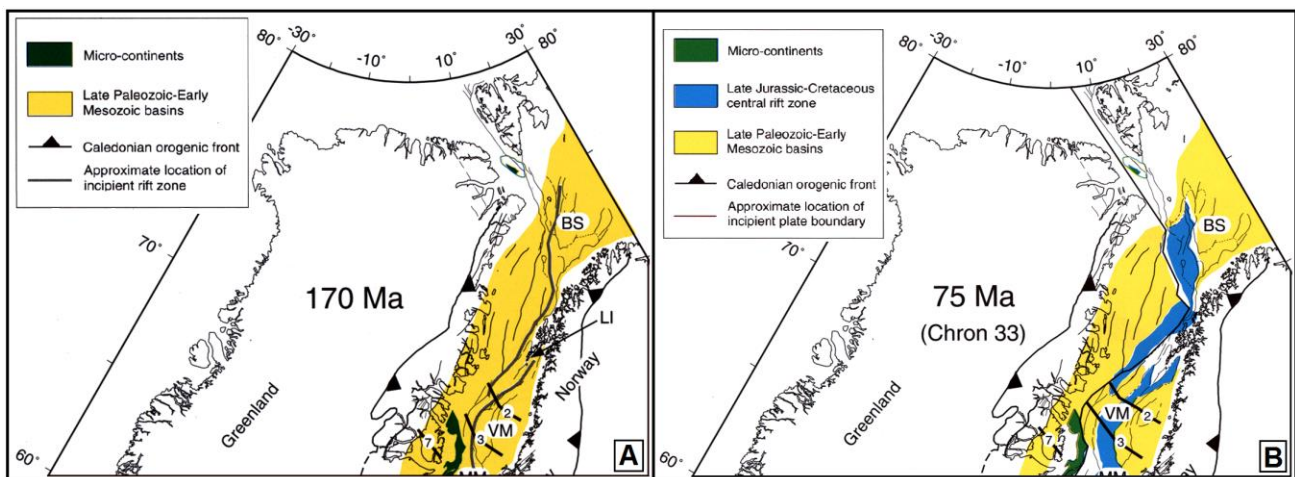
Fig. 2.5: (A) *Plate reconstruction at 170 Ma (Middle Jurassic);* **(B)** *Plate reconstruction at 75Ma (Late Cretaceous). VM: Voring margin, LI: Lofoten Islands, BS: SW Barents Sea (modified from Skogseid et al., 2000).*

Eocene: Continental break-up in the Norwegian-Greenland Sea at the Paleocene-Eocene transition at ~55–54 Ma initiated the formation of the mainly sheared western Barents Sea-Svalbard continental margin which experienced both transtensional and transpressional deformation during Eocene time (**Fig. 2.4** and **Fig. 2.6**) (Faleide et al., 1993). It culminated in a 3–6 m.y. period of massive magmatic activity during breakup and onset of early sea-floor spreading opening of the Norwegian-Greenland Sea, formation of the Vestbakken Volcanic Province, and extensional faulting and uplift along the Senja Fracture Zone. Breakup-related magmatism in the Vestbakken Volcanic Province was followed by down-faulting and deposition of thick Eocene strata (Faleide et al., 2008).

Oligocene: Structural rejuvenation took place along the continental margin (Faleide et al., 1993). In earliest Oligocene time, Greenland (and North America) moved in a more westerly direction with respect to Eurasia. The early Oligocene rifting associated with the change in plate motion (**Fig. 2.7**),

reactivated mostly NE-SW trending faults in the Vestbakken Volcanic Province. Also, renewed volcanic activity took place. Transpressional movements west of Svalbard were replaced by oblique rifting and incipient seafloor spreading when relative plate motions changed in the earliest Oligocene, and narrow grabens developed along the Svalbard margin. At the western Barents Sea margin, a Late Miocene uplift event increases in amplitude eastwards within the Vestbakken Volcanic Province and may be related to pre-glacial tectonic uplift of the Barents Shelf (Jebsen and Faleide, 1998).
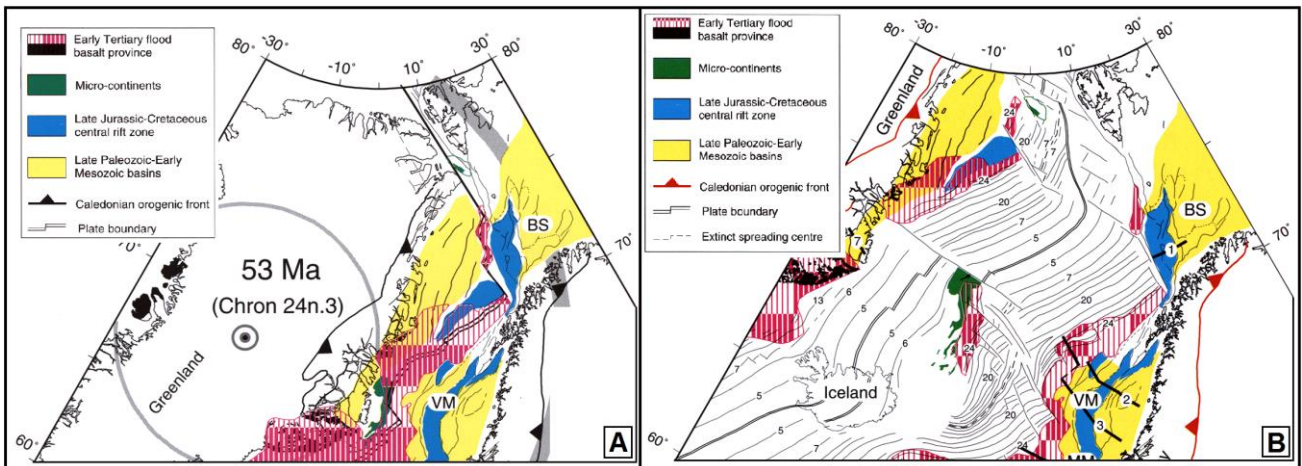
Fig. 2.6*: **(A)** Plate reconstruction at 53Ma (early Eocene) when the continental break-up occurred; **(B)** Present day tectonic setting (modified from Skogseid et al., 2000).*
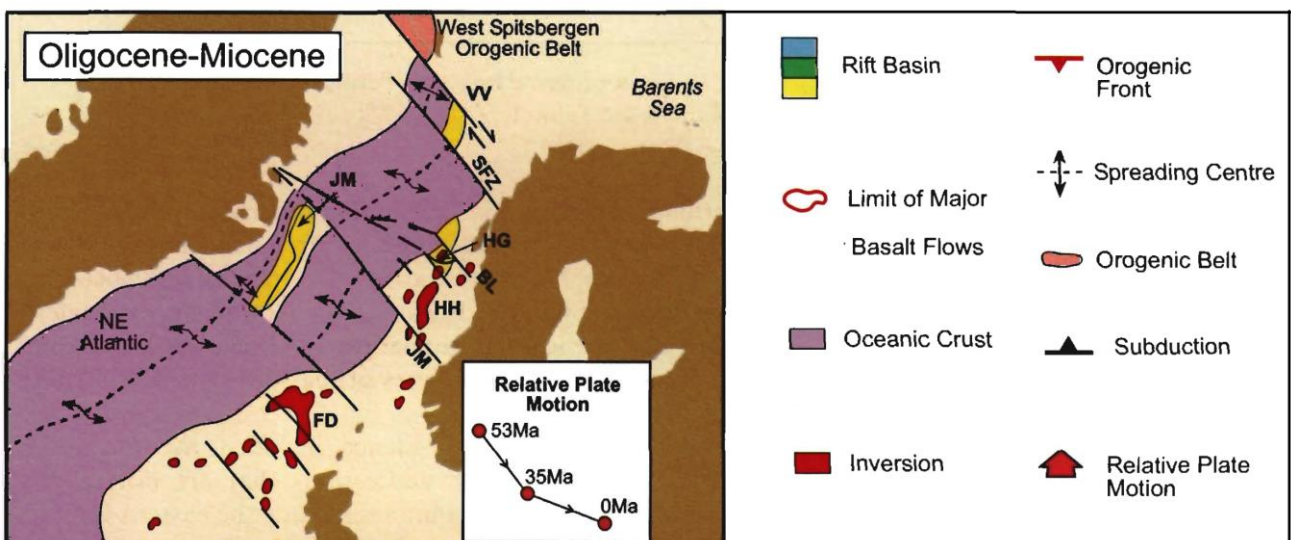
Fig. 2.7*: Plate reconstruction at Oligocene-Miocene emphasizing the change in relative plate motion at 35Ma (early Oligocene), (modified from Doré et al., 1997).*

Since Oligocene times oceanic crust has been generated along the entire Barents Sea margin (**Fig. 2.6B**), followed by subsidence and burial by Neogene and Quaternary sediments in an elastic wedge

sourced by the uplifted Barents Sea area. Initial uplift was tectonic in nature and occurred in several phases during the Cenozoic times, but the most severe uplift and erosion was in the Plio-Pleistocene times and was closely associated with glaciations (Doré et al., 1999). Mechanisms able to explain repeated events of regional uplift and erosion in the south-western Barents Sea include thermal effects associated with shifts in mantle convection patterns and crustal thinning, elastic response to regional intraplate compressional stresses associated with ridge push or other processes associated with plate boundary stresses, elastic response to glaciation, erosion and redeposition and combinations of these (Gabrielsen et al., 1997).

2.5 Cenozoic stratigraphy of the Southwestern Barents Sea

Cenozoic deposits are widespread throughout the Barents Sea (Ryseth et al., 2003). The main Cenozoic lithostratigraphic units observed in the southwestern Barents Sea are shown in the lithostratigraphic summary chart of **Fig. 2.8** and include:

Nordland Group

The Neogene sediments of the Nordland Group are related to a marine to glacial setting (Dalland et al., 1988; Nøttvedt et al., 1988). This group involves: sand and clays grade into sandstones and claystones, the sand content increasing upwards. Cobbles and boulders of quartzite, granite and different metamorphic rocks occur with clay in the upper parts of the group. The clay is grey to greyish green, soft to firm, blocky, non-calcareous, and in parts silty (www.npd.no).

Sotbakken Group

The whole Barents Shelf was transgressed in the mid-Paleocene and a uniform sequence of outer sublittoral to deep shelf claystones were deposited (**Fig. 2.8**). The group is dominated by claystones, with only minor siltstone, tuffaceous and carbonate horizons (www.npd.no).

Nygrunnen Group

This group is represented by open marine, deep shelf environments which in the west passed into shallower starved shelf regimes (uplifted at times) in the east (**Fig. 2.8**), (www.npd.no). Lithologies involve: greenish grey to grey claystones with thin limestone intervals in the Tromsø Basin and western parts of the Hammerfest Basin pass eastwards and southeastwards into more calcareous or sandy condensed sequences (www.npd.no).

These are the main three groups observed in the Cenozoic history of the Southwestern Barents Sea as well as in the Vestbakken Volcanic Province. However, note that the Nygrunnen Group primarily covers the Late Cretaceous time interval and only a small part of the early Paleocene (Danian).
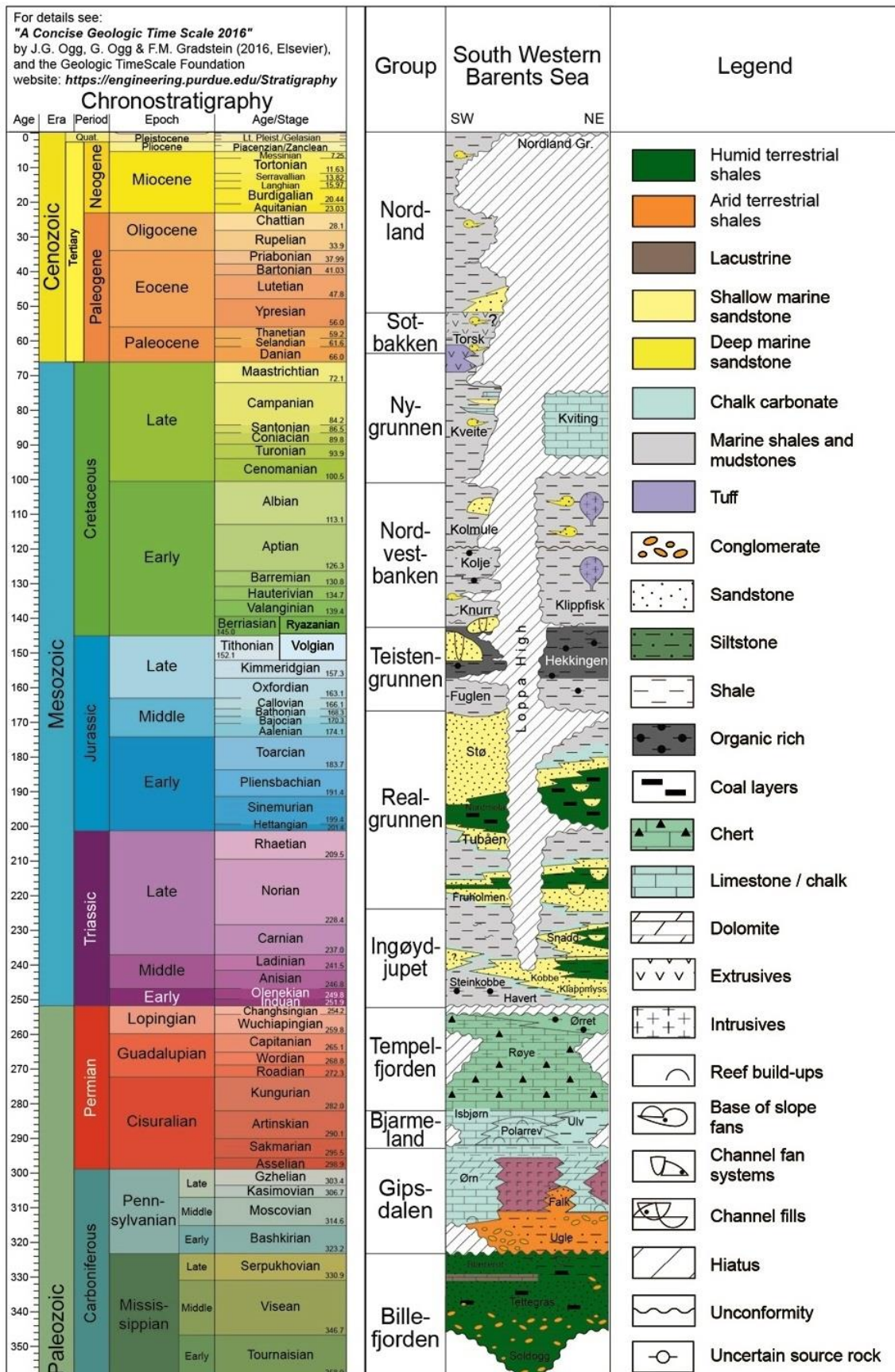
Fig. 2.8*: Lithostratigraphic summary chart of the Southwestern Barents Sea (modified from the Norwegian Stratigraphic Lexicon, Natural history museum based on Gradstein et al., 2010, see also upper left corner for references).*

Chapter 3

3   Data and methods

3.1   Data

The data set of this study includes 2D seismic reflection data from several surveys and well data in the Vestbakken Volcanic Province. The 2D seismic coverage is shown in **Fig. 3.1**. Data coverage is less dense in northern part of the study area. Typical spacing of seismic lines is 4km. Well 7316/5-1 (see **Fig. 3.1** for location) has been used to correlate the seismic data with formation tops in the study area (**Fig. 3.2**) whereas paper based correlations have provided calibration and age of each seismic horizon mapped (e.g. Eidvin et al., 1998; Ryseth et al., 2003). General information for the well is provided in **Table 3.1**. Three stratigraphic groups are present in the well (**Fig. 3.2**), the Nordland Group (473 – 945m); the Sotbakken Group (945-3752m) and Nygrunnen Group (3752-4014m), (Eidvin et al., 1998; www.npd.com). The stratigraphic control provided from Eidvin et al. (1998) is based on studies of the micropaleontology and palynology of cores, thus, calibration and ages are considered to be reliable.

Wellbore name	7316/5-1
Type	Exploration
Purpose	Wildcat
Main area	Barents Sea
Status	Plugged & Abandoned
Seismic location	NH 9109-112 & SP. 543.49
Drilled in production license	184
Drilling operator	Norsk Hydro Produksjon AS
Water depth [m]	450.0
Total depth (MD) [m RKB]	4027.0
Bottom hole temperature [°C]	183
Oldest penetrated age	Late Cretaceous
Geodetic datum	ED50
NS degrees	73° 31' 11.89'' N
EW degrees	16° 25' 59.7'' E
NPDID wellbore	1987
NPDID discovery	45092
Discovery year	1992
Entered date	21.07.1992
Completed date	05.10.1992

Table 3.1: *General information of well 7316/5-1 (modified from www.npd.no).*

Ryseth et al. (2003) have provided correlation of well 7316/5-1 with the nearby Cenozoic stratigraphy of Sørvestsnaget Basin in well 7216/11-1S showing stratigraphic sequences, time correlations, unconformities and lithologies, and hence, further increasing the reliability and validity of horizons, through their observations and inferences.
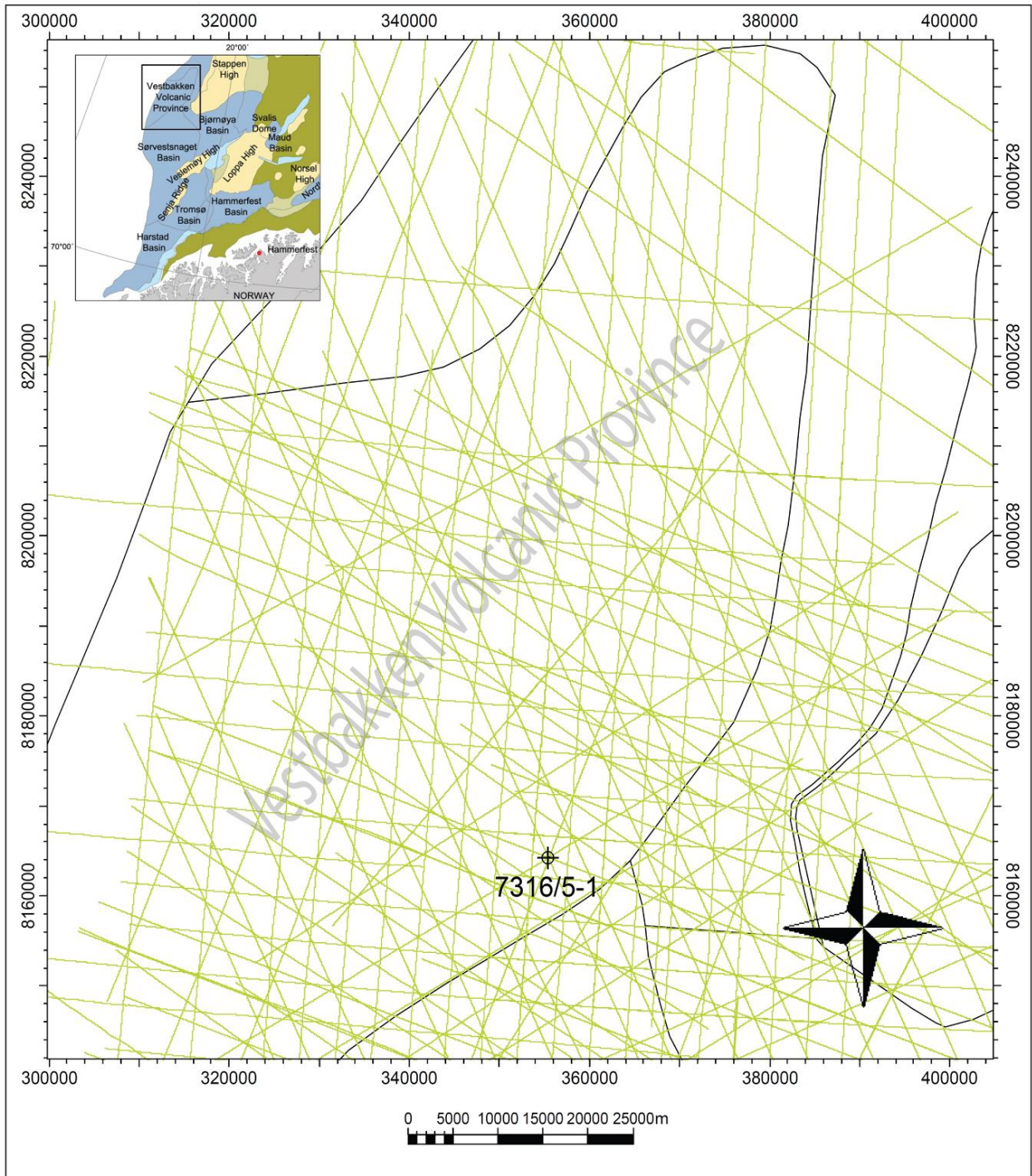
Fig. 3.1: 2D seismic coverage map of the study area. Note that several surveys are shown together. Well location of borehole 7316/5-1 is included. Structural boundaries are loaded into Petrel software and are based on NPD FactMaps. Inset (upper left corner) shows the location of the study area (modified from Henriksen et al., 2011).
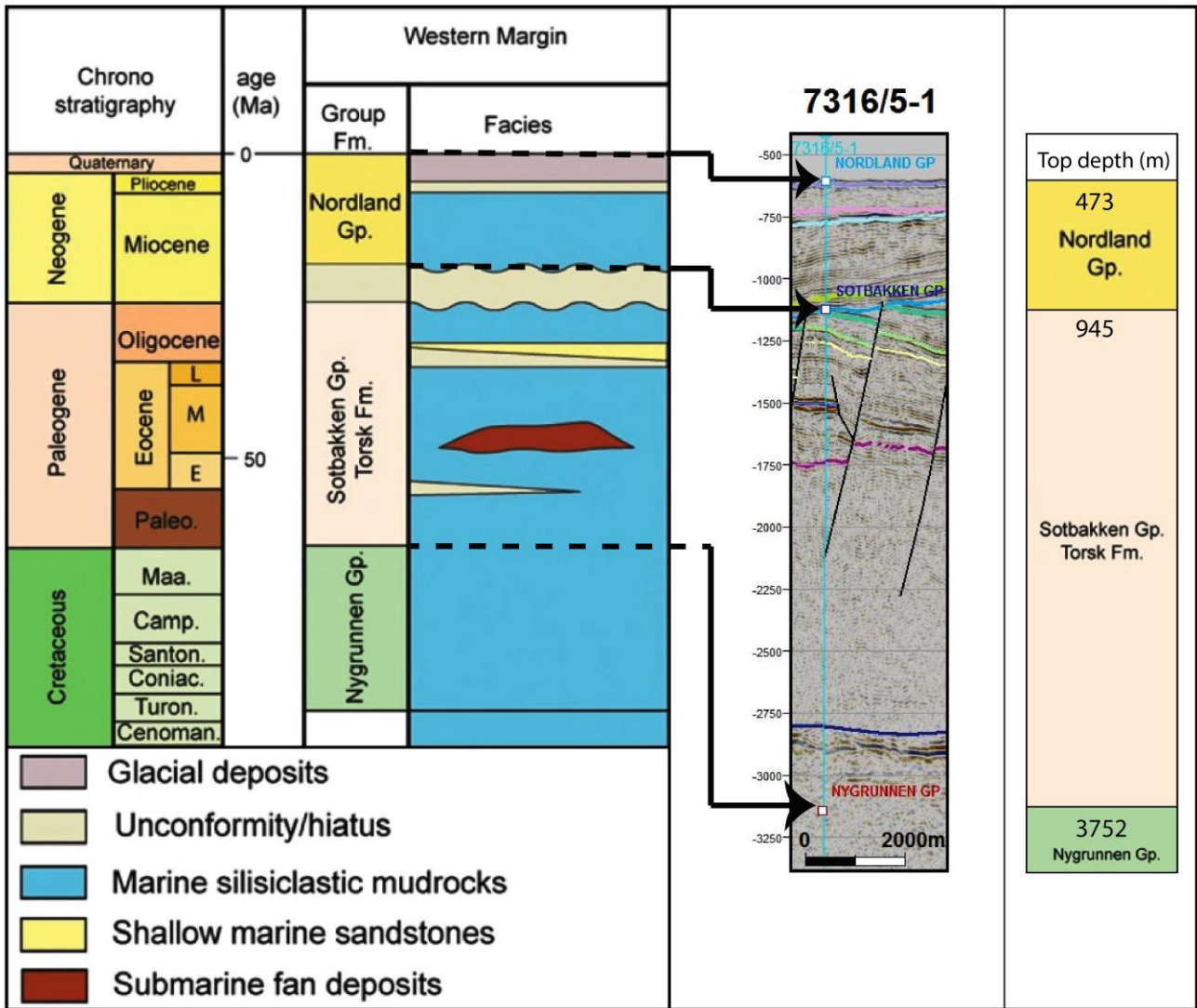
Fig. 3.2: *Seismic well tie and calibration. Chronostratigraphy, stratigraphic groups and facies (modified from Henriksen et al., 2011) are shown and are representative for the western Barents Sea margin. Top depths for each group are placed as obtained from the Norwegian Petroleum Directorate (www.npd.no). Location of well 7316/5-1 is shown in **Fig. 3.1**. Seismic section is part of line BV-04-86 (**Fig. 4.3**) and vertical axis is given in TWT (ms).*

3.2   Methods

The generalized workflow of **Fig. 3.3** summarizes methodologies and data used at each stage throughout the progress of this thesis work. The software used for seismic interpretation was "Petrel E&P Software Platform 2016". Petrel is a software platform used in exploration and production sector of the petroleum industry and is developed by Schlumberger (slb.com). Microsoft Windows is the operating system on which it runs. Adobe Illustrator was selected as the main software for editing and modifying figures, maps and images.

After the data import process in Petrel software, seismic to well tie and calibration was made as shown in **Fig. 3.2** and described in section 3.1. During the seismic interpretation process, five key

horizons were selected and mapped in the entire study area. These horizons include: the early Eocene, the intra middle Eocene, the intra lower Oligocene, the intra lower Miocene and the intra upper Pliocene and are described in Chapter 4 (Results). Some other horizons were mapped in a lesser extent at the early phase of seismic interpretation but were not selected as key horizons (see **Fig. 4.3**).
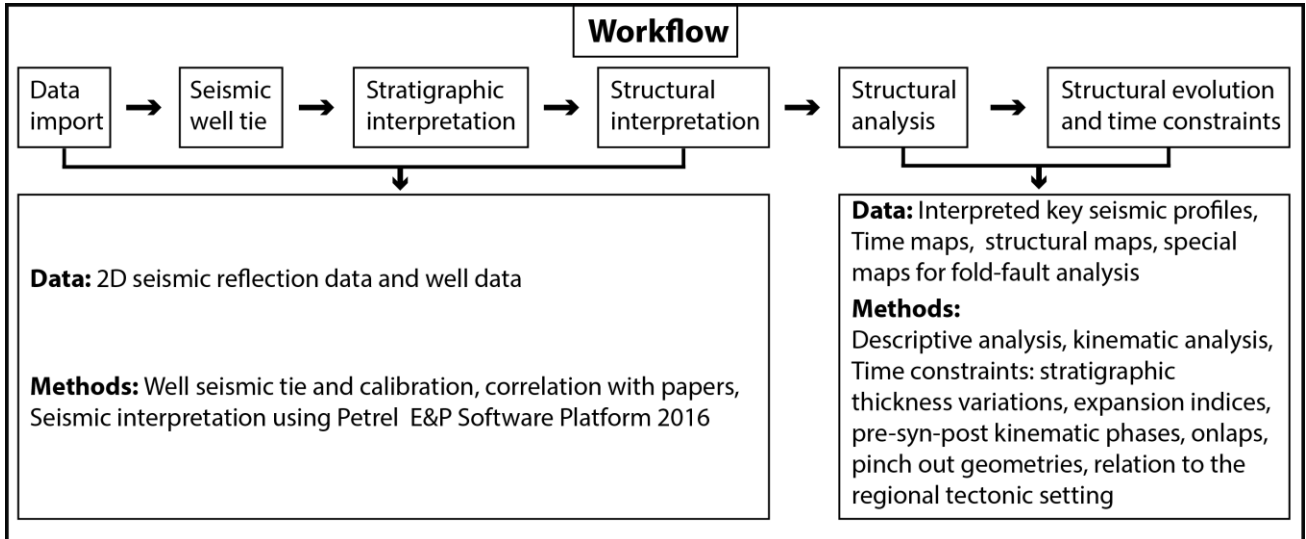
Fig. 3.3: *Generalized workflow describing the step by step research procedure with data and methods used.*

After the establishment of a confident interpretation of horizons, time structure maps were generated. Subsequent structural interpretation was the next step and consists of two parts: fault interpretation and fold interpretation. Fault interpretation in Petrel is a straightforward process but the interpretation of folds is more complicated and the method followed is illustrated in **Fig. 3.4**. Firstly, fold axes needed to be traced and mapped.
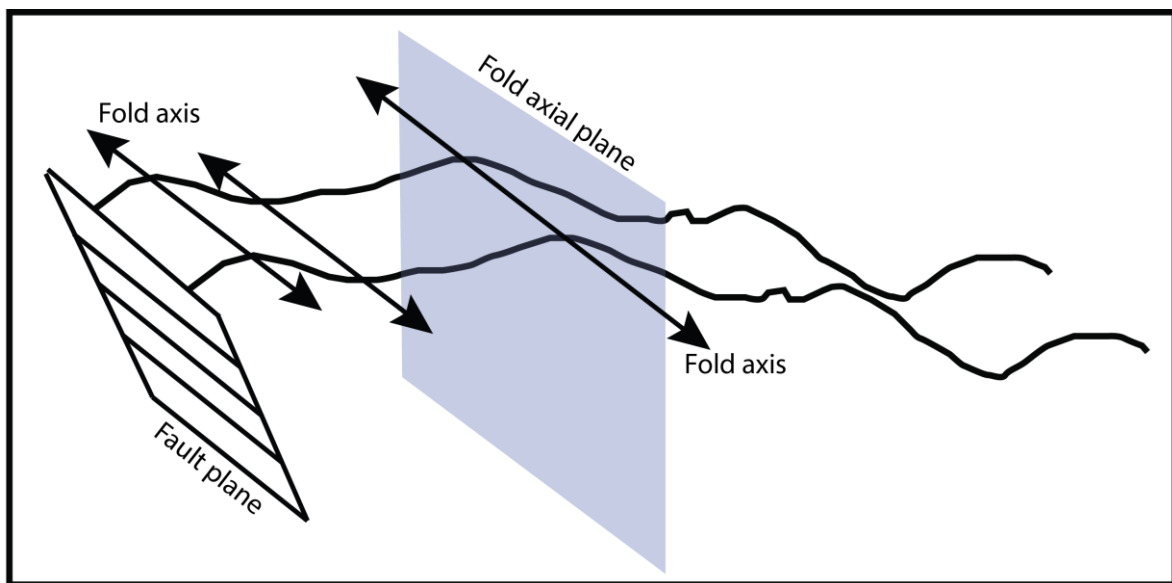
Fig. 3.4: *Example of fold axes tracking on the same interpreted horizon between two seismic lines. Axial planes can also be mapped based on axial trace interpretations in the cross-sectional view.*

This can be done among 2D seismic lines when detecting the hinge of the same fold on the same horizon (**Fig. 3.4**). The axial plane can be interpreted as a surface by mapping the axial trace in each 2D line and applying extrapolation for the space in between (as for fault planes). This is the best method for mapping fault planes and fold axial planes when only 2D data is available. The denser the 2D seismic grid is, the more reliable the interpretation becomes.

The next step was the structural analysis of faults and folds using interpreted 2D seismic lines. The structural analysis of faults is divided into two parts; the first part is the descriptive analysis and is incorporated in Chapter 4 (Results) whereas the kinematic analysis is the second part and is incorporated in Chapter 5 (Discussion). The descriptive analysis of faults involves: position in the study area, general geometrical characteristics (e.g. total length), fault type, strike, fault segmentation (vertical or/and lateral), dip geometry, stratigraphic tip points, hanging wall and footwall geometries, growth relations and age. The kinematic analysis involves: evolution of faults in time, normal/reverse reactivations, changes in shape/geometry, timing and causes, strain regime assessments.

Structural analysis of folds is similarly divided into two parts, the descriptive and the kinematic analysis. The descriptive analysis focuses on the description of the geometry of folds. The characterization and classification of folds is made based on the inclination of the axial plane, inter-limb angle, symmetry and harmony. The cross sectional view provides key measurements: amplitude and wavelength of the fold. When folds display inclined axial planes, amplitude needs to be measured along the axial trace, and since 2D seismic data provides a vertical axis given in TWT (ms), the average velocities obtained from the well data for each stratigraphic interval of interest must be used to calculate the amplitude in meters (as described in **Fig. 3.5**). The critical point here is that one should usually choose a specific orientation of 2D seismic lines (usually perpendicular to fold axes in map view to avoid erroneous apparent calculations of wavelengths) on which all measurements are to be calculated in the cross-sectional view. Note, that for this case study the orientation chosen is that of approximately NW-SE since the dominant orientation of fold axes was that of NE-SW. This is of particular importance when calculating shortening indicators (half wavelength/amplitude ratios). These are shown in special maps which emphasize the relationship between faults and folds. The kinematic analysis includes timing of folding. The determination of timing is based on geometrical characteristics such as onlapping strata onto the limbs of folds and typical pinch-out geometries. When these observations are expressed regionally, one can detect pre-, syn- and post-kinematic phases of contraction.

Finally, a relation to the regional setting was attempted based on observations made in the study area. The structural evolution of faults and folds in relation to the regional tectonic evolution is described in Chapter 5 (Discussion) and a similar tectonic setting in the Gulf of California is introduced for making comparisons with the study area in the Vestbakken Volcanic Province.
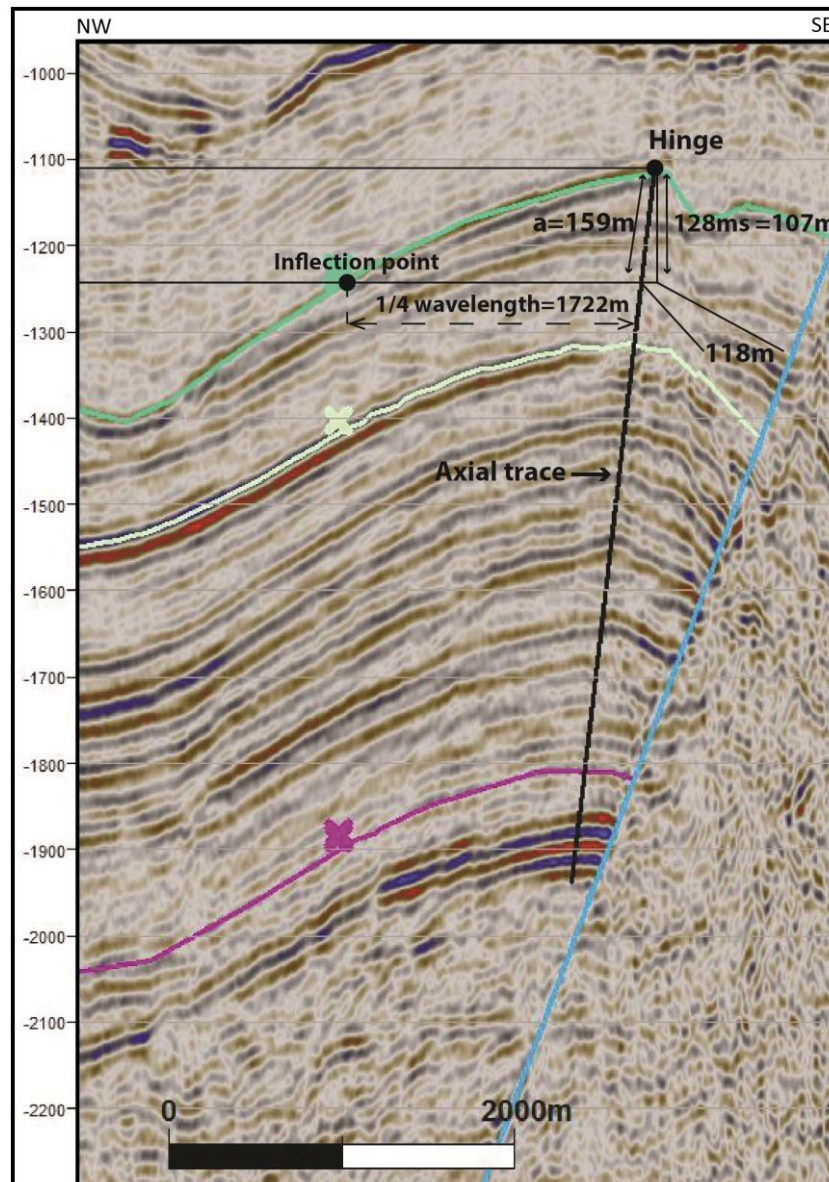
Fig. 3.5: *An example illustrating the calculation of amplitude (a) and ¼wavelength. The average velocity is determined from well data for the corresponding stratigraphic interval.*

CHAPTER 4

4   Results

The study area is located within the Vestbakken Volcanic Province (**Fig. 4.1**) and covers approximately 7174 km^2. It is bounded by an eastern boundary fault (EBF in **Fig. 4.1**) which is a part of the Knølegga Fault Complex and is one of the two master faults in the study area together with the central fault (CF). The Knølegga Fault Complex separates the Vestbakken Volcanic Province from the marginal Stappen High further east. To the south and southeast the Vestbakken Volcanic Province drops gradually into the Sørvestsnaget Basin through the southern extension of the eastern boundary fault and its associated faults. To the west and north the area is delineated by the continent – ocean boundary/transition (marked as COB in **Fig. 4.1**).

According to Faleide et al. (1988) this province can be defined seismically by a level which is expressed by high amplitude reflections (HARs) that represent early Eocene lava flows. The VVP was structured after the formation of these lavas (Faleide et al., 1988; Gabrielsen et al., 1990) within a pull-apart basin setting which was attributed to a releasing bend of the Eocene dextral shear margin (Faleide et al., 2008).

Study area was divided into five subareas (on the basis of tectonic and paleo-topographic criteria) and each of them is characterized by a distinct and homogeneous structural development (**Fig. 4.1**). All five subareas together with mapped structural features such as faults and folds are shown in the structural contour map (**Fig. 4.1**) and time maps (**Fig. 4.4** and **Fig. 4.5**) which were constructed based on the seismic interpretation.

The following subsections of Chapter 4 include an introduction to the study area and the main structural features through the description of a structural map, a stratigraphic interpretation, a description of time structure maps which help on understanding the evolution of the area through time and finally, a detailed structural analysis of faults and folds. Also, the determination of the timing of folding is defined based on observations. Several interpreted key seismic lines are presented for supporting the stratigraphic interpretation, the detailed descriptive structural analysis of faults and folds and finally, for further helping on the analysis of the kinematic history.

All abbreviations used in this chapter can be found in the list of abbreviations (**Table 4.1**). In addition **Table 4.2** and **Table 4.3** of this chapter include all fault abbreviations and **Table 4.4** and **Table 4.5** include all fold abbreviations.

Abbreviation	Full name
CF	Central Fault
COB	Continent Ocean Boundary
EBF	Eastern Boundary Fault
F1-F18	Folds 1 – 18
FM	Formation
GP	Group
HARs	High Amplitude Reflections
KFC	Knølegga Fault Complex
SF1-SF10	Secondary Faults 1 – 10
VVP	Vestbakken Volcanic Province
V1-V3	Volcanoes 1 – 3

Table 4.1: List of abbreviations.

4.1   Structural map

The stratigraphic level of the intra middle Eocene was selected in the structural contour map (**Fig. 4.1**) since it was found a representative level for studying faults and folds, retaining the imprint of Cenozoic tectonic activity and displaying a greater areal extent in comparison with other horizons. Therefore, all faults displayed in the structural map were mapped at this stratigraphic level. The heave of faults at this stratigraphic level is colored black in maps presented herein to illustrate amount of displacement. On the contrary, the procedure of mapping fold axes turned out to be more difficult and the continuation and fold growth was better expressed in stratigraphic levels as shown in **Fig. 4.1**.

Areas with light gray color represent wide NE-SW oriented domal structures. Dome 1 is located on the southern part of the study area and southwest of the well site. This dome has also been mapped by Jebsen (1998) and in his study is referred as *Langdomen*. Dome 2 is located further north, 10 kilometers northwest of the northern termination of the EBF. Dome formation mechanisms will be discussed in Chapter 5.

In the western part of the study area three Volcanoes were additionally mapped and marked as V1, V2 and V3. Volcanoes V1 and V2 are of Oligocene age whereas Volcano 3 is of early Eocene age (Faleide et al., 1988). Volcanoes are discussed in chapter 4.5.

Division into subareas

➢ Subarea I: This subarea is a depression with basinal geometry representing a half-graben (syncline F3, **Fig. 4.1**) developed in a NNE-SSW orientation in the area between the eastern boundary fault and the central fault. The stratigraphic interval on which subarea (I) can be observed is from intra middle Eocene to intra lower Miocene. Based on the interpretation of 2D
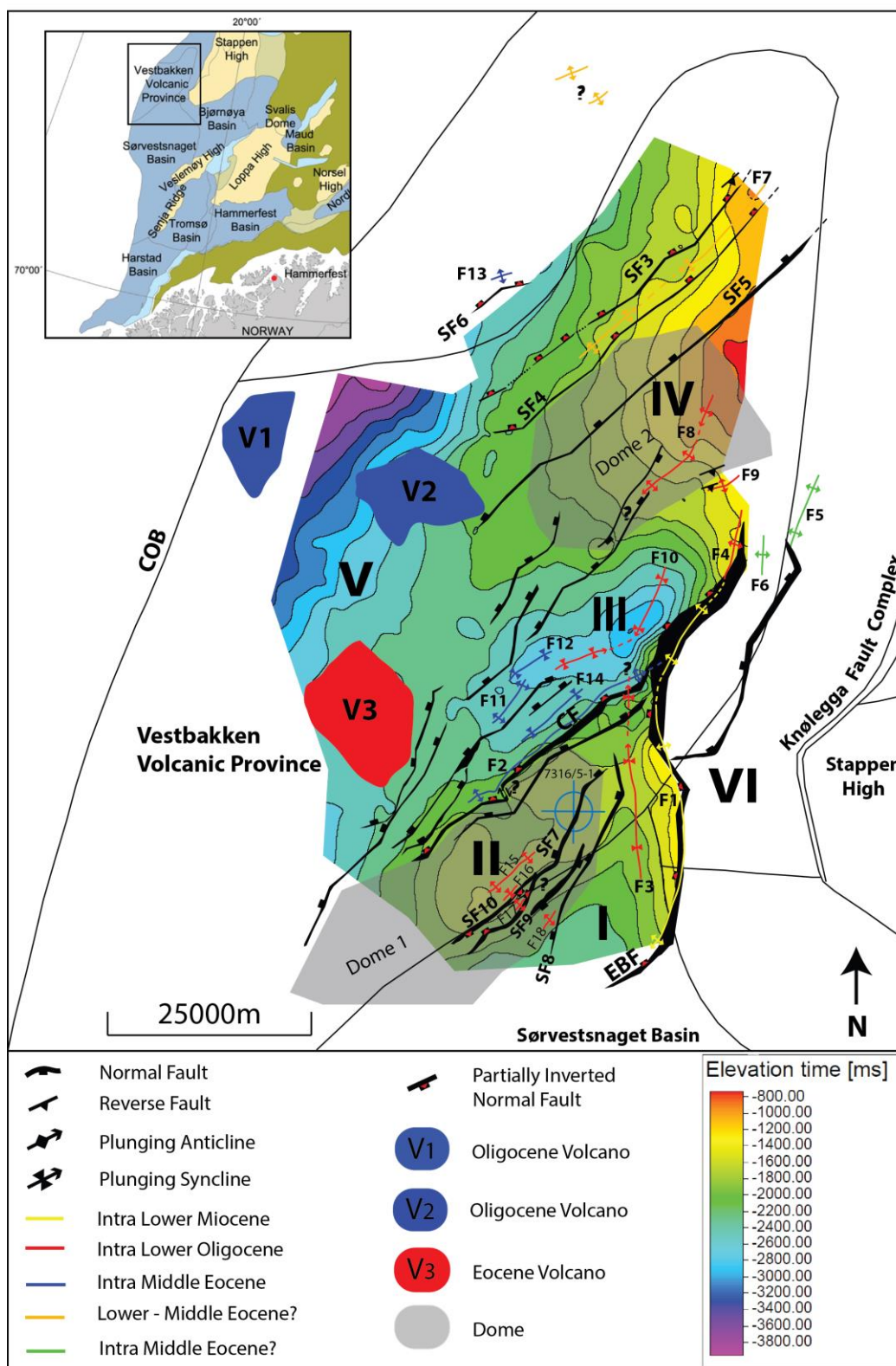
Fig. 4.1*: Structural contour map of the study area within the Vestbakken Volcanic Province. Fault interpretations are displayed at Intra middle Eocene level. Fold axes are mapped at various stratigraphic levels as shown in the legend. Inset (upper left corner) shows the location of the study area (modified from Henriksen et al., 2011). COB: Continent-Ocean boundary. EBF: eastern boundary fault, CF: central fault. All fault and fold abbreviations are shown in the list of abbreviations of **Table 4.1**. All subareas are described in this chapter and are shown with their corresponding Latin numbers I, II, III, IV, V and VI.*

seismic data (e.g. **Fig. 4.7**) one can infer that before segmentation due to down faulting in Oligocene times (e.g. Eidvin et al., 1998), subarea (I) together with subarea (III) were united forming a larger basin.

➢ Subarea II: This subarea shows a high with elongated domal geometry oriented NE-SW (Dome 1 in **Fig. 4.1**). It is associated with the central fault and located on its footwall fault block. To the southeast it gradually drops into subarea (I) and is segmented by normal faults (SF7, SF8, SF9 and SF10 in **Fig. 4.1**). The stratigraphic interval on which subarea (II) can be observed is from early Eocene to intra lower Miocene.

➢ Subarea III**:** This subarea has a basinal geometry representing a NE-SW trending half-graben and introduces the most well preserved Cenozoic sedimentary succession that can be observed adjacent to the eastern boundary fault. In **Fig. 4.1** this area is represented by a syncline (syncline F10). To the west a mild N-S high marks the boundary between subarea (III) and subarea (IV). The stratigraphic interval on which subarea (III) can be observed is from early Eocene to intra lower Miocene.

➢ Subarea IV: This subarea is a high with domal geometry (Dome 2 in **Fig. 4.1**) as subarea (II) and is oriented NE-SW. It develops in a wide area (≈20km) and elevation (ranging from ≈800ms to 2000ms in TWT) consistently decreases toward SW. This subarea is expressed in all stratigraphic levels. There is no cogent evidence that this structuring is a result of faulting.

➢ Subarea V: This subarea is characterized by slope geometry gradually deepening towards west and is better expressed in the intra upper Pliocene time structure map (**Fig. 4.5**). Other stratigraphic levels show this topographic character mainly at the western part of the study area.

➢ Subarea VI: The footwall fault block of the eastern boundary fault is uplifted and the apparent elevation contrast can be seen only in the early Eocene time structure map where this stratigraphic level is preserved in both footwall and hanging wall fault blocks. Note that according to Blaich et al. (2017) the Stappen High was uplifted during the Early Cenozoic due to footwall uplift associated to the Knølegga Fault Complex.

Description of faults in map view

The Vestbakken Volcanic Province is characterized by both extensional and contractional structures (e.g. Jebsen, 1998; Faleide et al., 2008; Blaich et al., 2017). Cenozoic tectonic activity has left its imprint at the eastern part of the study area (**Fig. 4.1**) where most of the structures are observed. There are two mapped master faults, the eastern boundary fault (EBF) and the central fault (CF). The EBF is a N-S striking and W-dipping normal fault with a sigmoid shape. It shows generally

steeper dips in the south compared to north. The CF is a NE-SW striking and NW-dipping normal fault with linear character in map view. However, as shown in map of **Fig. 4.1** there is an area of abrupt lateral shift of the strike of this fault.

All other faults in this map are secondary faults, mainly acting as accommodation structures to the master faults. Starting from the southern part of the area and south of the well site, a population of secondary faults is expressed as an anastomosing development with branched and rejoined faults. Faults SF7 and SF8 are both NNE-SSW striking and WNW dipping synthetic normal faults in relation to the EBF (which shows top-to-the-west displacement). On the contrary, the closely located secondary faults SF9 and SF10 are both NNE-SSW striking and ESE dipping antithetic normal faults in relation to the EBF. At the central and northern part of the study area secondary faults primarily display an isolated character. SF5 is NE-SW striking and NW dipping normal fault with linear expression. SF4 and SF3 show similar characteristics with SF5. However, the southwestern expression of SF3 is not clear. SF6 is a NE-SW striking and NW dipping normal fault. Reverse faulting has occurred locally within the study area and few reverse faults are shown at the northern part of the structural map (**Fig. 4.1**).

Description of folds in map view

Fold F1 is an anticline the axis of which, is parallel and close to the eastern boundary fault (EBF) displaying similar sigmoid shape in map view general N-S orientation. Note that at its southern part it gradually becomes a south plunging fold. Similarly, NE plunging fold F2 has the same relationship with the central fault (CF) with its axis oriented NE-SW. Fold F3 is a north plunging fold and is located between the two master faults within the subarea I and its axis is oriented N-S. Note that the northern continuation of this fold is unclear. Fold F4 is located at the northern part of the EBF and its axis is oriented N-S. Folds F5 and F6 are located a few kilometers eastern on the uplifted footwall of the EBF and their axes are NNE-SSW and N-S oriented, respectively. The doubly plunging fold F7 is running parallel to the strike of fault SF4 with its axis oriented NE-SW and its continuation at the central part (on which it is plunging) is unclear. The SW plunging fold F8 has a NE-SW oriented axis and was divided into two parts since its continuation was found to be unclear. Fold F9 has NE-SW oriented axis, fold F13 is a locally developed fold along fault SF6 and its axis is oriented NE-SW. Fold F10 is a doubly plunging fold toward its central part with a NNE-SSW axis orientation at the northern part and a more ENE-WSW axis orientation at the southwestern part. Folds F11, F12, and F14 constitute a set of folds that develop among secondary synthetic normal faults in relation to the CF and their axis is oriented NE-SW. At the southern part of the area, folds F15, F16, F17 and F18 constitute a set of locally developed folds among the secondary normal faults SF7 – SF10. Their axes are NE-SW oriented.

__Summarized observations on structural contour map__

Cenozoic tectonic activity is concentrated at the eastern part of the study area. Six tectonically divided subareas are defined as follows (**Fig. 4.1**):

- Subarea I: NNE-SSW trending half-graben between the two master faults (EBF and CF).
- Subarea II: fault controlled domal structure (NE-SW orientation) on the footwall fault block of the central fault (CF).
- Subarea III: NE-SW trending half-graben. Fault controlled subarea associated with the eastern boundary fault (EBF) to the northeast and the central fault (CF) to the southwest.
- Subarea IV: domal structure (NE-SW orientation) located in the area north and NNW of the EBF.
- Subarea V: characterized by slope geometry and affected by volcanoes,
- Subarea VI: uplifted footwall block of the eastern boundary fault (EBF).

Numerous normal faults, folds and reverse faults were identified and mapped (**Fig. 4.1**). The dominant strike of normal faults is that of NE-SW, with the exception of the eastern boundary fault, which has a more N-S strike at its central part. Most of the normal faults are generally NW-dipping. Exceptions are faults SF9 and SF10 that are interpreted as SE-dipping antithetic normal faults (top-to-the-east displacement) to the EBF. Occasionally, some secondary faults exhibit the same character. Studied contractional structures are chiefly oriented parallel to the strike of the faults as shown in the map of **Fig. 4.1**, keeping a general NE-SW direction and include plunging synclines, plunging anticlines and occasionally blind thrust faults and reverse faults.

4.2   Stratigraphic interpretation

Interpreted seismic profile of **Fig. 4.3** (and **Fig. 4.2** restricted in well site) represents the starting point of the seismic interpretation stage, with well 7316/5-1 for stratigraphic control and correlation. **Fig. 4.2** shows the seismic characteristics and ages of all horizons interpreted. Note that the calibration and age of each horizon (**Fig. 4.2** and **Fig. 4.3**) is based on Eidvin et al. (1998) and was defined based on data obtained from the micropaleontology and palynology of well 7316/5-1.

__Lithostratigraphic units in the well site__

This study covers the early Eocene to Base Pliocene (**Fig. 4.2**). The latter represents the sequence boundary between glacial and pre-glacial sediments while early Eocene the top of Volcanic flows. Three lithostratigraphic groups are present in the well (**Fig. 4.2**), the Nordland Group (473 – 945m) of Pliocene-Pleistocene age; the Sotbakken Group (945-3752m) of lower Miocene to Paleocene age and the Nygrunnen Group (3752-4014m) of Cretaceous age (e.g. Eidvin et al., 1998; NPD factpages). Note that according to Eidvin et al. (1998), upper Oligocene sediments and those of earliest Oligocene age are not proved in the well. Also upper middle and upper Eocene sediments are absent.
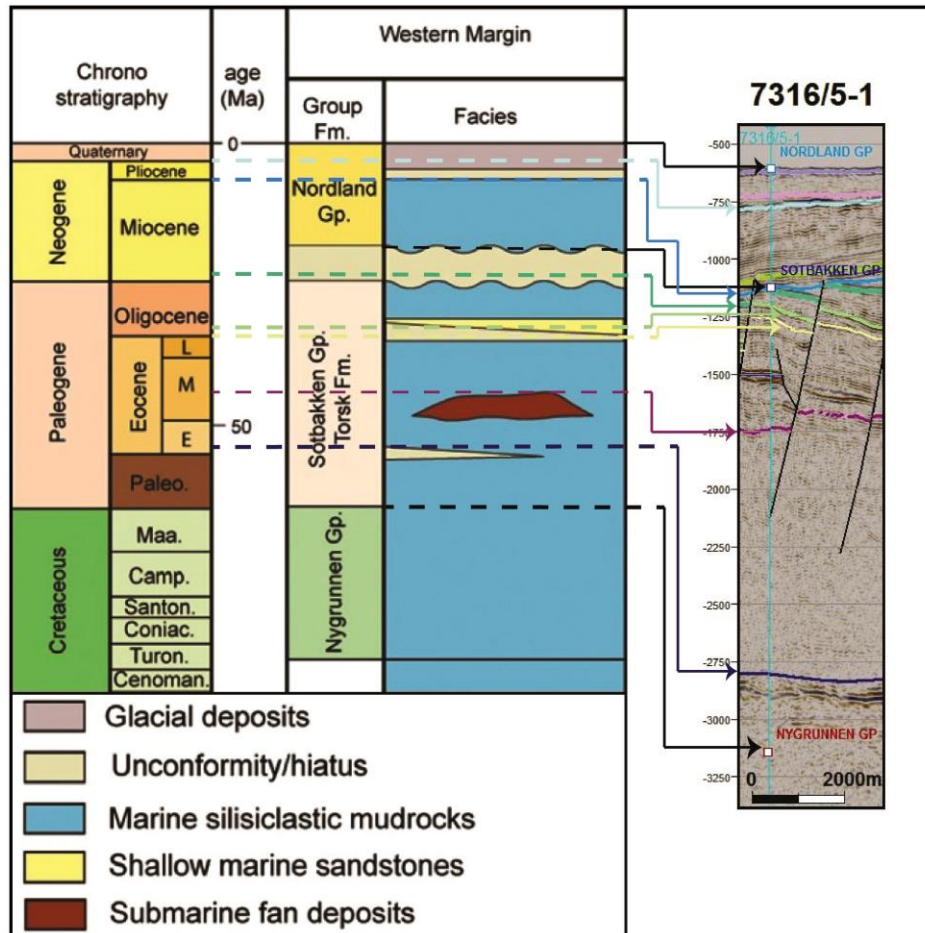
Fig. 4.2: *Chronostratigraphy, groups and facies (modified from Henriksen et al., 2011) correlated with interpreted seismic horizons in well site. Seismic section is part of line BV-04-86 (**Fig. 4.3**) where the detailed legend for all horizons is also provided. Vertical axis is given in TWT (ms).*

Depositional environments

Pleistocene to upper Pliocene sediments were deposited in a bathyal to glacial marine depositional environment (Eidvin et al., 1998; npd.no). The lower Miocene and lower Oligocene sequences in the well site were deposited on the middle to outer shelf depositional environment (Eidvin et al., 1998). In addition, Eidvin et al. (1998) suggested that much of the Middle Eocene sequence was deposited in relatively deep open marine environment proposing an outer to middle shelf depositional environment.

Seismic stratigraphy and architecture

Northeast of the well location the Base Pliocene unconformity is present expressed as an erosional surface separating pre-glacial (older) from glacial sediments (**Fig. 4.3**). However, the same unconformity is eroded to the southwest (in reference to the well location) by the younger intra upper Pliocene erosional surface (angular discordance) which acts similarly truncating progressively older pre-glacial sediments. Note that the intra Upper Pliocene erosional surface is the most dominant and regionally expressed in the whole study area.
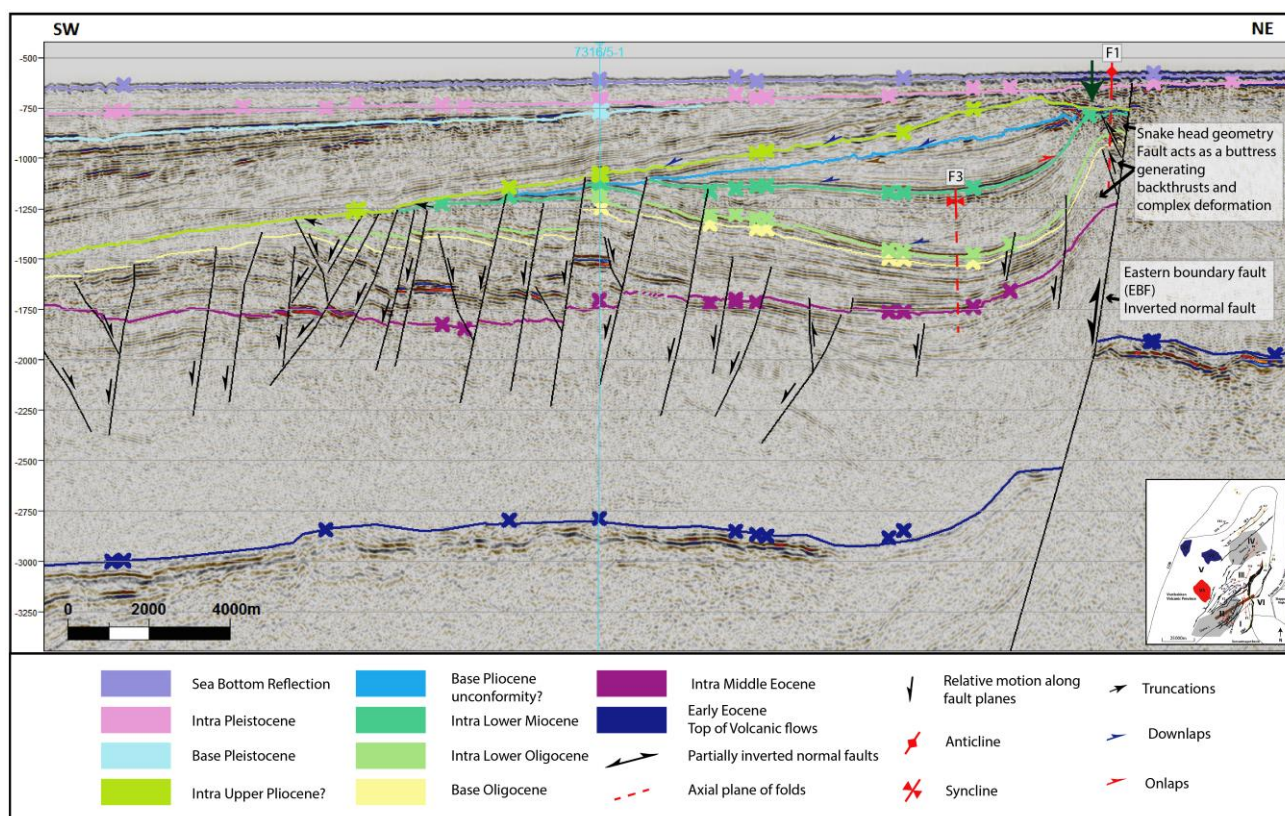
Fig. 4.3: *Interpreted seismic profile of line BV-04-86 showing well location with interpreted seismic horizons and major unconformities, master fault EBF with hanging wall structures and basinal development of subarea (I). See* *Fig. 4.6* *for location of line and structures. Note that this legend applies for all interpreted seismic profiles. Vertical axis is given in TWT (ms).*

To the east of the well site stratigraphic units between intra lower Miocene and Base Pliocene have lens-shaped geometry with parallel reflections displaying eastward onlap and westward downlap terminations. Stratigraphic units between the intra lower Oligocene and the intra lower Miocene have similar lens-shaped geometry and display subparallel medium amplitude reflections that downlap toward the west. Prograding clinoforms indicate sediment transport from the east toward the west. Horizons intra lower Miocene and the intra lower Oligocene seem to be truncated to their westward extension. This is generally evident in the whole study area. Stratigraphic units included from the intra middle Eocene to the intra lower Oligocene thicken toward west and adjacent to the eastern boundary fault, strata included in the core of anticline F1 display deformation and reflections become discontinuous. All stratigraphic units in this anticline are absent in the footwall of the eastern boundary fault. Exception is the lower Eocene horizon (top of volcanic flows/extrusives, high amplitude reflections). This is generally evident all along the eastern boundary fault except for the southern part. To the east of the well site most reflections are parallel to subparallel and continuous with strong amplitudes but toward the west they become weak and difficult to interpret. The stratigraphic unit from the early Eocene to the middle Eocene is volumetrically the most important with thicknesses reaching 1500 ms (TWT). However, the seismic character within this unit is chaotic and observations are limited. One can barely notice westward downlap on the lower Eocene volcanic flows.

4.3   Time structure maps

Time structure maps (TWT) were generated for five (5) stratigraphic levels, the selection of which is based on the following criteria: regional extent, structural (and thus tectonic) importance, stratigraphic importance (e.g. unconformities, hiatus) and involvement of volcanic activity. These are: the early Eocene, the intra middle Eocene, the intra lower Oligocene, the intra lower Miocene and the intra upper Pliocene stratigraphic levels. The latter is a time structure map for the top of the volcanic flows (extrusives). However, note that this map is not an accurate isochronous map and was mainly created to show the topography and extent of volcanic flows within the study area. These maps give a sense of the topography and structural development (with contours representing elevation) for stratigraphic level. Note that that their development within the VVP is a result of several phases of rifting, uplift, erosion, tilting, volcanism and inversion during the Cenozoic (e.g. Jebsen 1998; Faleide et al., 1988; Faleide et al., 2008; Richardsen et al., 1990; Eidvin et al., 1998). The tectonic subdivision of the study area into subareas was described in chapter 4.1 on intra middle Eocene stratigraphic level and is also used here for the detailed description of time structure maps.

Early Eocene – Top of Volcanics time structure map

The early to the middle Eocene was a period of massive volcanic activity in the Vestbakken Volcanic Province (Faleide et al., 1988). Distribution and topography of volcanic flows represented by HARs (High Amplitude Reflections) are shown in time structure map of **Fig. 4.4a**. Volcanic flows can be seen in both the hanging wall and footwall (subarea (VI)) fault blocks of the EBF despite the elevation contrast. All subareas can be still observed at this stratigraphic level. Subarea (I) can be also followed to the west while subarea (II) is expressed as a high approaching a conical shape. Subarea (III) has been affected by both master faults and shows half-graben geometry. This subarea seems to be topographically connected with subarea (I) to the southwestern termination of subarea (II) which generally acts as a boundary. Subarea (V) is bounded by the Eocene volcano (V3 in **Fig. 4.1**) and displays large elevation contrast to the west through a depression which reaches 4800ms (TWT), thus, introducing the deepest province of the study area. Subarea (IV) comprises a high that gradually deepens toward SW and to the south it drops into subarea (III).

Intra middle Eocene time structure map

All subareas are clearly developed in the intra middle Eocene time structure map (**Fig. 4.4b**). Note that intra middle Eocene strata are absent in the area eastern of the EBF due to erosion (e.g. Eidvin et al., 1998). The same applies for all following maps with more recent age. At this stratigraphic
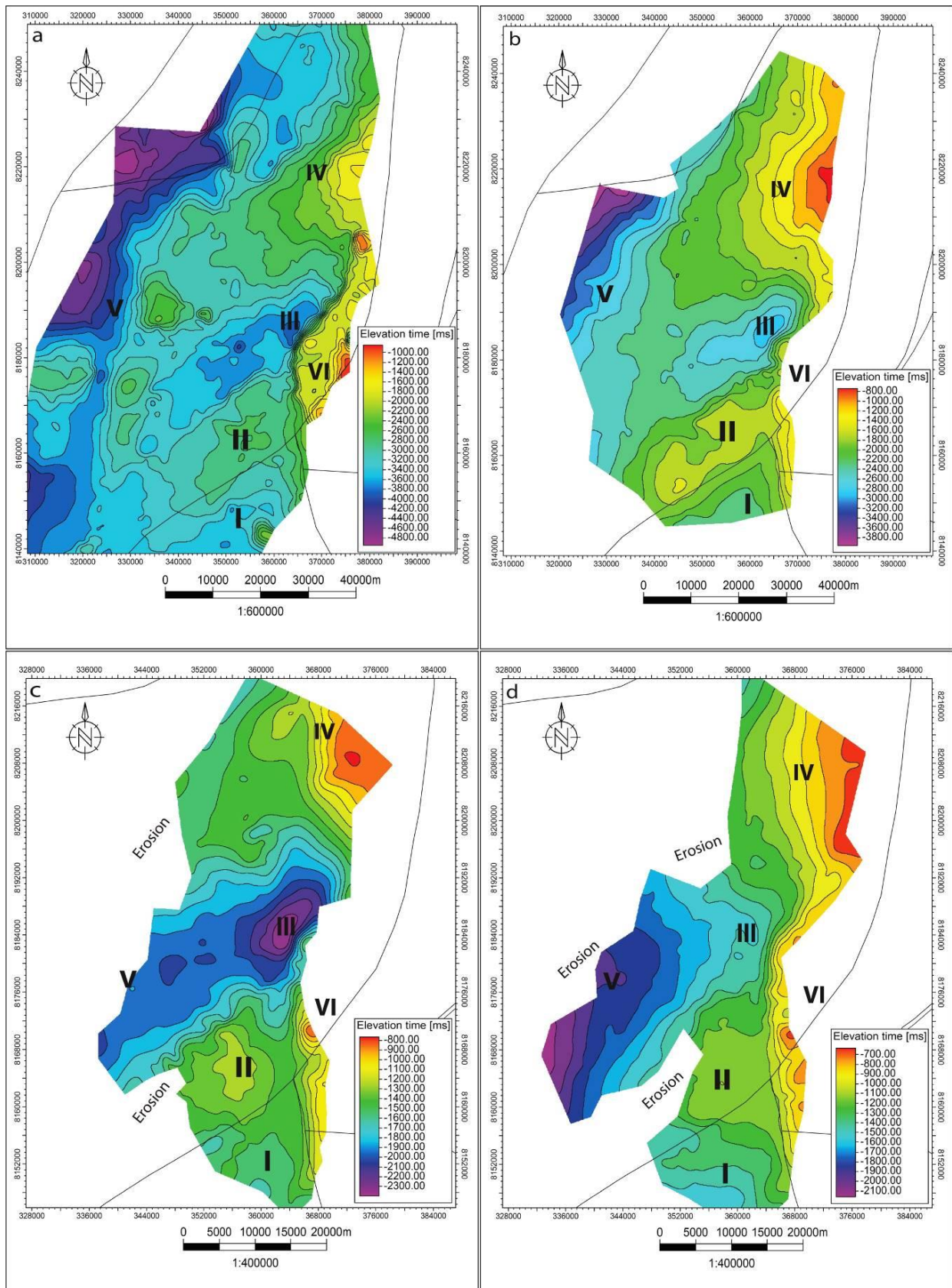
Fig. 4.4: a) Time structure map (TWT) of the top of volcanic flows representing early Eocene age, b) intra middle Eocene time structure map (TWT), c) intra lower Oligocene time structure map (TWT), d) intra lower Miocene time structure map (TWT). Subareas described in chapter 4.1 can be seen with their corresponding Latin numbers I, II, III, IV, V, and VI.

level, subarea (I) is clearly restricted with subarea (II) acting as boundary. The basin in subarea (I) gradually deepens from north, where the two master faults merge, towards south. Subarea (II) has a domal geometry but appears with a more ellipsoid shape with a NE-SW orientation. At least to some degree, it appears displaced by the central fault and segmented by several secondary normal faults, the displacement of which cannot be seen in the time map because is relatively low. Subarea (III) has been affected by both master faults and appears to reach depths of 3800-3900 ms (TWT). It keeps the general NE-SW structuring and to the west is bounded by a wide N-S oriented ridge which connects subarea (II) with subarea (IV). Subarea (IV) retains a general NE-SW orientation and gradually deepens towards SW. In this time map it appears to have a greater extent to the north and northwest compared to the early Eocene time map, but to the south it keeps the exact same pattern with it, gradually flexuring into subarea (III). Subarea (V) dips gently northwestwards where it reaches a maximum depth of 3900ms (TWT).

Intra lower Oligocene time structure map

The extent of this map (**Fig. 4.4c**) is laterally more confined in comparison with previous maps due to later erosion. The intra upper Pliocene erosional unconformity is present in the western, northern and southern part while the base Pliocene unconformity has affected the area adjacent to the EBF. Compared to the intra middle Eocene time structure map, subarea (I) is in this structure map dipping less and subarea (II) is expressed with a domal conical shape. Subarea (III) appears to have a larger extent in comparison with previous maps and forms a half-graben (e.g. F10 in **Fig. 4.1**) affecting the whole central area. This structuring is controlled by the master faults. Subarea (IV) is still expressed but lacks the sense of the previous NE-SW orientation. Area (V) cannot be observed.

Intra lower Miocene time structure map

Similarly with the intra lower Oligocene time structure map erosion has affected the extent of strata of intra lower Miocene age (**Fig. 4.4d**) on the hanging wall fault block of the eastern boundary fault and in the area of Dome 1. Subarea (I) becomes wider and deepens towards SW. Subarea (II) is still present as a high but lacks the previous sense of NE-SW structuring. In addition, it maintains the same stratigraphic level (≈1200ms TWT) in the area between the two master faults. In this time structure map, subareas (III), (IV) and (V) appear to have a similar structuring and steadily deepen towards SW. However, they keep their elevation contrast as displayed in previous time maps.

Intra upper Pliocene time structure map

This time structure map (**Fig. 4.5**) represents part of the sequence of westward prograding glaciogenic sedimentation forming gently westward-dipping strata. Therefore, it generally shows a slope geometry which gently dips toward the west with subarea (V) representing the entire area. However, pre-established depressions (e.g. in subarea III) and highs (subareas II and IV) slightly affect the topography. This map does not represent an isochronous surface since it is an unconformity.
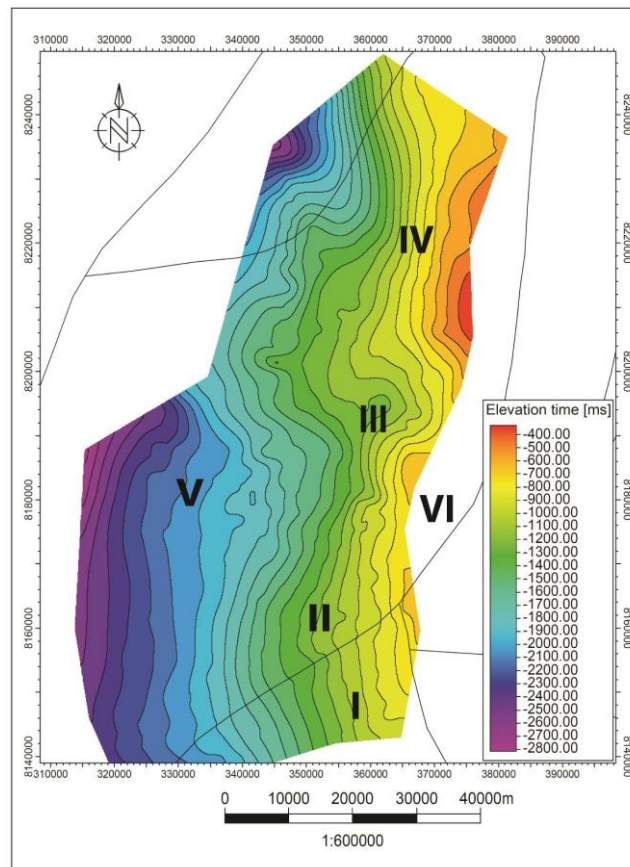
Fig. 4.5*: Time structure map (TWT) of intra upper Pliocene. Subareas described in chapter 4.1 can be seen with their corresponding Latin numbers I, II, III, IV, V, and VI.*

4.4   Structural analysis of faults and folds

The distribution of faults and folds as mapped in the study area is shown in the structural contour map of **Fig. 4.1** and in the same chapter the map view description of faults and folds is provided. This chapter focuses on the description of faults and folds in terms of geometry and structural development (descriptive analysis) and associates them with the regional geological setting. Location of all key seismic lines discussed in this chapter is shown in **Fig. 4.6**. The dominant observed structural styles are anticlines (e.g. F1, F2, F4 in **Fig. 4.1**) closely associated with extensional faults and synclines related with depocenters and half-grabens (e.g. F3 and F10 in **Fig. 4.1**).

4.4.1   Faults

Master Faults

There are two master faults in the study area, the eastern boundary fault (EBF) and the central fault (CF) (**Fig. 4.6**, **Fig. 4.7**, **Table 4.2**).
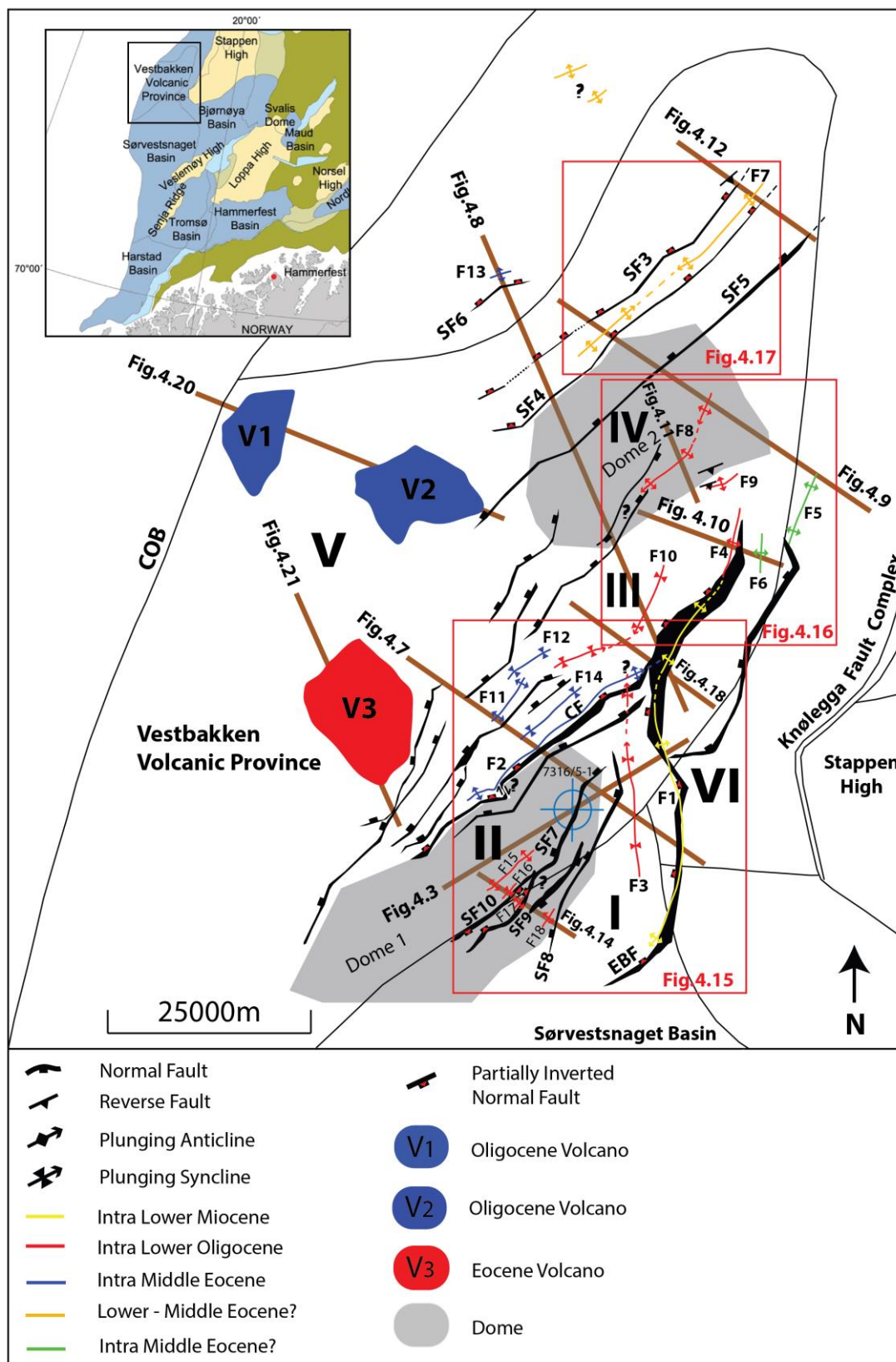
Fig. 4.6: *Structural map of the study area in the Vestbakken Volcanic Province showing mapped structural elements. Inset shows the location of the study area (modified from Henriksen et al., 2011). COB: Continent-Ocean boundary, EBF: eastern boundary fault, CF: central fault. All fault and fold abbreviations are shown in the list of abbreviations in* **Table 4.1**. *They can also be found within this chapter in* **Table 4.2** *and* **Table 4.3**. *Subareas described in chapter 4.1 are shown with their corresponding Latin numbers I, II, III, IV, V and VI.*

Master faults	General strike/ dip azimuth range of fault plane		Total Length	Maximum throw (TWT)	Remarks
Eastern boundary fault (EBF)	N-S	250^0-325^0	63.2 km	1980 ms	Partially inverted fault.
Central fault (CF)	NE-SW	310^0-340^0	38.3 km	670 ms	Partially inverted fault with mainly planar fault plane geometry.

Table 4.2: *Summary of main geometrical and structural characteristics of the master faults. For location of faults, see* **Fig. 4.6**. *Detailed description is provided in the text.*

Eastern boundary fault

The EBF is considered to be part of the broad Knølegga Fault Complex (**Fig. 4.6** and **Fig. 4.7**). **Table 4.2** summarizes the main structural characteristics of the EBF. This fault generally exhibits a normal top-to-the-west displacement, but locally shows evidence of being partially inverted. The EBF is a N-S striking fault with a sigmoid shape in map view. Note that the northernmost termination (fault trace) of the EBF is not clearly expressed. In most cases, the cross-sectional expression is defined as a single fault strand (e.g. **Fig. 4.7** and **Fig. 4.8**). Occasionally, displacement is vertically segmented shown as a distribution of closely located down-stepping fault blocks (e.g. **Fig. 4.10**). Maximum recorded throw was found to be 1980 ms within subarea (III) (**Fig. 4.6**). It is common that such faults along passive margins become listric in nature with depth (listric growth faults) and meet a regional detachment surface/fault at depth (e.g. Van, P. B. A., & Marshak, S. 2004). The fault plane geometry of the eastern boundary fault shows a slightly listric (concave up) geometry to the south (**Fig. 4.3** & **Fig. 4.7**) and to the north it seems that contraction has affected the fault plane which verges with decreasing dip angle towards east at the upper part (concave down geometry) (**Fig. 4.8**). In the cross-sectional view (Fig. 4.7) it seems that this master fault has an upper stratigraphic tip point located in intra Pleistocene. The downdip termination (tip point) of the EBF cannot easily be defined due to the chaotic seismic character and poor image at depth and therefore, a relationship of Cenozoic faults with older basement related zones of weakness such as faults is not possible. However, it was found that in the southern flank of the Stappen High, most of the Cenozoic faults (N-S trending, as the EBF in VVP) are decoupled from the deeper-seated faults and have different orientations (Blaich et al., 2017). The hanging wall fault block of this master fault hosts the anticline F1 (**Fig. 4.3** & **Fig. 4.7**) which runs parallel and very close to the strike of the EBF. Similarly, at the northernmost part of the EBF, in the hanging wall fault block, one can locate fold F4 (**Fig. 4.10**). These folds are generally located in the shallow part of the hanging wall of the EBF. Occasionally, small blind thrust faults associated with this master fault cut strata in fold F1 (**Fig. 4.3**) and it is common that extensional faults cut into the lower part (back limb) of the folds. The footwall fault block has a generally chaotic seismic character represented by sediments of mainly early to middle Eocene age. In the northern part of the fault it was possible to identify and map fold F6 (**Fig. 4.10**). The general character at this position is expressed with highly deformed and folded

strata. The EBF displays variable degrees of throws with generally decreased throws toward its southern extension. Maximum throws were found at the position of seismic line in **Fig. 4.8**.

Timing: this fault generally cuts the early Eocene surface which represents volcanic flows (**Fig. 4.7**). Therefore, it is obvious that the fault came later and after the cessation of early Eocene volcanic activity. Growth wedge geometries in middle Eocene strata suggest fault activity and subsidence of the hanging wall fault block at this time (**Fig. 4.8**). However, related observations are restricted in the central part of subarea (III) (**Fig. 4.6**) and contractional deformation has overprinted the initial fully developed character. The early Oligocene plate reorganization (e.g. Faleide et al., 1993; Faleide et al., 2008; Doré et al., 1999) has reactivated mainly the northern half part of the EBF that has a more NNE-SSW orientation. This is supported by the wedge shape geometry (synrift) (**Fig. 4.8**) within the intra lower Oligocene – intra lower Miocene interval. The EBF slightly cuts the intra Pleistocene horizon which introduces the most recent reactivation of this fault.
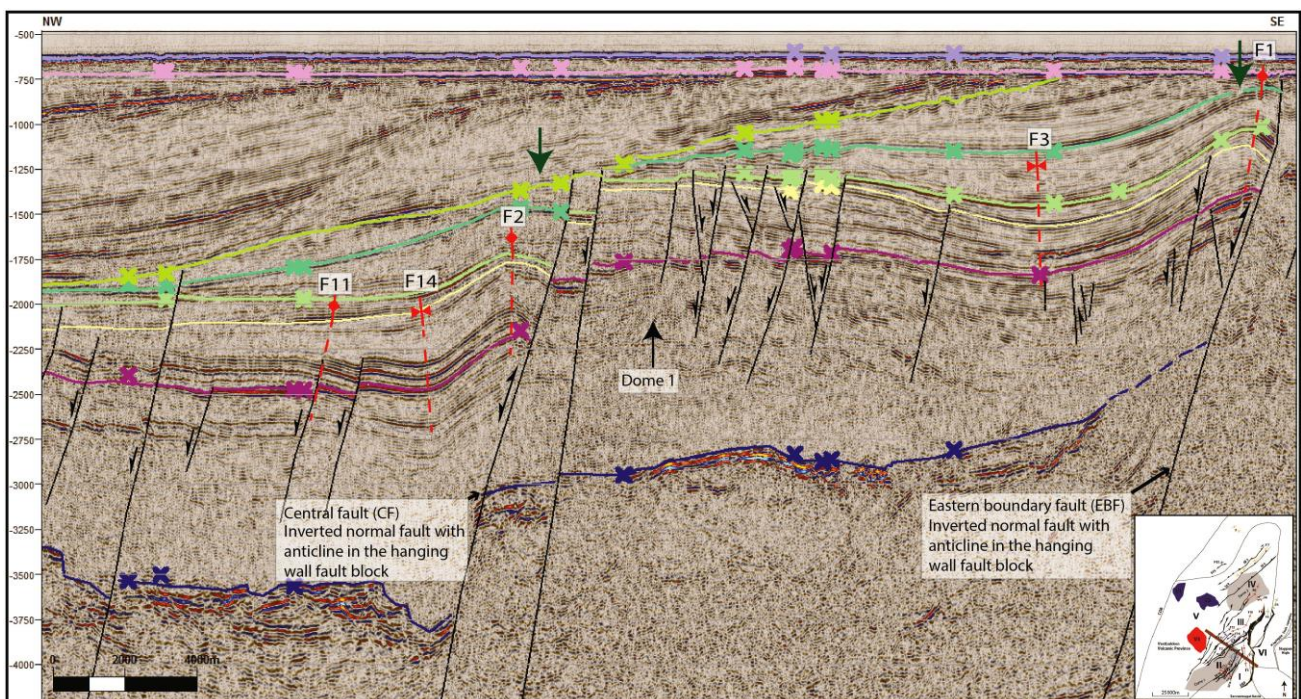

Fig. 4.7: *Interpreted seismic profile of line GBW-88-032Y showing master faults EBF and CF together with hanging wall structures and basinal development and segmentation into subareas (I), (II) and (III). Legend can be found in **Fig. 4.3**. See **Fig. 4.6** for location of seismic line, structures and subareas. Vertical axis is given in TWT (ms).*

Central Fault

This master fault (CF) is located at the central part of the study area, and is obliquely developed to the EBF and its linkage with it is found at the northeastern extension (**Fig. 4.7**). **Table 4.2** summarizes the main structural characteristics of the CF. It has a normal character but exhibits similar characteristics as the EBF and is interpreted as a partially inverted normal fault. It is a NE-SW striking normal fault with linear trace in map view and with top-to-the-NW displacement.
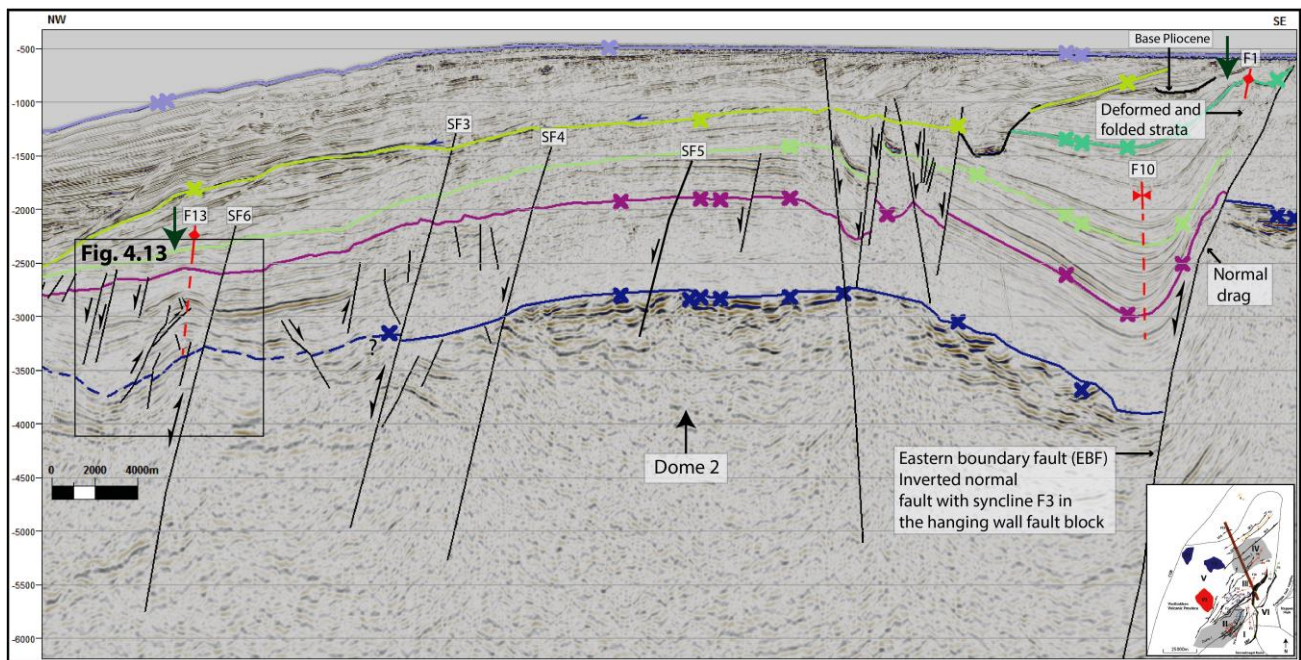
*Fig. 4.8: Interpreted seismic profile showing geometry of master fault EBF together with hanging wall structures and basinal development of subarea (III). In addition, secondary faults, fold F13 and dome 2 of the northern part of the study area can be seen. Legend can be found in **Fig. 4.3**. See **Fig. 4.6** for location of seismic line, structures and subareas. Vertical axis is given in TWT (ms). Data courtesy of TGS and Spectrum.*

However, the fault trace is found segmented in one position as shown in map of **Fig. 4.6**. The cross-sectional expression of CF is always defined as a single fault strand (**Fig. 4.7**) without evidence of vertical segmentation. The fault plane geometry of the CF shows a planar character and the upper stratigraphic tip point is located in the intra upper Pliocene unconformity (barely truncating it). The downdip termination cannot easily be defined due to the chaotic seismic character and poor imaging at depth. However, it is certainly located deeper than early Eocene and possibly within the Nygrunnen Group of Cretaceous age. The hanging wall fault block of this master fault hosts the anticline F2 (**Fig. 4.7**) which runs parallel to the CF. In addition, an anticline (F2) – syncline (F14) pair can be found in a more restricted area (**Fig. 4.6** and **Fig. 4.7**). The footwall fault block is generally segmented by secondary extensional faults and represents the main part of dome 1 (**Fig. 4.7**). The CF displays gradual decrease in throws toward its southwestern extension where it eventually tips out (see map view, **Fig. 4.6**).

Timing: this fault, as in the case of the EBF, cuts the early Eocene surface which represents volcanic flows. Thus, it is also considered to be younger than early Eocene. The synrift sedimentary wedge within the intra lower Oligocene – intra lower Miocene stratigraphic interval (**Fig. 4.7**) in the hanging wall block of the CF supports the previous statement since it records thickening toward the fault plane. Latest reactivations of the CF are found to affect intra upper Pliocene strata.

Secondary faults

Secondary faults form an inseparable part of the Cenozoic tectonic evolution of the study area and this subsection aims to describe the most important observations and to analyze these structures. **Fig. 4.6** displays all secondary faults mapped within the study area whereas **Table 4.3** summarizes

their main structural characteristics. Ten of those faults were found to be more important due to their structural development and association with structures such as folds. At the northern part of the study area, faults SF3 and SF4 are NE-SW striking and NW dipping normal faults and in map view are expressed with linear fault trace. They both have planar fault plane geometry. No vertical segmentation is observed. At their northeastern part their upper stratigraphic tip is located in middle Eocene (**Fig. 4.12**) but to the SW they affect more recent stratigraphic units and their upper stratigraphic tip is located within the intra upper Pliocene stratigraphic wedge (**Fig. 4.8** and **Fig. 4.9**). Their downdip termination is not clear but one can infer that it is below early Eocene – late Paleocene sediments. The hanging wall fault block of SF4 (or footwall block of SF3) hosts fold F7 (**Fig. 4.12**).

Secondary faults	General strike/ dip azimuth range of fault plane		Total Length	Maximum throw (TWT)	Remarks
Secondary fault 3 (SF3)	NE-SW	300^0-340^0	40.3 km	100 - 200 ms	Partially inverted normal fault
Secondary Fault 4 (SF4)	NE-SW	300^0-325^0	42.6 km	100 ms	Partially inverted normal fault
Secondary Fault 5 (SF5)	NE-SW	300^0-330^0	52.9 km	100 ms	Fault with normal character
Secondary Fault 6 (SF6)	NE-SW	275^0-300^0	8.1 km	50 ms	Partially inverted normal fault
Secondary Fault 7 (SF7)	NNE-SSW	300^0-335^0	28.8 km	25 ms	Synthetic fault to the EBF
Secondary Fault 8 (SF8)	NNE-SSW	265^0-310^0	26.0 km	60 ms	Synthetic fault to the EBF
Secondary Fault 9 (SF9)	NNE-SSW	110^0-160^0	10.1 km	60 ms	Antithetic fault to the EBF
Secondary Fault 10 (SF10)	NNE-SSW	120^0-150^0	10.2 km	30 ms	Minor antithetic fault to the EBF forming a mild push-up inversion structure (anticline F17) with SF7.

***Table 4.3**: Summary of main geometrical and structural characteristics of mapped secondary faults. Note that EBF shows a general top-to-the-west displacement and is mentioned due to the use of terms synthetic and antithetic secondary faults. For location of structures, see **Fig. 4.6**.*

This kind of geometrical character is indicative of contractional deformation/inversion and therefore, these faults are interpreted as partially inverted faults. In addition, reverse faults and associated small scale minor folds can be seen in the hanging wall block of SF3. Faults SF5 and SF6 (**Fig. 4.8** and **Fig. 4.9**) are NE-SW striking and NW dipping normal faults with linear map view expression and planar fault plane geometry. The upper stratigraphic tips of SF5 and SF6 are located in lower Miocene and lower Oligocene strata, respectively, while the downdip tips for both faults are located within early Eocene – late Paleocene strata. The hanging wall block of SF6 hosts anticline F13 which is accompanied by small scale blind thrust faults. These structures are indicative of contractional deformation/inversion. This fault exhibits a reversal of slip direction and is interpreted as a partially inverted fault. In the well site, there is a group of several secondary faults

that is developed in a general oblique orientation to the CF (**Fig. 4.6** and **Fig. 4.14**). Fault SF8 is a NNE-SSW striking and NNW dipping synthetic normal fault to the EBF whereas SF9 displays same strike but opposite dip direction (antithetic fault to the EBF). Fold F18 is located between these two faults that act as buttress. Similarly, as shown in **Fig. 4.14**, a few hundred meters to the NW, secondary faults SF7 and SF10 display the exact same structuring with fold F17 located in between. These four secondary faults exhibit a clear upper stratigraphic tip at intra lower Miocene while their downdip termination seems to affect strata of early to middle Eocene age but without affecting the early Eocene horizon. The previous type of structuring with all accompanied geometrical features in footwall and hanging wall blocks is supported by several parallel to subparallel brittle faults forming fault splays and creating an anastomosing map view picture. In addition, the footwall fault block of the CF (and part of Dome 1) is segmented by closely located parallel secondary faults that seem to strike obliquely to the CF (**Fig. 4.3** and **Fig. 4.7**) and affect the same stratigraphic interval as secondary faults SF7 – SF10.
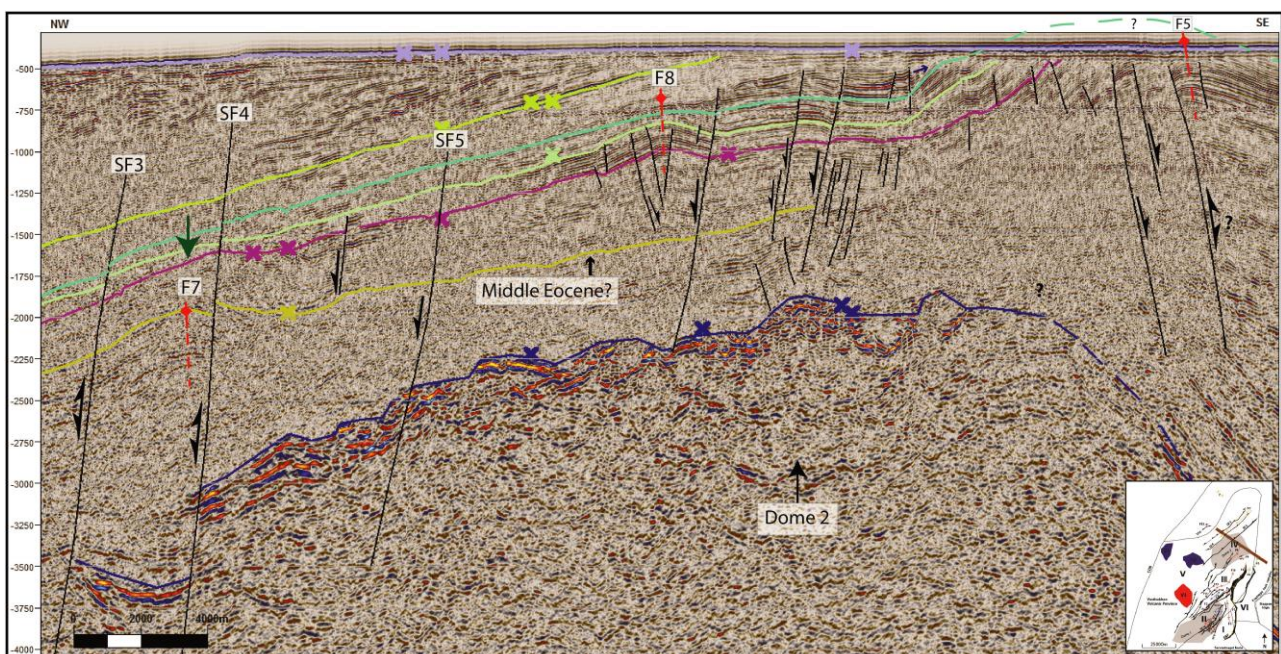

Fig. 4.9: *Interpreted seismic profile of line BV-04-87 showing secondary faults SF3, SF4 and SF5 together with folds F7, F8 and F5 and dome 2 (subarea (IV)). Legend can be found in* **Fig. 4.3**. *See* **Fig. 4.6** *for location of line, structures and subareas and text for detailed description. Vertical axis is given in TWT (ms).*

In summary, secondary normal faults seem to develop mostly at the central and southern part of the study area as branch faults with anastomosing character or isolated character. They affect strata of early Eocene to intra lower Miocene age but rarely cutting the early Eocene horizon (top of volcanic flows) and therefore, they are considered to be decoupled from the basement. They exhibit a general NE-SW to NNE-SSW strike and NW to NNW dip direction. They all display planar fault plane geometry. All of the numbered mapped secondary faults seem to have been involved and played a role at the stage of folding since several of the mapped folds are closely associated with these faults some of which act as buttress.

4.4.2   Folds

There are 18 mapped structures (folds) which record bedding-parallel shortening within the study area (**Fig. 4.6**) and these are mainly anticlines and synclines. In addition, thrust faults occur locally. The geometrical and structural characteristics of folds are summarized in **Table 4.5** whereas their stratigraphic development is shown in **Table 4.4**. Based on structural development and regional extent, folds F1, F2 F3, F7 and F10 are deemed to the most important folds within the study and are described in the following paragraphs. The remaining folds are described thereafter. Structural styles are classified based on geometrical characteristics: (i) inter-limb angle, (ii) axial plane inclination. Plunge is included whenever observed and symmetry of each fold is also mentioned. Fold styles that are identified include: Close and upright anticlines, close and steeply inclined anticlines, open and steeply inclined anticlines, open and upright anticlines, open and steeply inclined synclines, open and upright synclines, gentle and upright synclines and kink-like upright anticlines and synclines. They are grouped into two general categories: (a) upright to steeply inclined close to open anticlines with snakehead (head on) geometries (b) upright or steeply inclined gentle to open synclines.

Fold	Stratigraphic level of tracking	Time span of observed development
Fold 1 (F1)	Intra Lower Miocene	Middle Eocene – Intra Lower Miocene
Fold 2 (F2)	Intra Mid Eocene	Middle Eocene – Intra Lower Miocene
Fold 3 (F3)	Intra Lower Oligocene	Middle Eocene – Intra Lower Miocene
Fold 4 (F4)	Intra Lower Oligocene	Middle Eocene – Middle Oligocene?
Fold 5 (F5)	Middle Eocene?	Middle Eocene – Middle Oligocene?
Fold 6 (F6)	Middle Eocene?	Middle Eocene?
Fold 7 (F7)	Middle Eocene?	Middle Eocene?
Fold 8 (F8)	Intra Lower Oligocene	Southwest part: Oligocene Northeast part: Middle Eocene – Intra Lower Oligocene
Fold 9 (F9)	Intra Lower Oligocene	Oligocene?
Fold 10 (F10)	Intra Lower Oligocene	Middle Eocene –Intra lower Miocene?
Fold 11 (F11)	Intra Mid Eocene	Middle Eocene
Fold 12 (F12)	Intra Mid Eocene	Middle Eocene – Lower Oligocene?
Fold 13 (F13)	Intra Mid Eocene	Middle Eocene
Fold 14 (F14)	Intra Mid Eocene	Middle Eocene – Lower Oligocene?
Fold 15 (F15)	Intra Lower Oligocene	Middle Eocene – Lower Oligocene
Fold 16 (F16)	Intra Lower Oligocene	Middle Eocene – Lower Oligocene
Fold 17 (F17)	Intra Lower Oligocene	Middle Eocene – Lower Oligocene
Fold 18 (F18)	Intra Lower Oligocene	Middle Eocene – Lower Oligocene

Table 4.4*: Stratigraphic level of fold tracking for each structure and stratigraphic interval of observed development. For location of structures, see **Fig. 4.6**. Detailed description of each fold is provided in the text.*

Fold F1

Fold F1 strikes N-S and is a gently south plunging inclined close anticline closely associated with the EBF master fault (**Fig. 4.3**, **Fig. 4.7**, **Fig. 4.8** and **Fig. 4.15**). It runs parallel to the strike of the EBF and

is located in the hanging wall fault block. F1 generally affects strata of middle Eocene to intra lower Miocene age and the cross sectional geometry of this fold has a general symmetrical shape and has an axial plane parallel to the EBF (**Fig. 4.15**). In addition, this fold is locally seen to have been dissected by compressional faults (such as thrust faults). These faults mainly affect the limbs of F1 (**Fig. 4.3**).

Fold	General strike / dip azimuth range of axial planes		Half wavelengh (width)	Amplitude	Classification
Fold 1: Anticline	N-S	250^0 - 325^0	3-4 km	160-580m	Close inclined fold, inclined to upright at central part
Fold 2: Anticline	NE-SW	$325^0 – 360^0$	2-3 km	180 -230m	Close and steeply inclined fold
Fold 3: Syncline - Southern part	N-S	$250^0 – 275^0$	6-7 km	130m	Gentle to open upright fold
Fold 3: Syncline -Northernmost part	N-S	$270^0 – 280^0$	5-6 km	189m	Open and steeply inclined fold
Fold 4: Anticline	N-S	$300^0 –275^0$	3 km	310m	Close and upright fold
Fold 5: Anticline	NNE - SSW	110^0 - 120^0	3-3.5 km	146m	Open and steeply inclined fold
Fold 6: Anticline	N-S	275^0	1.5 km	144m	Close and upright fold
Fold 7: Anticline	NE - SW	125^0-150^0	4-5 km	433m (NE part) – 217m (SW part)	Doubly plunging upright to inclined fold. Close at northeastern part, open at southwestern part
Fold 8: Anticline	NE - SW	125^0 - 150^0	3-4 km	111m	Open and upright fold
Fold 9: Anticline	NE - SW	325^0 - 360^0	3 km	45m	Open and upright fold
Fold 10: Syncline – Northeastern Part	NNE - SSW	$75^0– 125^0$	5-7 km	500m	Open and upright fold
Fold 10 Syncline – Southwestern Part	NE - SW	330^0 - 340^0	6 km	72m	Gentle and upright fold
Fold 11: Anticline	NE-SW	310^0 - 320^0	3 km	31m	Open and steeply inclined fold
Fold 12: Syncline	NE-SW	320^0 - 330^0	5 km	78m	Open and steeply inclined fold
Fold 13: Anticline	ENE - WSW	330^0	2 km	101m	Close and upright fold
Fold 14: Syncline	NE-SW	130^0 - 150^0	1.5-2 km	68m	Open and steeply inclined fold
Fold 15: Anticline	NE-SW	310^0-325^0	2-3 km	46m	Open and steeply inclined fold
Fold 16: Syncline	NE-SW	125^0 and 315^0	1-1.5 km	44m	Kink-like fold (upright)
Fold 17: Anticline	NE-SW	300^0-315^0	2 km	50m	Kink-like fold (upright)
Fold 18: Anticline	NE-SW	125^0	3.5 km	68m	Open and upright fold

Table 4.5: *Summary of main geometrical and structural characteristics and classification of mapped folds. For location of structures, see* **Fig. 4.6***. Detailed description for each fold is provided in text.*

Values for the width of this fold (or half wavelength) range from 3 to 4 km (**Fig. 4.15**) whereas amplitude varies between 160-580m. Maximum amplitude was measured at horizon intra middle Miocene and at the northern part of the fold ½wavelength/amplitude ratio is 5/1 indicating that this area represents the highest amount of shortening recorded (**Fig. 4.15**). Wavelength variations along strike are shown in **Fig. 4.15** and show a stable range of wavelength except for its southern part where it gradually becomes wider. Also, its southern part shows lower ratios indicating less but generally fixed total amount of shortening. Growth relationships are not possible since most of the horizons are absent in the footwall fault block. Toward its northern extension, F1 is found truncated by a more recent geometrical feature that resembles incised valley or canyon/channel infill as shown in **Fig. 4.10**. This fold is interpreted as a buckle fold and its formation is related to the period of reverse reactivation of the EBF master fault. However, there are areas that indicate possible additional mechanisms that affected its formation. These are discussed in chapter 5.

Fold F2

Fold F2 strikes NE-SW and is a NE plunging close anticline with steeply inclined axial plane (**Fig. 4.7**). Similarly with F1, it runs parallel to the CF master fault and is closely associated with it. It develops in the hanging wall block and in the cross sectional view, it exhibits a generally symmetrical shape with its axial plane oriented parallel to subparallel to the fault plane of CF and dips toward NW (**Fig. 4.7** and **Fig. 4.15**). The width (or half wavelength) of this fold varies between 2 to 3 km and its amplitude between 180 to 230 m. Maximum amplitude was measured at horizon intra middle Eocene and ½wavelength/amplitude ratios range between 10/1 and 16/1 indicating a generally stable degree of shortening without high deviations. Its northeastern continuation is found to be unclear and the fold either terminates in the area of linkage of the EBF with the CF or it continues to the NNE along the EBF. Half-wavelength variations along strike are shown in **Fig. 4.15** displaying an overall constant half wavelength along its strike apart from its southwestern part which becomes gradually wider. This fold, as in the case of F1, is interpreted as a buckle fold and its formation is related to the period of reversal of slip direction of the CF master fault. In chapter 5 there is an extended discussion on folding mechanisms.

Fold F3

Fold F3 strikes N-S and is a gentle to open upright syncline mainly developed in subarea (I) (**Fig. 4.6**). It generally affects strata of middle Eocene – intra Lower Miocene age. In cross sectional view, it has a basinal geometry with widths in the order of 7km and amplitudes of 170-180 meters (**Fig. 4.3**, **Fig. 4.7** and **Fig. 4.15**). Half-wavelength variations show a general tightening of the fold towards north indicating increased shortening. Its northern continuation becomes unclear at the area of linkage of the two master faults. Despite the fact that it is located relatively far (approx. 3-4 km) from the EBF it seems that the axial trace follows the strike of the EBF and mimics its sigmoid trace (**Fig. 4.15**). In addition at the northern part, the axial plane starts dipping towards east in contrast with the fault plane of the EBF. This syncline is interpreted as mildly inverted depocenter.
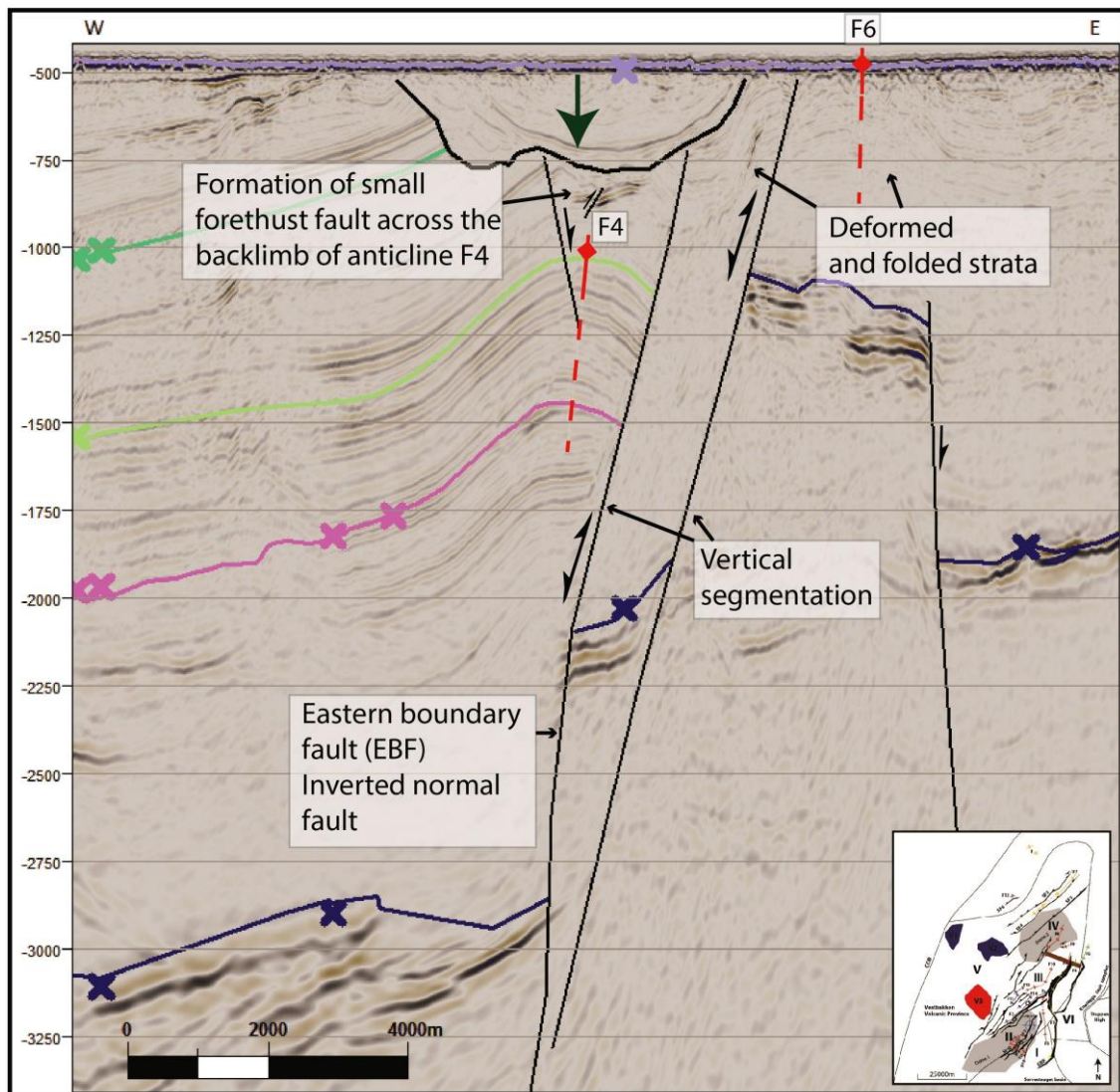
*Fig. 4.10: Interpreted seismic profile showing vertical segmentation of the displacement of the eastern boundary fault, formation of fold F4 in the hanging wall fault block and of fold F6 in the footwall fault block accompanied by highly deformed and folded strata. Legend can be found in **Fig. 4.3**. See **Fig. 4.6** for location of line and structures and text for detailed description. Vertical axis is given in TWT (ms). Data courtesy of TGS and Spectrum.*

Fold F7

Fold F7 is located at the hanging wall fault block of SF4 as shown in **Fig. 4.6**. It is a doubly plunging fold and comprises two parts since its central lateral continuation was untraceable. At the northeastern part (**Fig. 4.12**), it is expressed as a NE-SW striking and SW plunging inclined close anticline and runs parallel to the SF4. In cross sectional view, it has a general asymmetric shape and its axial plane dips toward SE, in contrast with the fault plane of SF4. At its southwestern part (**Fig. 4.9**), it is expressed as a NE-SW striking and NE plunging upright open anticline. This configuration shows that the amount of shortening is higher at the northeastern part of F7 with a lower half wavelength/amplitude ratio in comparison with the southeastern part (**Fig. 4.17**). This fold is interpreted as a buckle fold.
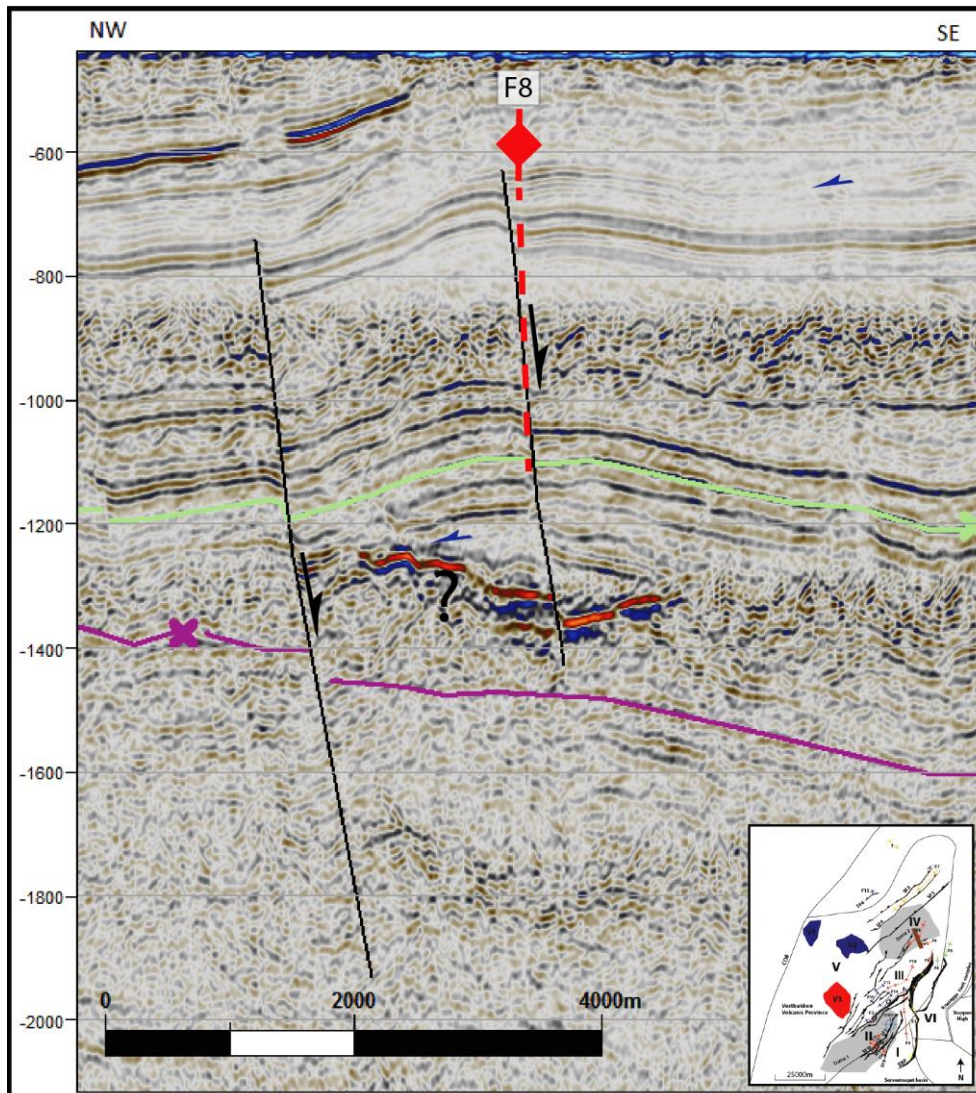
Fig. 4.11: *Interpreted seismic profile of line showing a minor normal fault bisecting fold F8. Note the formation of a small scale anticline in the footwall block of the minor fault. Blue arrows represent downlaps. Legend can be found in **Fig. 4.3**. See **Fig. 4.6** for location of line and structures and text for detailed description. Vertical axis is given in TWT (ms). Data courtesy of TGS and Spectrum.*

Fold F10

Fold F10 is a doubly plunging fold and is divided into two parts that both develop within subarea (III) (**Fig. 4.6**). The northern part is a SSW plunging and NNE - SSW oriented open upright syncline. It affects strata of middle Eocene to intra lower Miocene age. The cross sectional geometry of this fold (**Fig. 4.8**) has a generally asymmetrical shape and has an axial plane that slightly dips toward ESE in contrast with the fault plane of EBF (**Fig. 4.16**). However, it displays a reversal at the southern part (as displayed in **Fig. 4.16**) where it gradually starts dipping towards WNW. Typical values for the width of this fold (or half wavelength) range from 5 to 7 km (**Fig. 4.16**). The southern part of this fold (**Fig. 4.15**) is a NE plunging and NE-SW striking gentle upright syncline. The axial plane dips towards NW. This fold is interpreted as a partially inverted depocenter.
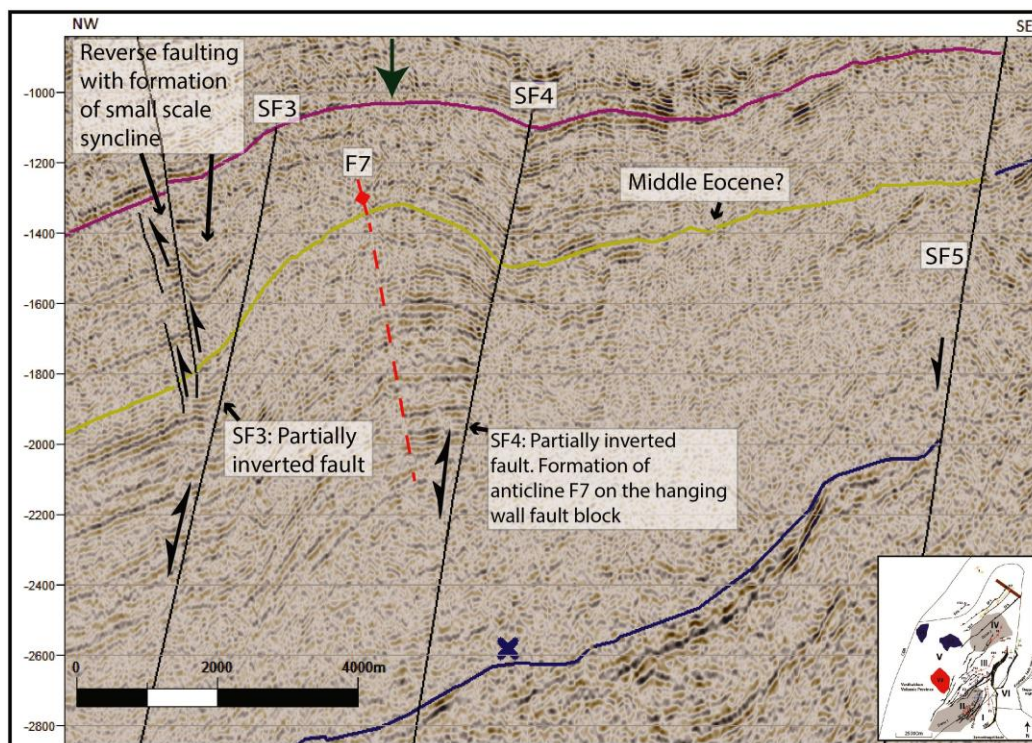
Fig. 4.12: *Interpreted seismic profile of line BV-12-86 showing folds F7 in the hanging wall of the secondary partially inverted fault SF4. Green arrow shows cogent evidence for the characterization of this fault. In the hanging wall of SF3 one can observe reverse faults and minor folds which suggest mild reactivation of SF3 in a reverse sense. Legend can be found in *Fig. 4.3*. See *Fig. 4.6* for location of line and structures and text for detailed description. Vertical axis is given in TWT (ms).*
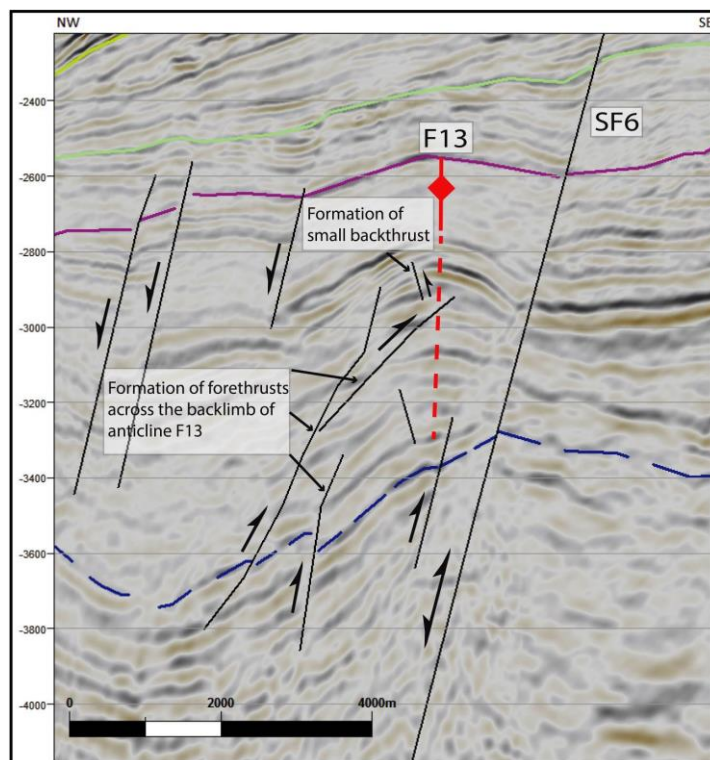
Fig. 4.13: *Detailed interpretation of the northwestern part (black rectangle) of seismic profile in *Fig. 4.8* showing thrusting across the backlimb of fold F13 in the hanging wall of the partially inverted secondary normal fault SF6. Legend can be found in *Fig. 4.3*. Vertical axis is given in TWT (ms). Data courtesy of TGS and Spectrum.*

Other folds

Fold F4

Fold F4 is a N-S oriented and upright close anticline, which is closely related to the EBF master fault (**Fig. 4.6** and **Fig. 4.10**). As mentioned above, fold F1 is truncated at this particular area and F4 essentially constitutes its continuation (dashed line in **Fig. 4.6**) to the north but at different stratigraphic levels (middle Eocene - intra lower Oligocene interval). The half wavelength/amplitude ratio recorded is 10/1 and shows relatively high amount of shortening for the study area (**Fig. 4.16**). Typical value for the width of this fold is 3 km whereas amplitude is 310m. This fold is interpreted to be a result of buckling associated with a period of reverse reactivation of the EBF master fault.
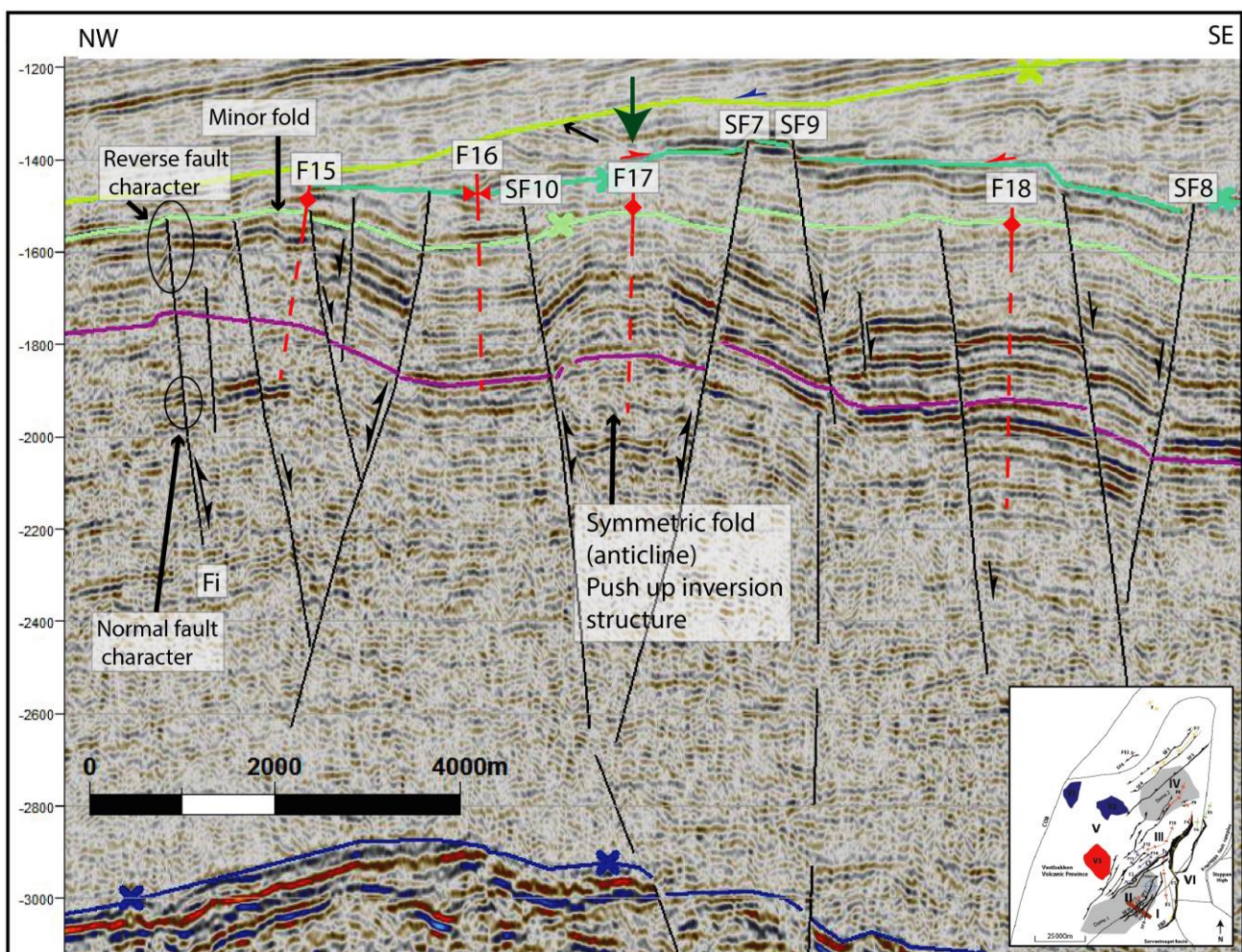

Fig. 4.14: Interpreted seismic profile of line (GBW-88-054) showing a series of folds, the formation of which is strictly controlled by secondary faults. Downlaps are shown with blue arrows, onlaps with red, and truncations with black arrows. Green arrow indicates reasoning for characterizing SF7 and SF10 faults as partially inverted normal faults, based on a push up inversion structure marked as fold F17. Fi fault shows both normal and reverse character, and hence, is interpreted similarly. Legend can be found in **Fig. 4.3**. See **Fig. 4.6** for location of line and structures and text for detailed description. Vertical axis is given in TWT (ms).

Fold F5

This fold is a NNE-SSW oriented and steeply inclined open anticline with its axial plane dipping toward WNW (**Fig. 4.6** and **Fig. 4.9**) and is associated with a SE dipping normal fault. It is considered to affect strata of middle Eocene to middle Oligocene age. The half wavelength/amplitude ratio of this fold is 21/1 whereas typical values for the width and amplitude are 3.5km and 146m, respectively (**Fig. 4.16**).

Fold F6

This locally developed fold is located 3 kilometers to the SW in relation to fold F5, at the footwall fault block of the EBF (Subarea (VI), **Fig. 4.6**) and is a N-S oriented upright close anticline (**Fig. 4.10**). It is considered to affect strata of middle Eocene age. The half wavelength/amplitude ratio of this fold is 13/1 showing relatively high degree of shortening for the case of this study area (**Fig. 4.16**). Typical values for the width and amplitude are 1.5km and 144m, respectively. Adjacent to this fold, strata are highly deformed and more folds can be observed. These folds are locally developed and are untraceable from line to line.

Fold F8

This fold (**Fig. 4.6**) was divided into NE part (**Fig. 4.9**) and SW part (**Fig. 4.11**) since its continuation was unclear. However, both parts display similar geometrical characteristics and fault relations. Fold F8 is interpreted as NE-SW oriented and open and upright anticline. The half wavelength/amplitude ratio is 25/1 and typical values of fold width and amplitude are 3.5km and 111m, respectively.

Fold F9

This is a locally developed fold (**Fig. 4.6** and **Fig. 4.16**) and is interpreted as a NE-SW oriented and open and upright anticline. It affects Oligocene strata and its half wavelength/amplitude ratio is 60/1 indicating relatively low amount of shortening. Typical values of fold width and amplitude are 3km and 45m, respectively.

Folds F11, F12 and F14

These folds are located at the distal part of the hanging wall fault block of the CF master fault (**Fig. 4.6** and **Fig. 4.7**) and are all NE-SW oriented folds. Fold **F11** is an open and steeply inclined fold with its axial plane dipping toward NW. It mainly affects middle Eocene strata with typical values of fold width and amplitude as 3km and 31m, respectively (**Fig. 4.15**). The half wavelength/amplitude ratio is 96/1 indicating low amount of shortening. Fold **F12** is interpreted as an open and steeply inclined syncline with its axial plane dipping toward NW. It affects strata of middle Eocene to lower

Oligocene age and its half wavelength/amplitude ratio is 71/1 indicating relatively low amount of shortening. Typical values of fold width and amplitude are 5km and 78m, respectively. Fold **F14** is an open and steeply inclined syncline (**Fig. 4.7**) with its axial plane dipping toward SE. It mainly affects middle Eocene to lower Oligocene strata and its half wavelength/amplitude ratio is 38/1 indicating moderate amount of shortening. Typical values of fold width and amplitude are 2km and 68m, respectively (**Fig. 4.15**).
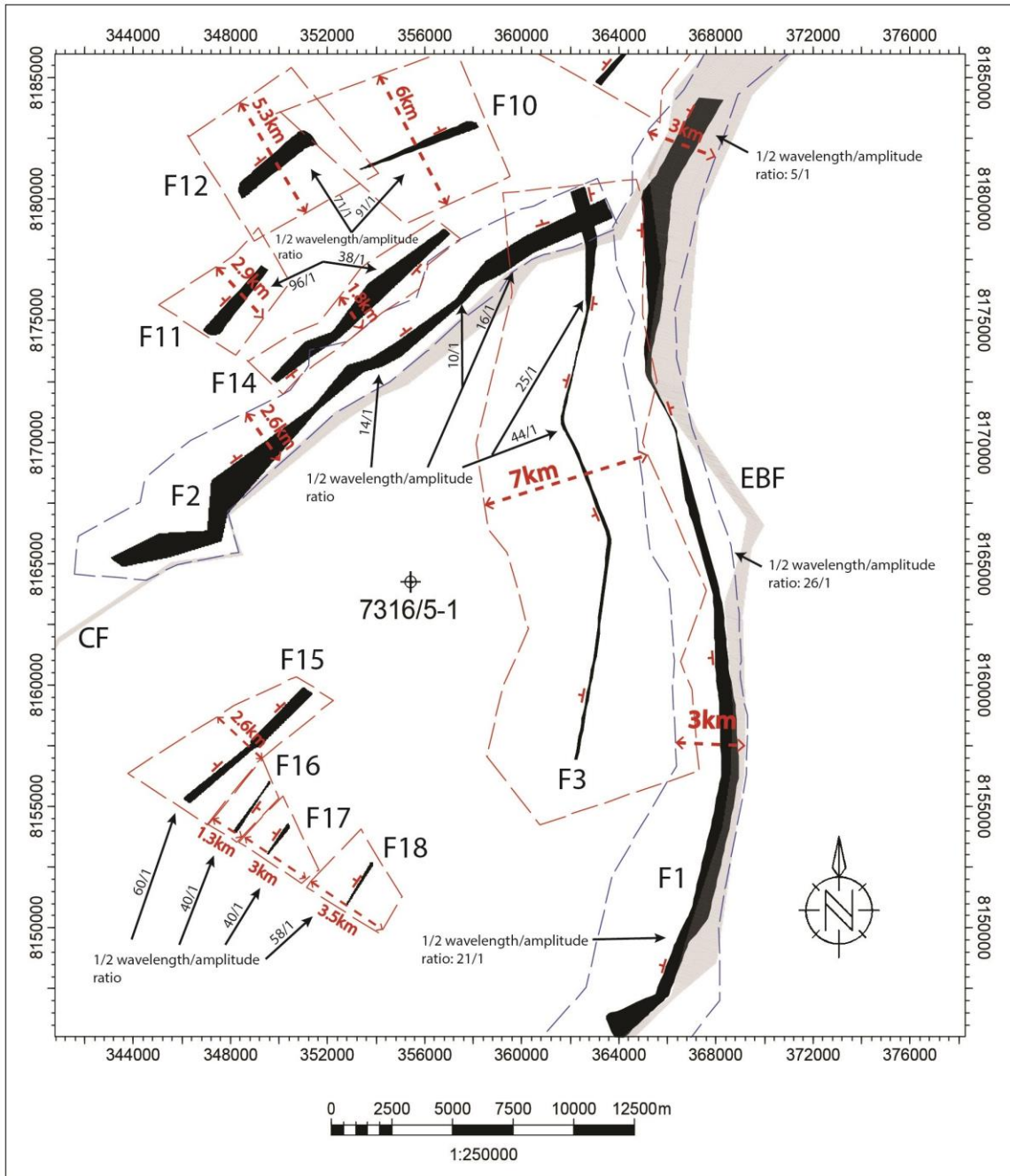
Fig. 4.15*: This map illustates the half-wavelength (or fold width between inflection points) – axial plane relationship of folds and gives a sense of their geometric spatial development showing their along-axis variations in wavelength and relations with master faults EBF and CF. In addition, half-wavelength/amplitude ratios are shown for making comparisons among folds (or along the same fold) in terms of shortening. Light grey color: master faults, Black color: axial planes, Red symbols: dip azimuth of axial planes, Dashed lines: wavelength (Note that different colors are used just for avoiding confusion among wavelegths). Ratios were calculated in lines oriented approximately NW-SE. See **Fig. 4.6** for location.*
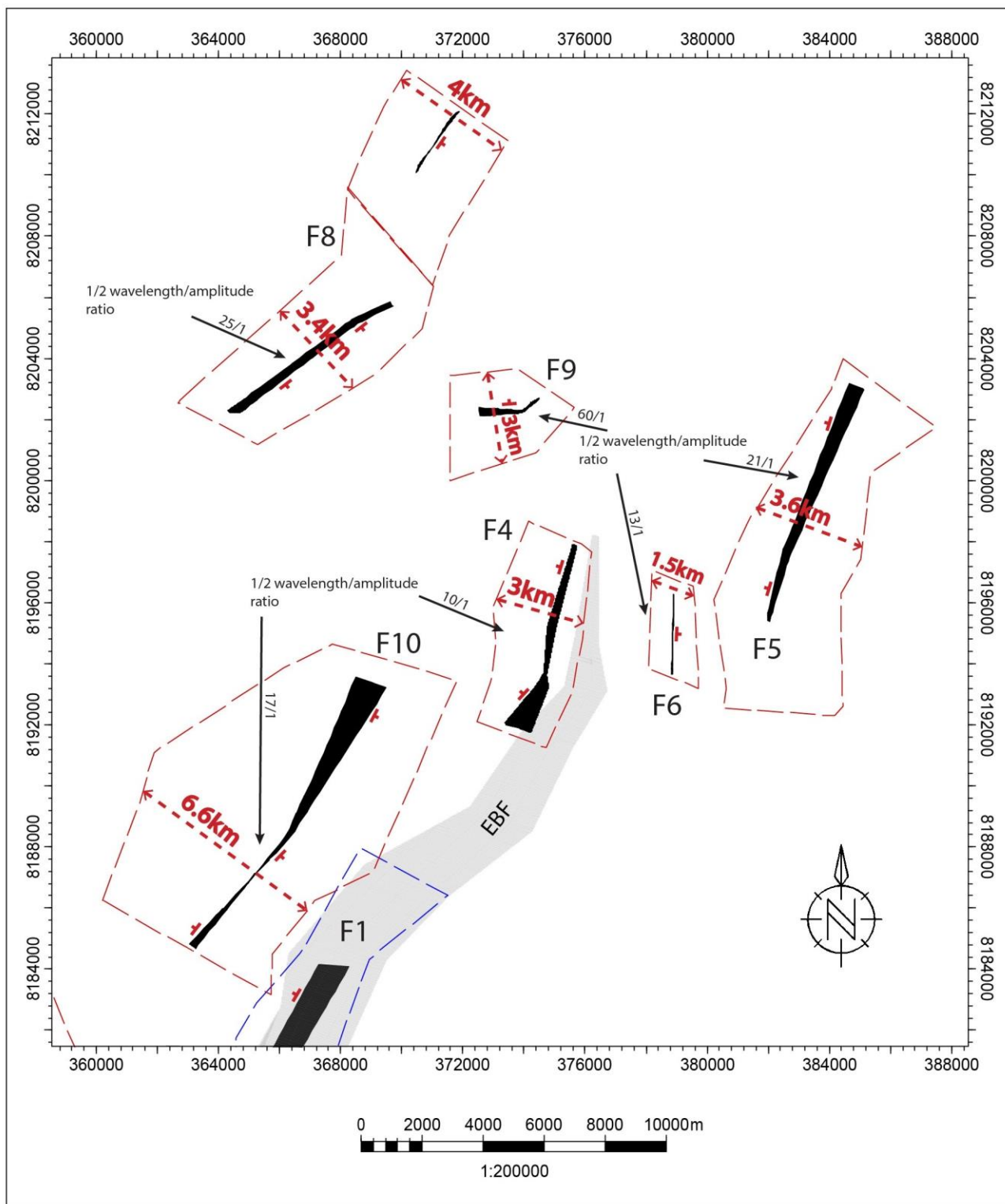
Fig. 4.16*: This map illustates the half-wavelength (or fold width between inflection points) – axial plane relationship of folds and gives a sense of their geometric spatial development showing their along-axis variations in wavelength and relations with master fault EBF. In addition, half-wavelength/amplitude ratios are shown for making comparisons among folds (or along the same fold) in terms of shortening. Light grey color: master fault EBF, Black color: axial planes, Red symbols: dip azimuth of axial planes, Dashed lines: wanelength (Note that different colors are used just for avoiding confusion among wavelegths). Ratios were calculated in lines oriented approximately NW-SE. See **Fig. 4.6** for location.*

47

Fold F13

This is a locally developed fold located at the northern part of the study area as shown in map of **Fig. 4.6**. It is an ENE-WSW oriented upright close anticline (**Fig. 4.13**) located in the hanging wall fault block of secondary fault SF6. The back-limb of this fold is dissected by thrust faults. It affects strata of middle Eocene to lower Oligocene age. The half wavelength/amplitude ratio of this fold is 19/1 showing relatively moderate degree of shortening for the case of this area. Typical values for the fold width and amplitude are 2km and 101m, respectively. This fold is interpreted as a fault propagation fold.
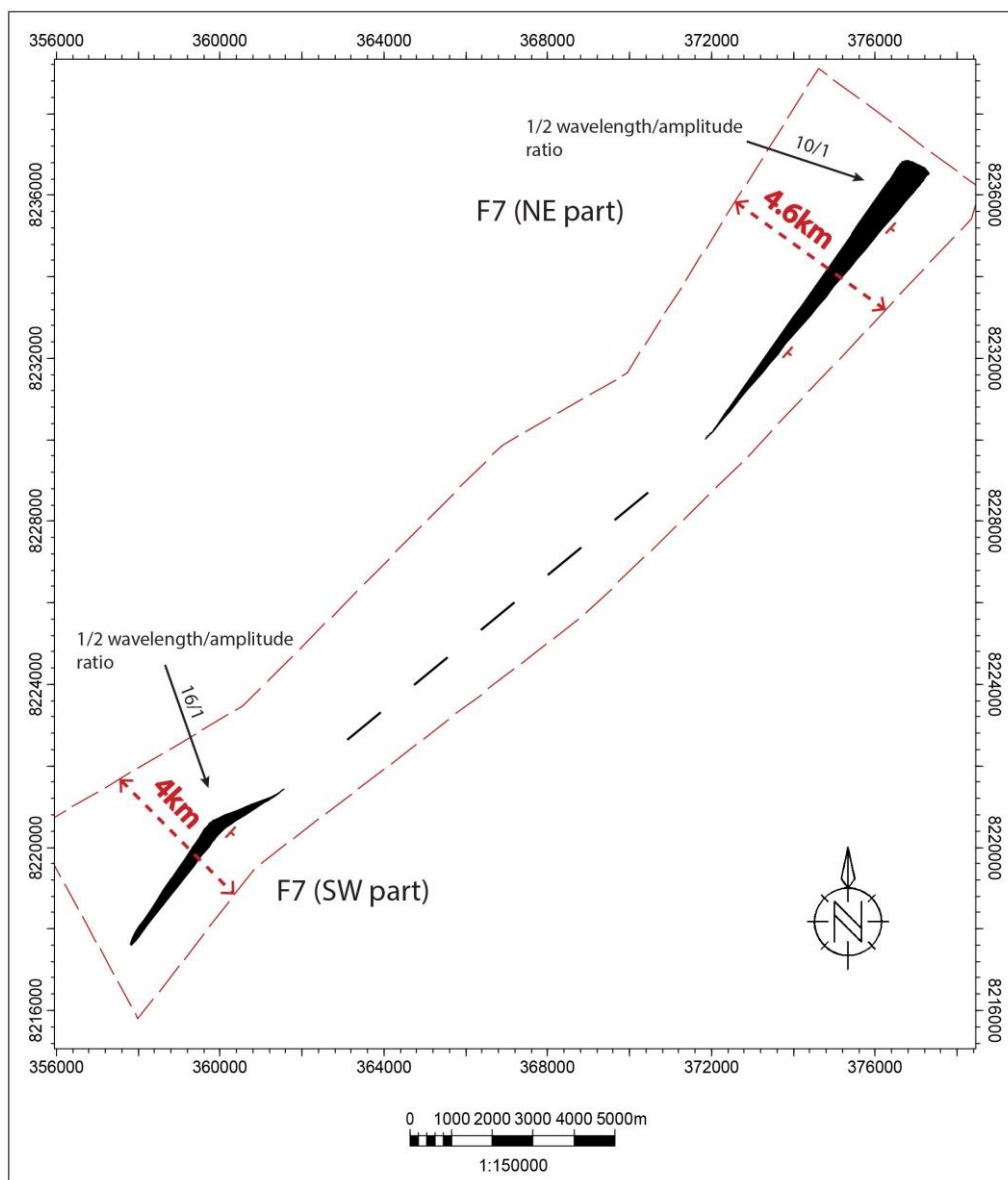

Fig. 4.17: *This map illustates the half-wavelength (or fold width between inflection points) – axial plane relationship of folds and gives a sense of their geometric spatial development showing their along-axis variations in wavelength. In addition, half-wavelength/amplitude ratios are shown for making comparisons among folds (or along the same fold) in terms of shortening. Black color: axial planes, Red dashed lines: wanelength, Black dashed line: assumable fold continuation. Ratios were calculated in lines oriented approximately NW-SE. See **Fig. 4.6** for location.*

__Folds F15, F16, F17 and F18__

These folds are developed at the southern part of the study area and are laterally restricted within areas that are mainly controlled by faulting (secondary faults SF7, SF8, SF9 and SF10), (**Fig. 4.6**, **Fig. 4.14** and **Fig. 4.15**). All of these folds are NE-SW oriented. Fold **F15** is an open steeply inclined anticline with its axial plane dipping toward NW. Minor folding and reverse faulting (fault Fi, **Fig. 4.14**) affect the limbs of this anticline. Typical values of width and amplitude for this fold are 2.5km and 46m, respectively. The half wavelength/amplitude ratio is 60/1 showing a relatively moderate to low amount of shortening. Fold **F16** is interpreted as an upright kink-like syncline. Typical values of width and amplitude are 1-1.5km and 44m, respectively. The half wavelength/amplitude ratio is 40/1 indicating relatively moderate amount of shortening. Fold **F17** is interpreted as a relatively asymmetric upright kink-like anticline expressed as a push-up (or pop-up) inversion structure between conjugate secondary faults SF7 and SF10 (**Fig. 4.14**). Typical values of width and amplitude are 2km and 50m, respectively. The half wavelength/amplitude ratio is 40/1 indicating relatively moderate amount of shortening. Fold **F18** is an open and upright anticline. Typical values of width and amplitude are 3.5km and 68m, respectively. The half wavelength/amplitude ratio is 58/1 indicating relatively moderate to low amount of shortening.

__Timing of inversion and folding__

Deformation is by principle younger than the age of the younger layer affected. The analysis of the cross-sectional view of several lines shows consistency on key observations such as onlaps and pinch out-geometries that provide time constraints on the initiation of fold growth and reverse reactivation of pre-existing faults. Two examples of seismic profiles are illustrated and show onlaps (red arrows) of Miocene strata onto the limb of folds (**Fig. 4.18** and **Fig. 4.19**). **Fig. 4.18** is located in subarea (III) and shows a red-colored area which represents the Miocene unit with stratal onlaps onto the backlimb of fold F1 near the eastern boundary fault. Pinch-out geometry is also observed (black double-arrows) and together with onlaps they indicate syn-growth sedimentation. This unit is truncated by the base Pliocene unconformity and this is evident in the entire area. Hence, the timing of the termination of fold growth remains controversial.

Fig. 4.19 shows similar configuration and concerns fold F2 which is related to the central fault. This profile is located in subarea (III) but to the SW of the previous seismic line. Early Miocene stratal onlaps (red-colored unit) onto the backlimb of fold F2 seem to migrate towards the hinge of the fold. Pinch-out geometry can also be observed. The Miocene unit, in this case, is observed truncated by the intra upper Pliocene unconformity. A discussion on the timing of folding and fold growth is extended in chapter 5.
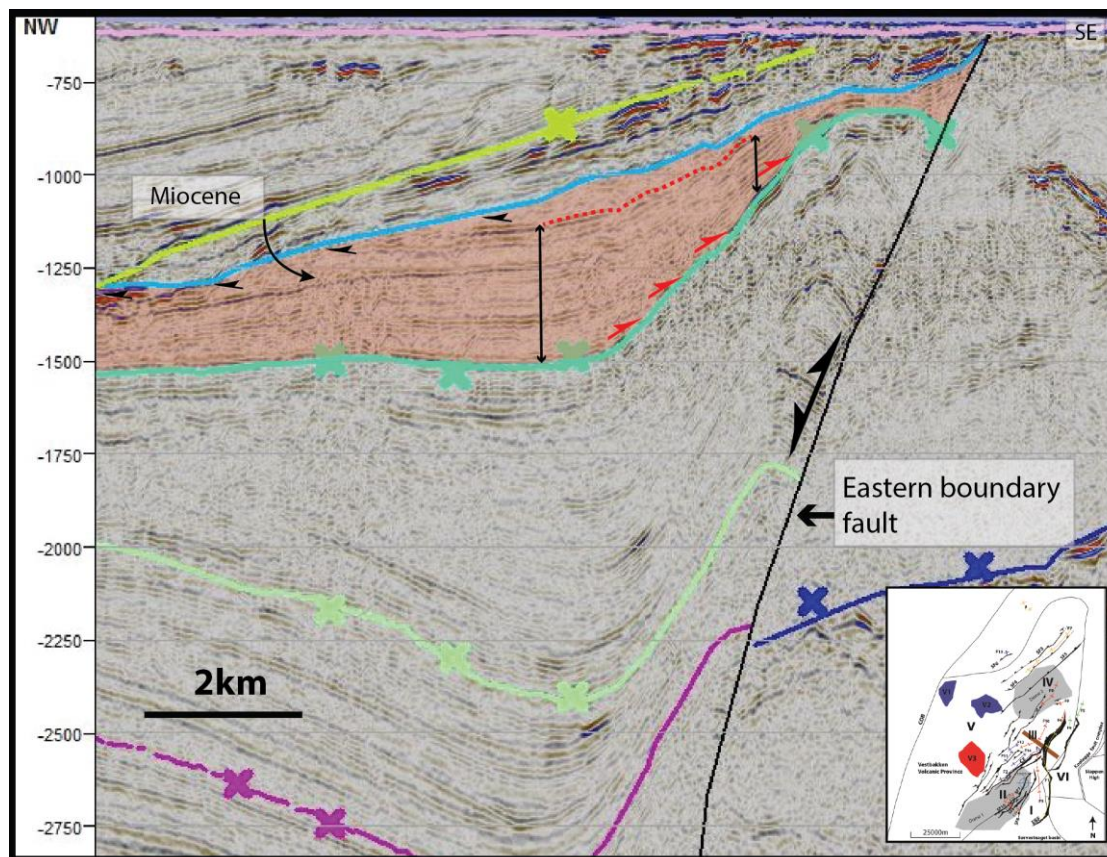
Fig. 4.18: Interpreted seismic profile of line BV-10-86 showing onlaps onto the intra lower Miocene horizon and pinch-out geometry as indicated with black arrows. Red-colored area represents strata of Miocene age. See *Fig. 4.6* for location of line and structures and text for detailed description. Vertical axis is given in TWT (ms).
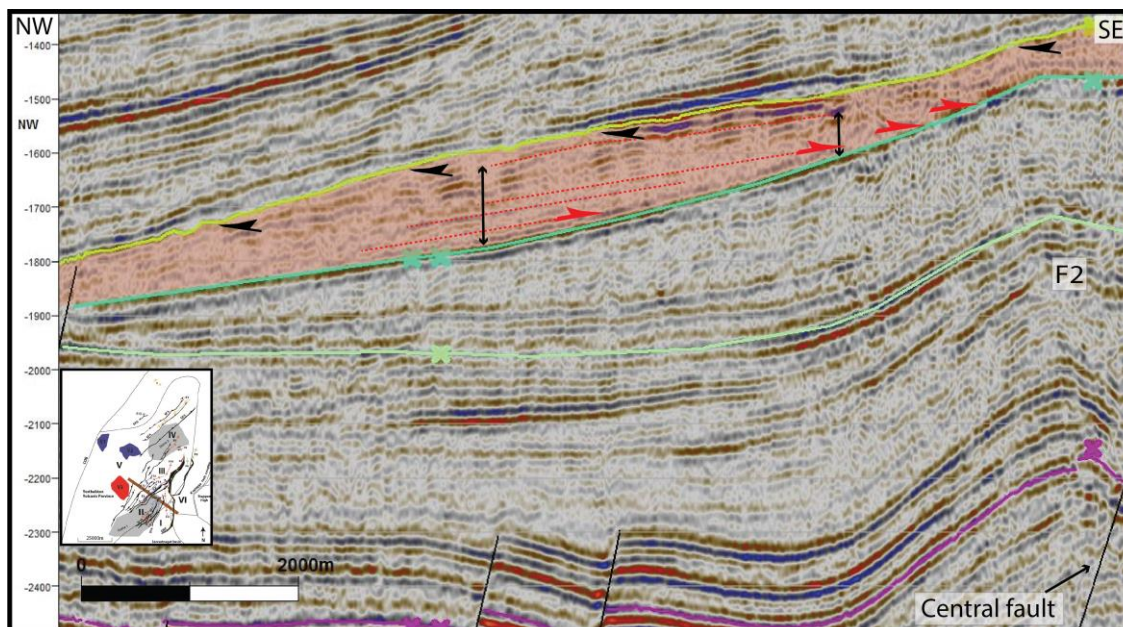

Fig. 4.19: Part of the Interpreted seismic profile of line BV-10-86 (in *Fig. 4.7*) showing onlaps onto the intra lower Miocene horizon and pinch-out geometry as indicated with black arrows. Red-colored area represents strata of Miocene age. See *Fig. 4.6* for location of line and structures and text for detailed description. Vertical axis is given in TWT (ms).

In summary

There are several contractional structures mapped in the study area. These include: a) upright to steeply inclined close to open anticlines (**Fig. 4.6**, e.g. folds: F1, F2, F4, F7 and F13) that are typically present in the hanging wall fault blocks and have wavelengths in the order of 2.5 to 4.5 kilometers, and amplitudes of several hundred meters. Usually, they appear with snakehead (head on) geometries and are interpreted as buckle folds, b) upright or steeply inclined gentle to open synclines that are interpreted as partly inverted hanging wall synclinal depocentres with wavelengths in the order of 5 to 7 kilometers (**Fig. 4.6**, e.g. folds: F3, F10, F12 and F14) and amplitudes of several tens of meters to several hundred meters. In comparison with the first category (a) which is described above, synclines generally display lower amounts of shortening. The dominant orientation of all these structures is NE-SW and most of the times they are closely associated with faults and run parallel to their strike (fault-related folds). Subarea (III) (**Fig. 4.1**) exhibits the highest amount of shortening within the study area expressed with an anticline-syncline pair (F1-F4 with F10) adjacent to the EBF and partly the CF master faults. Onlaps and pinch-out geometries show that fold growth commenced in early Miocene.

4.5   Volcanoes

There are 3 volcanoes in the Vestbakken Volcanic Province (Faleide et al., 1988; Jebsen, 1998). Their position is shown in map of **Fig. 4.6**. Volcano V3 (**Fig. 4.21**) is of early Eocene age since the intra middle Eocene horizon drapes the structure suggesting earlier cessation of volcanism for this volcano. However, volcanoes V1 and V2 (**Fig. 4.20**) seem to have been active for some period in Oligocene and lava flows can be observed above the intra lower Oligocene horizon which onlaps on the eastern flank of the volcano V2. Volcanoes V1 and V2 can now be found buried with mainly Plio-Pleistocene sediments as overburden load.
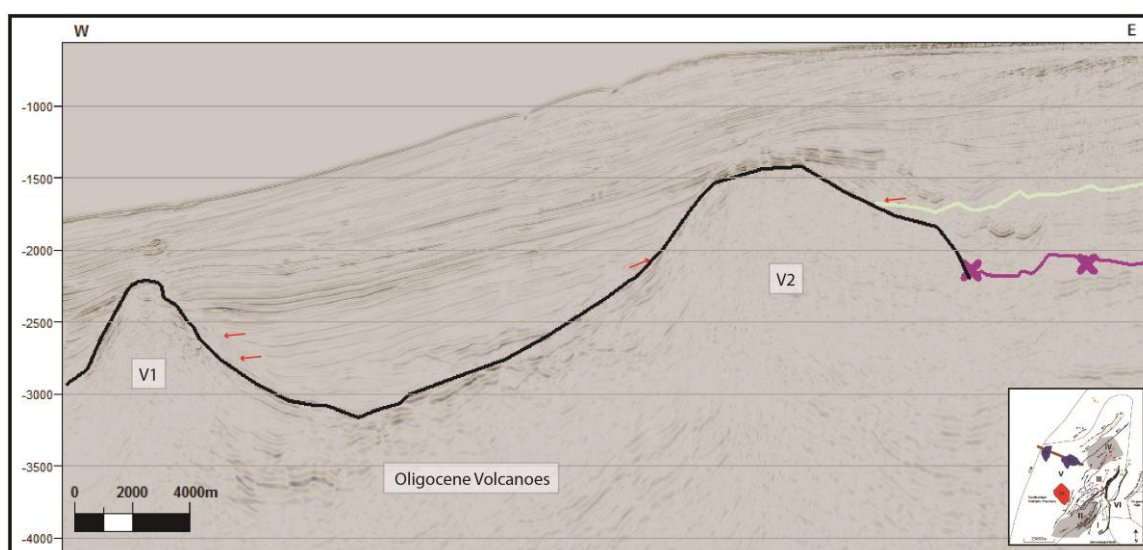

Fig. 4.20: *Seismic profile showing 2 Oligocene Volcanoes within the Vestbakken Volcanic Province. See **Fig. 4.6** for location. Vertical axis is given in TWT (ms). Data courtesy of TGS and Spectrum.*

According to Mørk & Duncan (1993) and their analysis of a shallow drill core of the scientific well 7316/3-U-1 there was an event of basaltic volcanism on the western Barents Margin in Late Pliocene time. They suggested that the volcanic eruption occurred at the continental side of the continent-ocean transition zone and that it was subaquatic in nature but also possibly including subaerial phases. Therefore, three volcanic events have been identified for the Vestbakken Volcanic Province (Faleide et al., 1988; Jebsen, 1998; Mørk & Duncan, 1993).
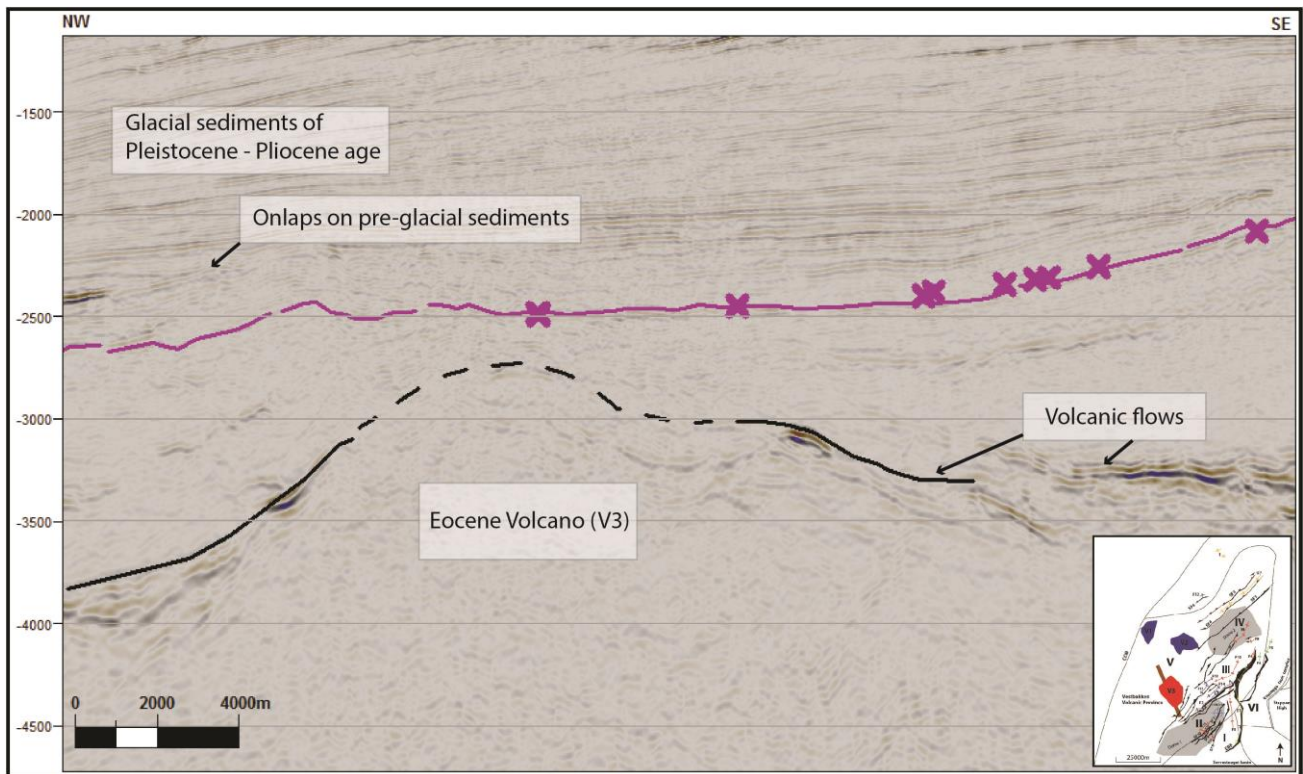

Fig. 4.21: *Seismic profile showing the early Eocene Volcano within the Vestbakken Volcanic Province. See **Fig. 4.6** for location and text for description. Vertical axis is given in TWT (ms). Data courtesy of TGS and Spectrum.*

Chapter 5

5   Discussion

This chapter concerns a discussion on structural styles and their relation to the regional tectonic setting based on an integrated approach which uses results presented in the previous chapter including: 2D interpreted key seismic lines, structural maps, time maps and special maps which focus on the geometrical and spatial relations among faults and folds. Conceptual models and literature-based information related to the study area and the regional setting are presented and correlated with key observations of this work. More specifically, the subjects involved in this chapter can be presented as follows:

- Geometry of faults and folds and their relation to inversion tectonics
- Strike-slip kinematics
- Fault kinematics
- Growth of folds and timing constraints
- Folding mechanisms
- Contractional folding in relation to the regional tectonic setting
- A modern example of similar tectonic setting

Table 5.1 includes all abbreviations used in this chapter and presents the legend which applies for all interpreted seismic lines presented in map of **Fig. 5.1**.

Abbreviation	Full name
CF	Central Fault
COB	Continent Ocean Boundary
EBF	Eastern Boundary Fault
F1-F18	Folds 1 – 18
FM	Formation
GP	Group
HARs	High Amplitude Reflections
KFC	Knølegga Fault Complex
SF1-SF10	Secondary Faults 1 – 10
VVP	Vestbakken Volcanic Province
V1-V3	Volcanoes 1 – 3

Sea Bottom Reflection

Intra Pleistocene

Base Pleistocene

Intra Upper Pliocene?

Intra Middle Eocene

Early Eocene
Top of Volcanic flows

Partially inverted normal faults

Axial plane of folds

Truncations   Downlaps

Base Pliocene
unconformity?

Intra Lower Miocene

Intra Lower Oligocene

Base Oligocene

Relative motion along
fault planes

Anticline

Syncline

Onlaps

Table 5.1: *All abbreviations used in this chapter are included in the table. Legend applies for all interpreted seismic profiles.*
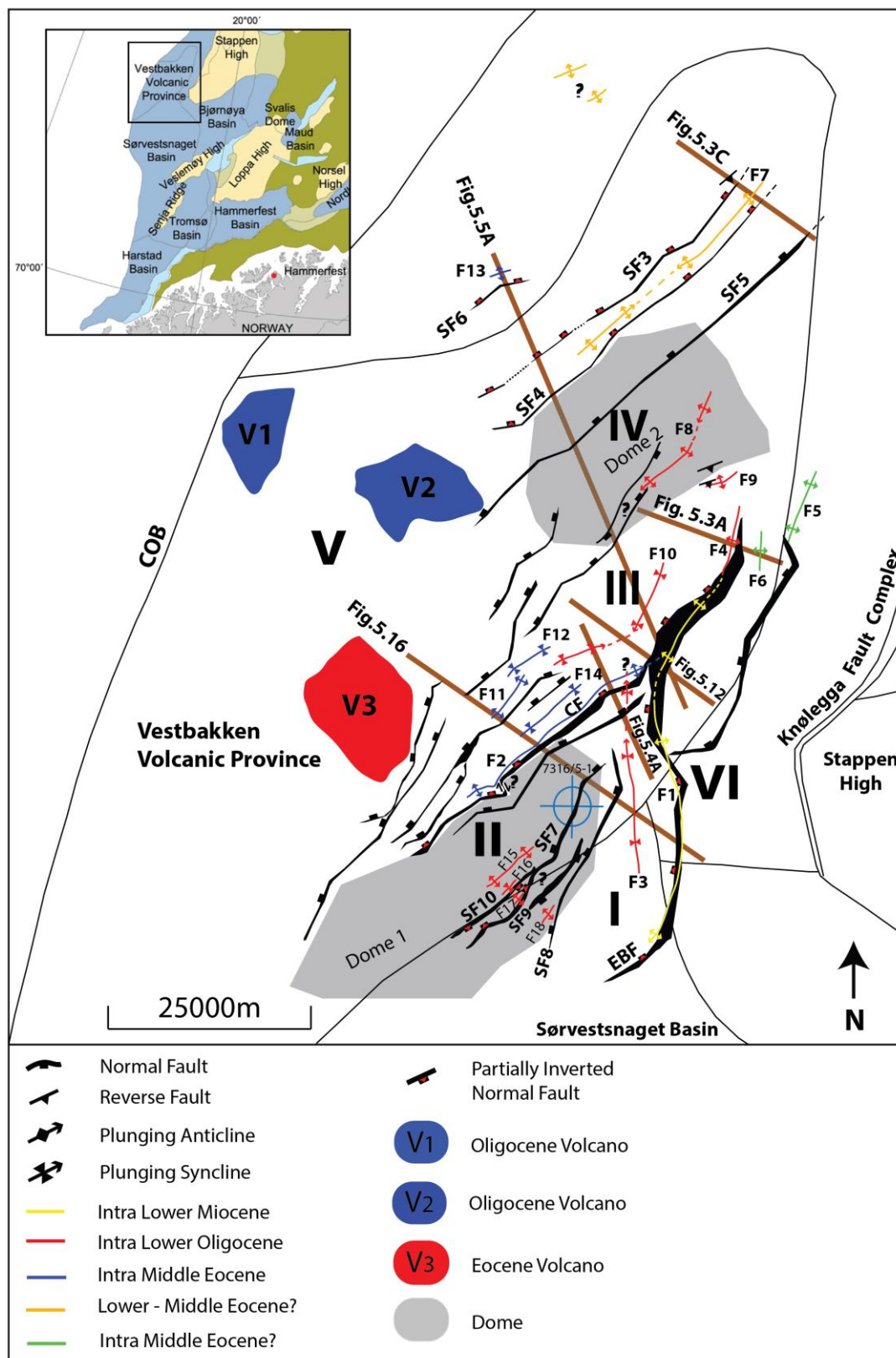
Fig. 5.1: *Structural map of the study area in VVP showing mapped structural elements. Inset (upper left corner) shows the position of the study area in SW Barents Sea (modified from Henriksen et al., 2011). All fault and fold abbreviations are shown in the list of abbreviations in **Table 5.1**. Subareas described in chapter 4.1 are shown with their corresponding Latin numbers I, II, III, IV, V and VI.*

5.1 Geometry of faults and folds – observations and inferences

5.1.1 Inversion

Several contractional structures and fold types have been identified in the study area (**Fig. 5.1**) and are related to inversion tectonics. These are discussed in the following paragraphs. Tectonic inversion is defined as the reactivation of pre-existing faults by a reversal of slip direction on the faults (e.g. Cooper et al., 1989; Van & Marshak. 2004). The main causes of inversion include: regional temporal variations in regional stress patterns, changes in plate boundary configurations and in relative plate motion (e.g. Williams 1989; Dewey 1989). Local inversion can also be observed in strike slip pull-apart basins. Inversion structures within a basin can be observed regionally or locally depending on the stress regime. These structures can be identified by several characteristics. Key geometric characteristics of mapped structures can provide diagnostic criteria for identifying inversion structures (e.g. Cooper et al., 1989; Cooper & Warren 2010; Turner & Williams 2004). Their geometry is highly dependent on the geometry of the original fault system (Cooper & Warren 2010). Cooper et al., (1989) defined tectonic inversion through an approach that relies on the concept of regional elevation (**Fig. 5.2a** and **Fig. 5.2b**.).
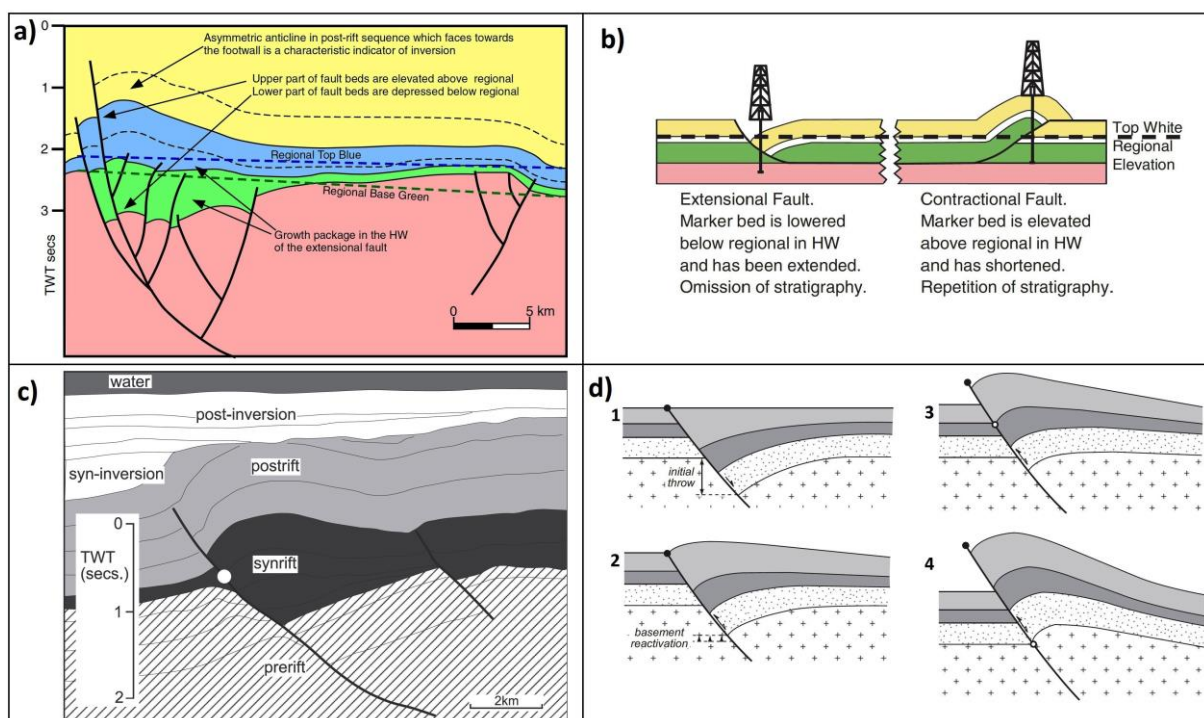

Fig. 5.2*: **(a) – (b)** Key geometric characteristics of an inversion structure incorporating the concept of regional elevation for discriminating between extensional and contractional faults (modified from Cooper & Warren 2010 after Uliana et al., 1995); **(c)** Typical inversion geometry in an inverted half-graben with emphasis on showing the pre-rift, and syn-rift sequences as well as the syn-inversion (onlaps on anticline) and the post inversion sequences (modified from Turner & Williams 2004 after Goudswaard and Jenyon 1988); **(d)** Structural geometries associated with (1) non-inverted rift basin, (2) mildly-inverted rift basin, (3) a moderately-inverted rift basin and (4) a strongly-inverted rift basin (modified from Jackson et al., 2013 after Song 1997).*

Deformation due to compression will elevate strata above regional elevation and extension will lower them. Williams et al., (1989) described the null point and its recognition on inverted normal faults. The change-over point (layers expressed at regional in the hanging wall) marks the null point (e.g. white dots in **Fig. 5.2c** and **Fig. 5.2d**) which is considered to be a diagnostic criterion that can be applied on inverted extensional faults.

However, when taking into account the extension to shortening ratios, erosion effects and tilting events within the Vestbakken Volcanic Province, it becomes obvious that null points and regional reference stratigraphic levels cannot easily be defined and detected for the master faults. In the case of the eastern boundary fault (**Fig. 5.12**, also, **Fig. 4.3** and **Fig. 4.8**) it seems that extension has dominated over later contraction and reference horizons have not been brought back to the null-position (neutral). Additionally, footwall fault block horizons are absent and stratigraphic correlations are impossible. In the case of the central fault (e.g. **Fig. 5.16**), extension has also dominated over contraction resulting to similar configuration.

The null point criterion can be applied occasionally, for example in the cases of folds F7 (**Fig. 4.14**) and F13 (**Fig. 4.15**). However, there is evidence of extensional reactivations of faults in the Vestbakken Volcanic Province (e.g. EBF and CF cutting intra Pliocene strata, Pliocene Volcanism) after the compressional phase which further increases the difficulty and complexity on accurately defining the null point.

Other diagnostic criteria for identifying reverse reactivation of normal faults and inversion structures include:

1. ### *The formation of folds known as 'snakehead structures' formed by reverse reactivation of faults, forced folds and buckle folds*

Typical examples of snakehead geometries can be seen in **Fig. 5.3A**, **Fig. 5.3C** and **Fig. 5.16** (see also **Fig. 4.3**) as folds (F1 and F2) adjacent to master faults EBF and CF. These geometries are indicative of inversion and are always fault-related. These are primarily buckle folds (see sketch **Fig. 5.3B** for comparison) which accommodate strain adjacent to faults (in the hanging wall fault blocks) due to buttress effects (e.g. Withjack et al., 2010). However, reverse reactivation of extensional faults, fault propagation, normal drag and load may have played a role on further modification of such folds and are discussed later in this chapter.
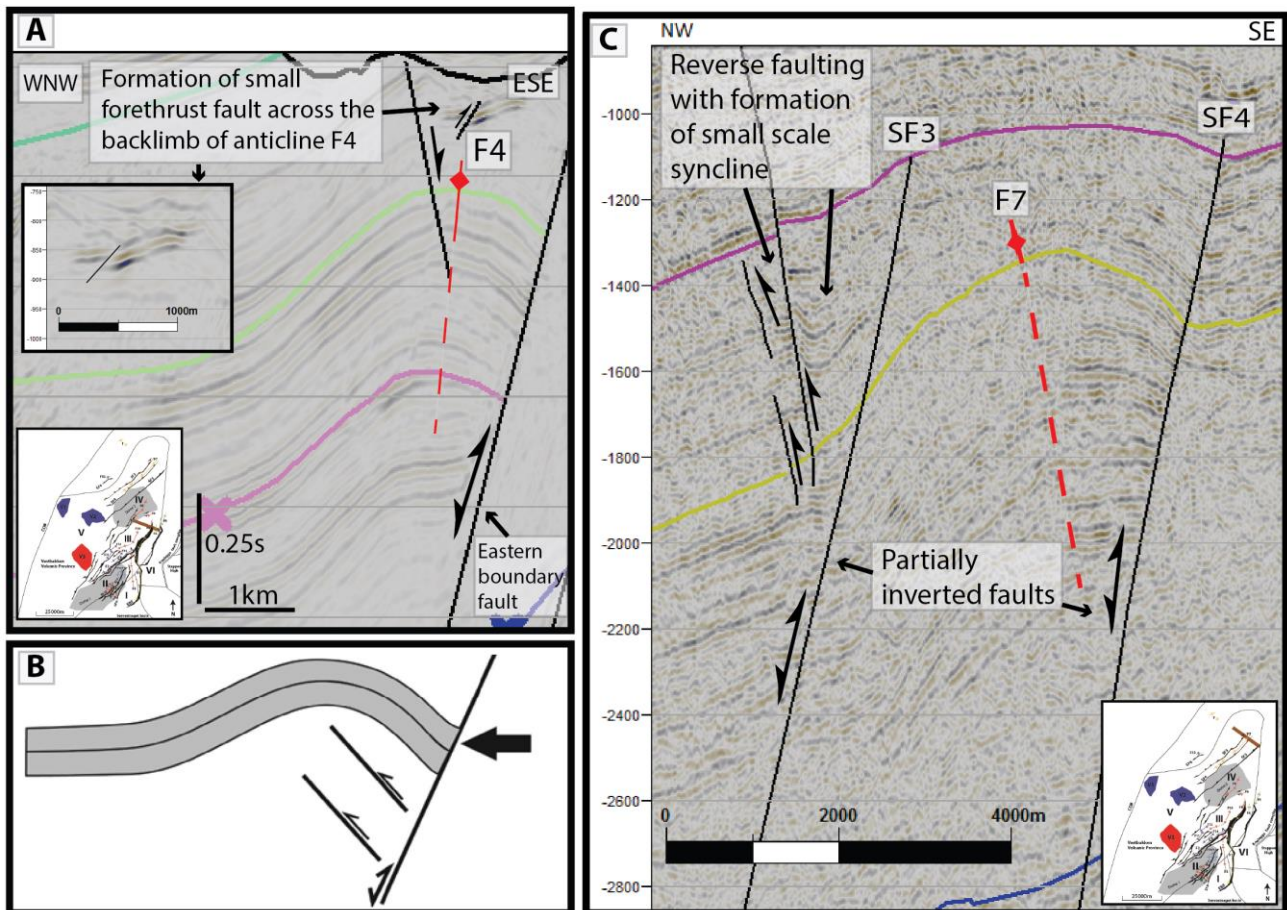
Fig. 5.3: ***(A)*** *Part of the interpreted profile in **Fig. 4.10** showing a buckle fold adjacent to the eastern boundary fault. Note formation of small forethrust that indicates a SE-directed tectonic transport direction; **(B)** Sketch showing typical geometry of a buckle fold is given for comparison (modified from Indrevær et al., 2016). Note that this configuration is indicative of inversion. **(C)** Interpreted profile showing buckle fold F7, partially inverted normal faults and reverse faults. Legend for the age of horizons can be found in **Table 5.1**. See **Fig. 5.1** for location of lines and structures. Vertical axis is given in TWT (s). Data courtesy of TGS and Spectrum.*

2. *Geometrically modified fault blocks and deformed fault planes*

It is obvious that the configuration shown in **Fig. 5.4A** that can be compared to sketch of **Fig. 5.4C** requires a contractional regime and is indicative of inversion tectonics. Fault reactivations in a reverse slip sense occur as a consequence of the change in stress pattern, and buckling due to head on contraction results in folding (**Fig. 5.4D**) and internal deformation of strata (**Fig. 5.4B**), (see also folds in **Fig. 4.7**, **Fig. 4.9**, **Fig. 4.10** and **Fig. 4.11**). **Fig. 5.4A** shows a series of tilted fault blocks which have been initially rotated during extension. Later contraction modified the fault planes that are slightly deformed (curved). Strata in the vicinity of these faults have also been affected as they are observed folded. This configuration is interpreted to be caused by the faults acting as buttresses and accommodating strain (e.g. **Fig. 5.4A**, fault plane of CF master fault). Hence, they control deformation by concentrating strain in their proximity.
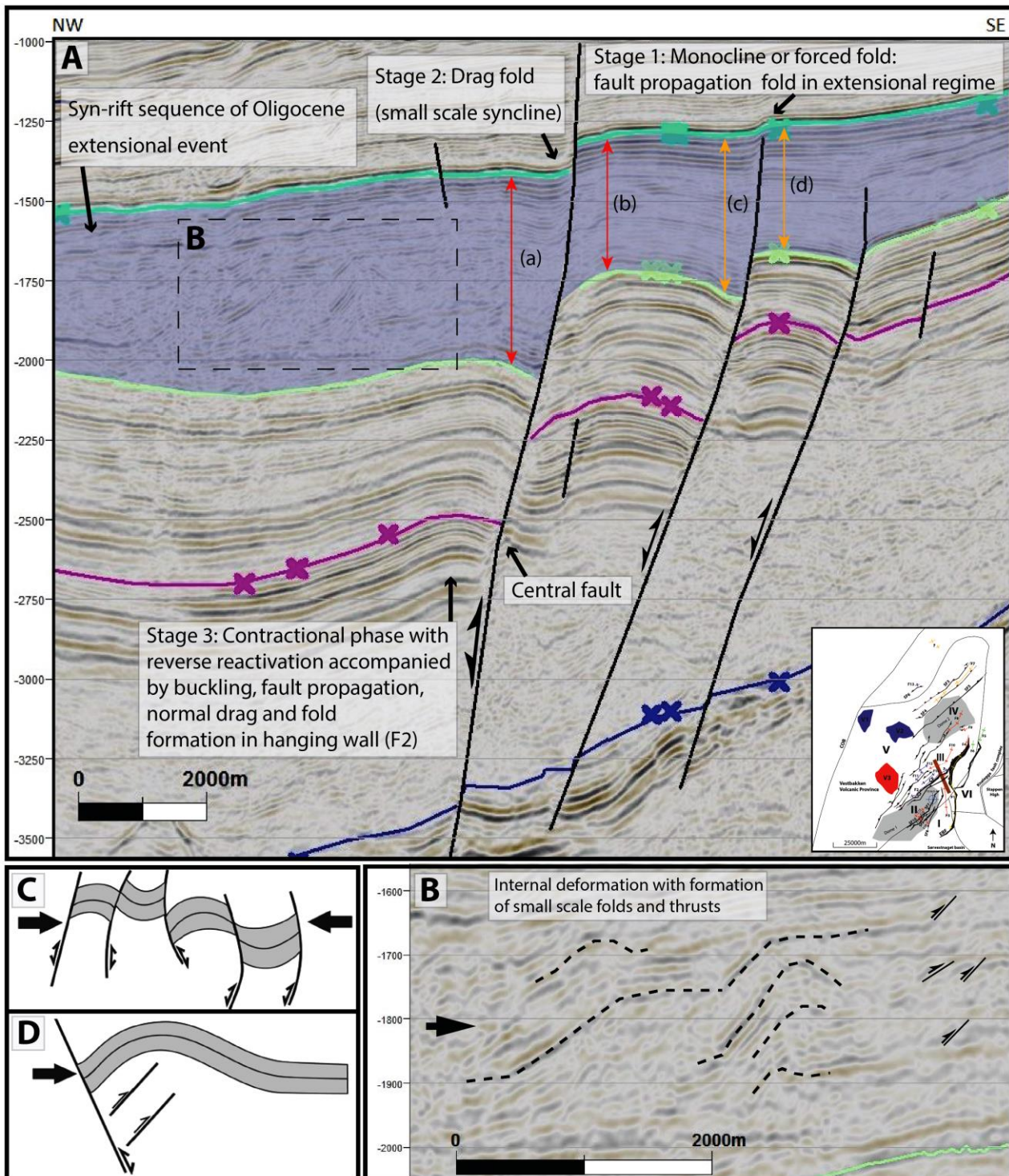
Fig. 5.4: (A) Interpreted seismic profile showing a series of slightly tilted deformed fault blocks and fault planes. Light blue color: syn-rift unit of Oligocene rift event. Stages mentioned, are described in Fig. 5.11 but note that they are not sequential in terms of age. Stages 1 and 2 refer to the Pliocene extensional event after the contractional phase of Miocene (stage 3). Expansion (growth) indices (E.I): a/b= 1.4, c/d=1.2; (B) Zoomed area of part of (A) showing internal deformation with folding and thrusting (flat-ramp-flat and duplex geometries), also indicating SE-directed tectonic transport direction; (C) Sketch showing typical geometries and types of deformed fault blocks is given for comparison. This configuration is indicative of inversion. (D) Sketch showing typical geometry of a buckle fold (sketches of C and D modified from Indrevær et al., 2016). Legend for the age of horizons can be found in Table 5.1. See Fig. 5.1 for location of line and structures. Vertical axis is given in TWT (ms). Data courtesy of TGS and Spectrum.

Fold F2 is better expressed (meaning low half wavelength/amplitude ratio) in deeper stratigraphic levels (intra middle Eocene – intra lower Oligocene) compared to, for instance, the intra lower Miocene stratigraphic level. A detailed study on the deformation pattern which occurs within the stratigraphic interval of intra lower Oligocene – intra lower Miocene (**Fig. 5.4B**) shows that this difference can be explained due to a partial release of strain. Folding and thrusting occurs in this interval through the formation of flat-ramp-flat folds, duplexes and thrust faults. This can be explained by the contrast in the mechanical nature of these rocks (e.g. mudstones, incompetent or unconsolidated sediments) in comparison with older deeper formations. The process described, shows that strain seems that it was partly "released" supporting that strain partitioning played a role on decreasing the amplification of F2 in this interval and in the vicinity of the CF. In addition, it indicates a SE-directed tectonic transport direction that is in agreement with the forethrust shown in **Fig. 5.4A** (see also **Fig. 5.9**).

3. _**Single fault rotation producing shortening along the hanging wall of the fault**_

According to Coward (1996) single faults which form the boundaries of extensional basins may invert and as a fault rotates the hanging wall flexes upwards while the footwall flexes down.
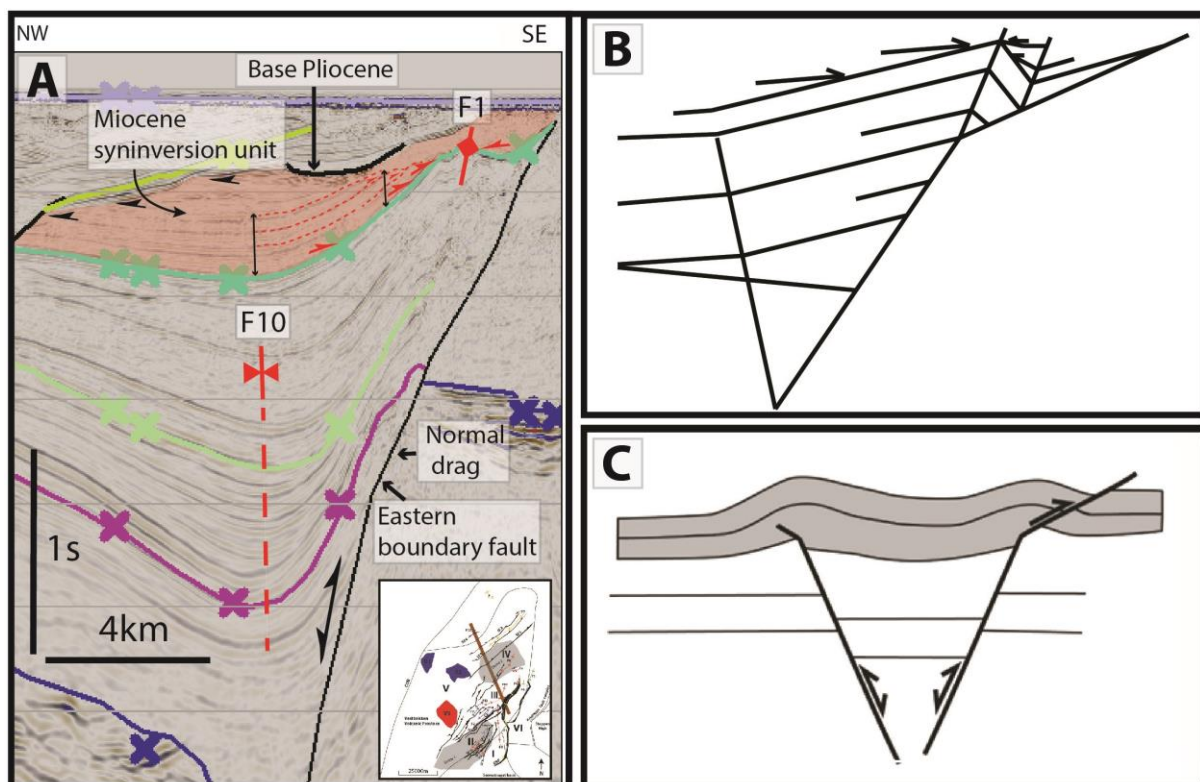
Fig. 5.5: **(A)** _Interpreted seismic profile showing a single rotated inverted fault. Apart from buckling, fault-bend folding could have contributed on folding of F1 in subarea (III) due to the change in the dip angle of the fault plane. This fold resembles snakehead geometry. Light red color: syn-inversion unit of Miocene age;_ **(B)** _Redrawn sketch after Coward (1996) illustrating the configuration described. The kink band fault-bend fold originates from the point where the fault changes dip;_ **(C)** _Snakehead structures with footwall cut-offs are indicative of inversion (modified from Indrevær et al., 2016). Legend for the age of horizons can be found in_ **Table 5.1**_. See_ **Fig. 5.1** _for location of line and structures. Vertical axis is given in TWT (s). Data courtesy of TGS and Spectrum._

The resultant folds are characterized by long back-limbs and steep forelimbs. The back-limbs can be modeled as fault-bend folds where the fault dip decreases upwards (**Fig. 5.5B**). In the Vestbakken Volcanic Province, one can observe this structural style within subarea (III) (**Fig. 5.1**) and adjacent to the EBF in the hanging wall fault block (**Fig. 5.5A**, see **Fig. 4.8** for entire profile). It is suggested that in this particular area, fault bend folding could contribute together with the reverse fault propagation and drag to form the fold (F1) observed. The geometry of this fold has geometry similar to a snakehead structure which is indicative of inversion (**Fig. 5.5C**).

4. *Inverted depocenters (or growth wedges) and domes*

Upright or steeply inclined gentle to open synclines are interpreted as partly inverted hanging wall synclinal depocentres (Fold F3 in **Fig. 5.6**, see also map in **Fig. 4.6**, e.g. folds: F3, F10, F12 and F14). Synclines generally display lower amounts of shortening with large wavelengths. The formation of these synclines is considered to relate with inversion and buckling due to a SE-directed contraction. Domes 1 and 2 (see **Fig. 5.1** for location and **Fig. 5.16** and **Fig. 4.8** for cross-sectional view) can also relate to a contractional phase since they seem to develop in a NE-SW orientation which is similar to the orientation of folds. However, dome 1 can also be related to the extensional phase of early Oligocene with processes related to footwall block rotation (or tilting) and uplift.
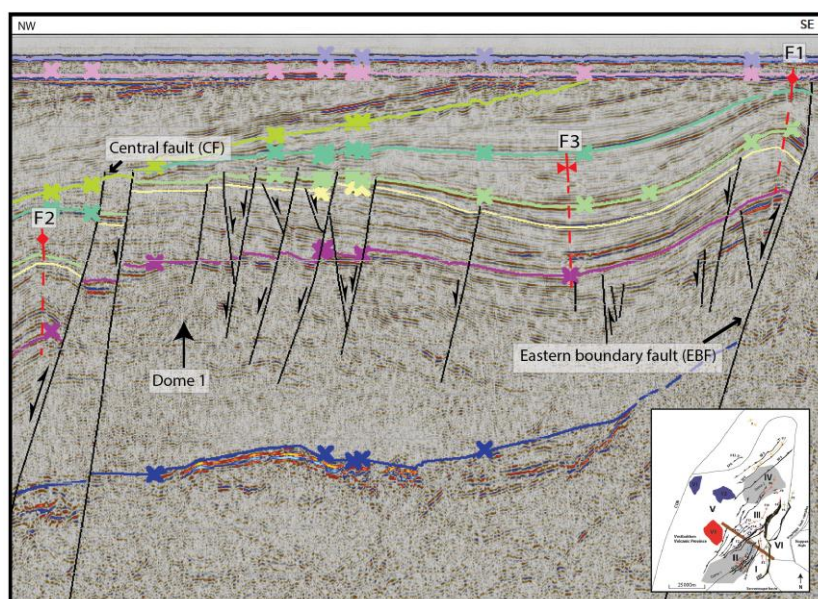
Fig. 5.6: *Part of interpreted profile in **Fig. 5.16** showing dome 1 and syncline F3. See text for description. Legend for the age of horizons can be found in **Table 5.1**. See **Fig. 5.1** for location of line and structures. Vertical axis is given in TWT (ms).*

This extensional phase is attributed to the plate reorganization at about 34Ma, (see Faleide et al., 1993, 2008). According to Ryseth et al., (2003) a bathymetrical high or positive structural feature may have been located in the fault zone between the Sørvestsnaget Basin and the Vestbakken area during the Oligocene - Miocene, possibly linked to the western marginal high of the Sørvestsnaget Basin. Perhaps, this could be correlated with dome 1. It is noteworthy, that one should keep in mind that there is an interplay between these structural features and vertical movements

attributed to events such as thermal cooling and local flexural stresses related to sediment loading or isostatic uplift due to erosion (erosion-isostatic rebound) and tectonic response to lithospheric thinning (see Grunnaleite et al., 2009) and this interplay constantly tries to reach an isostatic and stress equilibrium.

5.1.2   Fault-related folding and normal drag

Most of the anticlines studied, seem to be fault-related and more specifically, their fold axes tend to be located in the hanging wall fault block running close to, and parallel to the faults they are related to. Cogent examples are shown in **Fig. 5.7** and include the regionally expressed folds F1 and F2 which run parallel to the master faults EBF and CF, respectively. In addition, axial planes are parallel or sub-parallel to the fault surfaces and show a general same dip azimuth. The half wavelength/amplitude ratio is used in these figures as a normalized value for making comparisons among folds in terms of shortening, and is directly related to the stage of development of folds (Sattarzadeh et al., 2002); folds that are focused along pre-existing normal faults tend to have higher half wavelength/amplitude ratios in comparison with those that are not located adjacent to faults. This indicates that folding is mainly attributed to buckling due to a SE-directed compression and emphasizes the effect of fault buttressing and its significance on strain accommodation and fold formation in the study area.
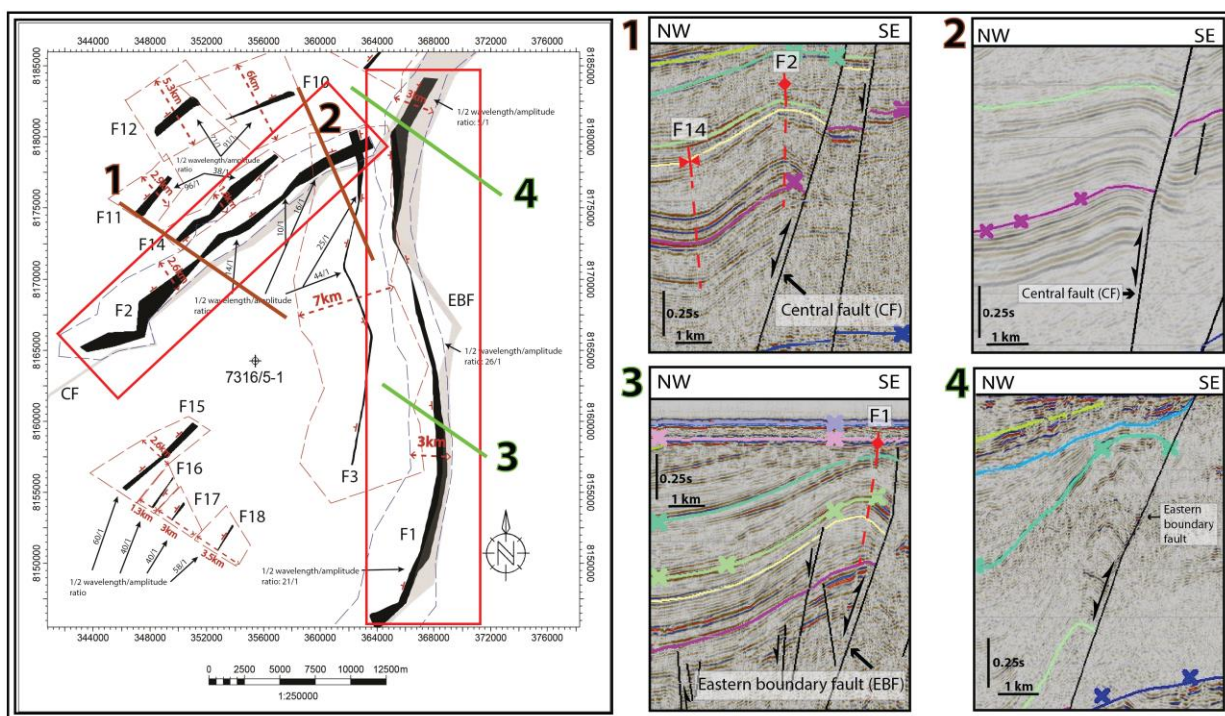
Fig. 5.7: *Map showing the distribution of folds and their relation to master faults. Black color: axial planes; Light grey: master faults. See **Fig. 4.15** for full description. Red rectangles show folds F1 and F2 striking parallel to master faults EBF and CF, respectively. Seismic lines oriented transversely to the strike of these structures show the cross-sectional relationship of faults and folds and support the first statement. Legend for the age of horizons can be found in **Table 5.1**. See **Fig. 5.1** for location of lines and structures. Vertical axis is given in TWT (ms). Data courtesy of TGS and Spectrum (line 2).*

Fault-related folds can be divided into three main categories according to the way the faults and the folds form (Brandes & Tanner 2014): (a) detachment, fault-bend, and fault-propagation folds. All fault-related folds are caused by changes in fault parameters and influence the geometry of related folds. Another detailed approach is that of Homberg et al., (2017) where they summarize all common types of fault-related folds in extensional and compressional regimes (**Fig. 5.8**).
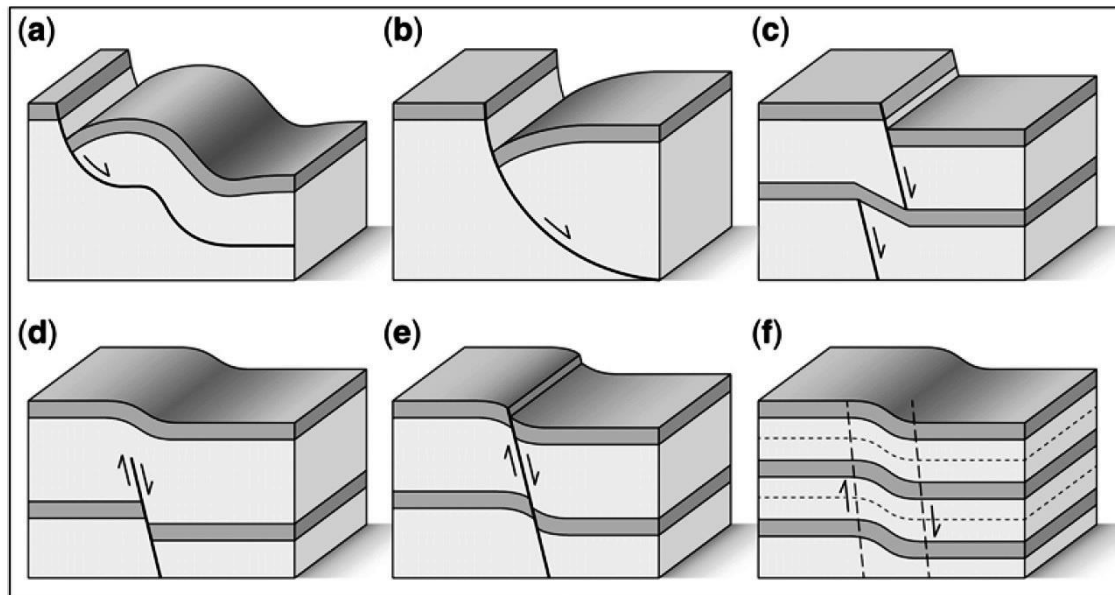
Fig. 5.8: Diagrams of the common types of fault-related folds: (a) fault-bend fold; (b) rollover anticline along listric fault; (c) fold between fault segments; (d) fault-propagation fold; (e) drag fold; and (f) shear fold. The folding mechanisms in (a) and (c)–(f) are drawn for normal faulting but are also common along reverse faults (after Homberg et al., 2017).

A combination of cases (d) and (e) (along reverse faults) of **Fig. 5.8** together with later contraction and buckling are the suggested means for the formation of fault-related folds within the study area. Occasionally, as shown in **Fig. 5.5A**, when fault plane geometry changes drastically, fault bend folding can partly participate. Fault propagation folding is suggested in the case of fold F13 (**Fig. 5.9**).

Note that transverse folds can occur in extensional regimes from along strike variations in fault displacement (Schlische 1995). This type of structuring could partly be used to explain later observed plunging (if any) of fault-parallel folds that formed due to contraction. In this scenario, folds can be divided into two generations owing to deferent regimes: transverse folds (extensional) and the fault-parallel folds (contractional).
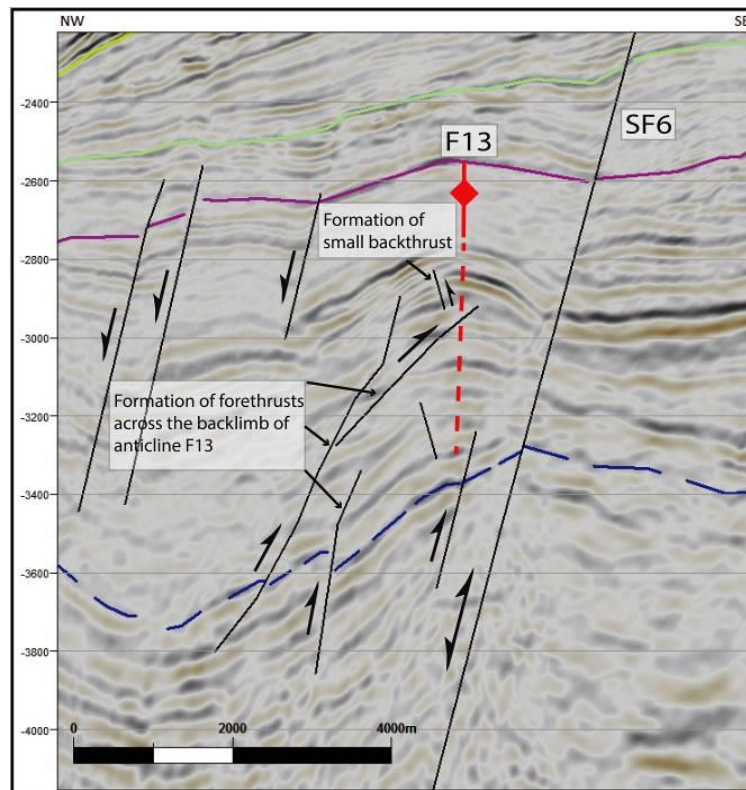
Fig. 5.9*: Interpreted seismic profile of the NW part of **Fig. 5.5A** showing a fault-propagation fold. Note the formation of forethrusts with emerging formation of frontal ramps. It is common that thrust faults ramp up in the direction of tectonic support indicating a SE direction. Small backthrust formed to accommodate excessive strain.*

Possible contribution of normal drag on folding

Fault drag, by definition, refers to the deflection of curved markers in the vicinity of a fault (see Grasemann et. al., 2005). Normal drag refers to a marker layer that is convex in the direction of slip, whereas reverse drag to a marker layer that is concave in the direction of slip. Grasemann et al. (2005) described normal and reverse drag along a fault (**Fig. 5.10**) and concluded than a mechanism to explain normal drag during fault slip is the caused heterogeneous displacement field. Ferrill et al. (2012) suggested that normal drag folds cannot form due to frictional forces as initially thought, but they form at the fault tip before being offset by the fault (e.g. **Fig. 5.8d**), (see also Homberg et al., 2017).
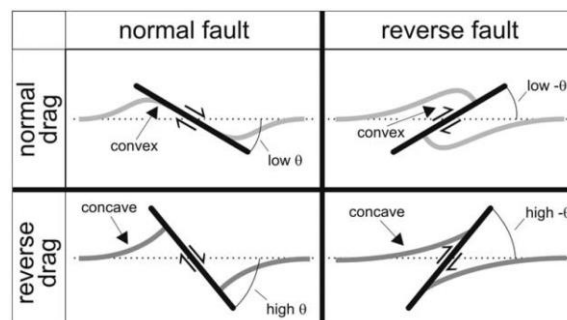
Fig. 5.10*: Sketch illustrating normal and reverse drag on normal and reverse fault. Note the relationship of the geometry of marker bed (concave/convex) for each case. Low angles favor normal drag whereas high angles favor reverse drag as visualized (modified from Grasemann et al., 2005).*

It is possible that drag mechanisms have contributed to amplifying folding during reverse reactivation in the study area since, locally, fault plane angles are relatively low (e.g. in subarea (III) adjacent to the EBF in **Fig. 5.1**) and marker beds show similar configuration as in **Fig. 5.10** (case of normal drag-reverse fault), (e.g. **Fig. 5.5A**). However, this is a theoretical scenario and cannot easily be proven. In addition, it is not suggested that this mechanism alone can form the large scale regionally expressed folds observed within the study area. An approach of incorporating possible drag contribution on folding during the evolution of faults through 3 stages is illustrated in **Fig. 5.11**.

5.1.3   Strike-slip kinematics

Structural styles and general structural patterns as mapped and described, cannot be correlated with pure strike-slip tectonics. Neither transtensional nor transpressional models could easily explain the present day configuration within the Vestbakken Volcanic Province and particularly that the fold axes strike parallel to the (extensional) master faults, suggesting that fold-strike has been influenced by head-on contraction (inversion against a structural buttress). It is accepted that strain partitioning can play a significant role on where to expect deformation and could influence structural orientations. According to Turner & Williams (2004), in pull-apart basins, most inversion episodes are non-coaxial, and oblique-slip or strike-slip kinematics are important modes of fault reactivation during inversion. Therefore, shortening strains will often be partitioned between faults displaying dip-slip, oblique-slip and strike-slip kinematics. Within the study area, such movements could be part of the compressional phase and cannot be excluded.

5.1.4   Fault kinematics

Fault - Fold relationships

Based on the above discussion, it is clear that fault kinematics within the Vestbakken Volcanic Province is challenging to resolve. **Fig. 5.11** represents a generalized and simplified approach of possible sequential stages for the evolution of master faults in the study area and comprises two scenarios. These are described by taking into consideration the fold formation. Timing of each phase will be addressed in Chapter 5.2. The first stage of the suggested model represents nucleation of a fault at depth and continued extension accompanied by fault propagation and formation of monocline above the fault tip. An example of this configuration is shown in **Fig. 4.11A** Stage 2 represents continued fault propagation where the fault cuts through the above-lying monocline and normal drag geometry is developed in both the hanging wall and footwall fault blocks (**Fig. 5.11B**).
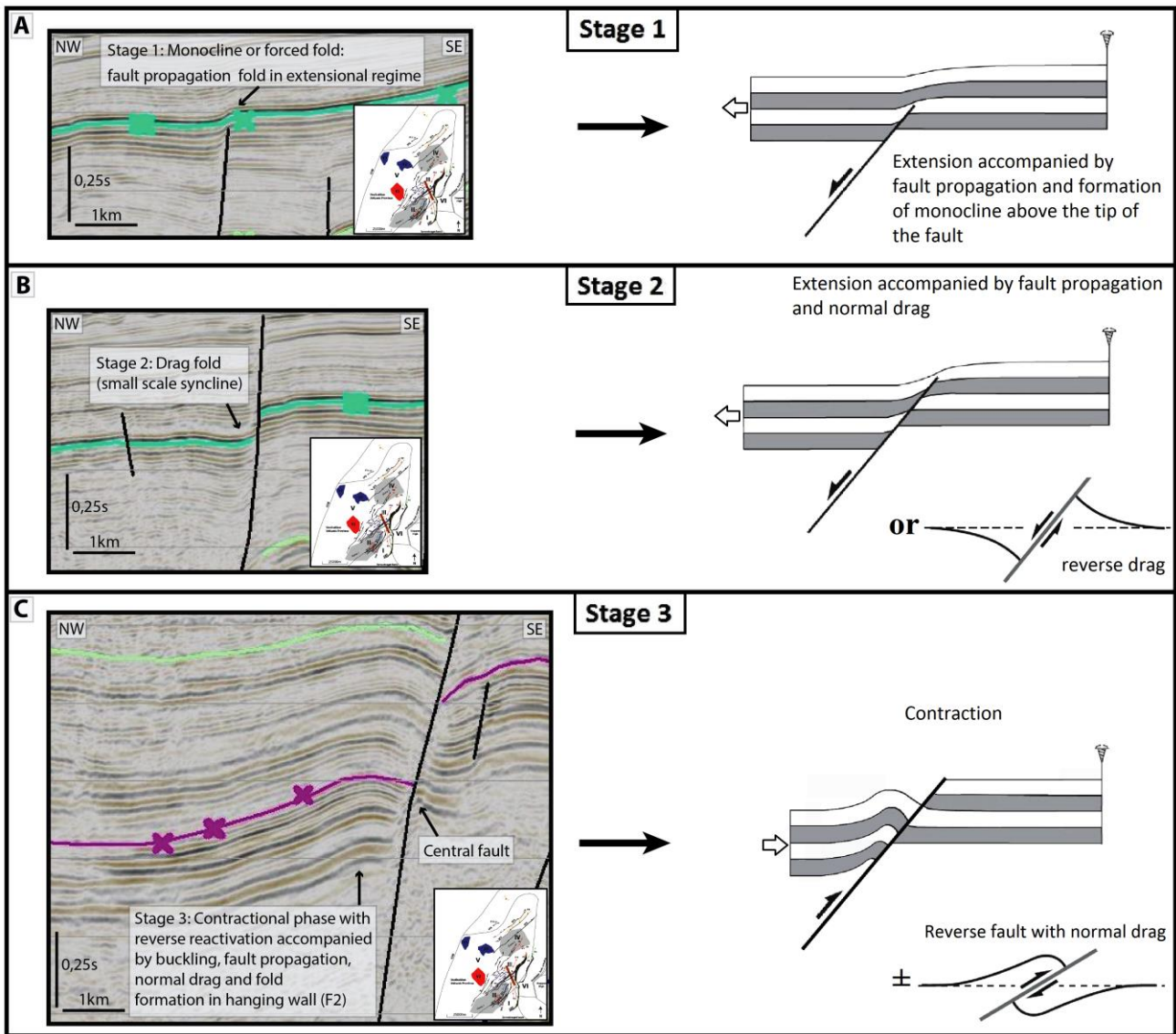
Fig. 5.11: Simplified sketches with examples of the study area representing possible generalized scenarios for the evolution of master faults in the area through 3 stages (A), (B) and (C). Note that this approach is conceptual based on observations but stages are not sequential in terms of age. Stages 1 and 2 refer to the Pliocene extensional event after the contractional phase of Miocene (stage 3). See text for description and comments. Main sketches on the right side of the figure are modified and partly redrawn (stage 3) from Brandes & Tanner (2014), the 2 smaller sketches referring to drag are modified from Grasemann et al., 2005). The three seismic profiles are part of the line in Fig. 5.4A, see Fig. 5.1 for location of line and structures. Legend for the age of horizons can be found in Table 5.1. Vertical axis is given in TWT (s). Data courtesy of TGS and Spectrum.

Stage 3 represents the contractional phase, which is accompanied by buckling and formation of folds parallel to the strike of faults accommodating shortening (**Fig. 5.11C**).

An alternative model for the formation of the observed snakehead geometries is a case where the first two stages would include formation of roll-over anticline (or reverse drag fold) during extension and a later stage where contraction would amplify shortening through buckling. Reverse reactivation of pre-existing normal faults could be accompanied by normal drag depending on the angle of the fault plane (e.g. if the fault plane was partly rotated with decreased dip angle due to

compression), thus, favoring the formation of anticlinal geometries. The second model preconditions the existence of listric fault geometry and fold amplitude and wavelength fitting this geometry. However, gently listric geometry is only observed for the eastern boundary fault and theoretical amplitude and wavelength of roll-overs do not fit this geometry. Therefore, the second model is less realistic and is found less likely to have occurred. Note that the seismic images (**Fig. 5.11**) are selected as representative examples of described configurations and are not time-sequential.

Fault kinematics and evolution based on observations and relation to plate reconstruction

It is well established from previous work that two main extensional tectonic episodes have affected the Vestbakken Volcanic Province during Cenozoic times (see Faleide et al., 1988; Faleide et al., 1991; Rasmussen et al., 1995; Jebsen, 1998; Faleide et. al., 2008; Faleide et al., 2010). Late Cretaceous-Paleocene extension between Norway and Greenland is correlated with the northward progradation of the Atlantic rifting (**Fig. 5.13**). A pull-apart setting established in the Vestbakken Volcanic Province in early Eocene. It is suggested that down-faulting started from the east through the Knølegga Fault Complex and fault activity gradually migrated to the west within the study area with normal faulting along the EBF after cessation of early Eocene volcanism, possibly accompanied by thermal uplift. This is based on the fact that extrusives of early Eocene age are observed on the elevated footwall fault block of the EBF (**Fig. 5.12**, additionally, **Fig. 4.3**, **Fig. 4.7** and **Fig. 4.10**). Moreover, thermal cooling caused rapid subsidence during middle Eocene (e.g. Eidvin et. al., 1998) but Vestbakken Volcanic Province subsided differentially with respect to the Sørvestnaget Basin (Ryseth et. al., 2003) through the southern extension of the EBF and its associated faults. Observations of thick successions of early to middle Eocene age can be seen in **Fig. 5.12**. The syn-rift sequence is not easily distinguishable due to the chaotic seismic character. However, there is evidence of normal drag along the EBF within subarea (III) (**Fig. 5.5A**) together with thickening of strata toward the fault plane indicating syn-rift sedimentation. Note that the initial nature of this configuration is partly obscured and distorted by a later contractional phase which resulted in shortening. The second extensional episode is related to the early Oligocene plate reorganization (**Fig. 5.13**, app. 34Ma, Greenland started moving more westerly with respect to Eurasia) which resulted in reactivation of mainly NE-SW striking faults. The hanging wall fault block of the CF master fault subsided providing accommodation space and as seen in **Fig. 5.4A** and **Fig. 5.16** (same seismic line) the stratigraphic interval from intra lower Oligocene to intra lower Miocene records a thickening toward the fault plane with an expansion (growth) index E.I=1.4 (and 1.2 for a nearby fault), but once more, compressional forces resulted in a change of the initial configuration.
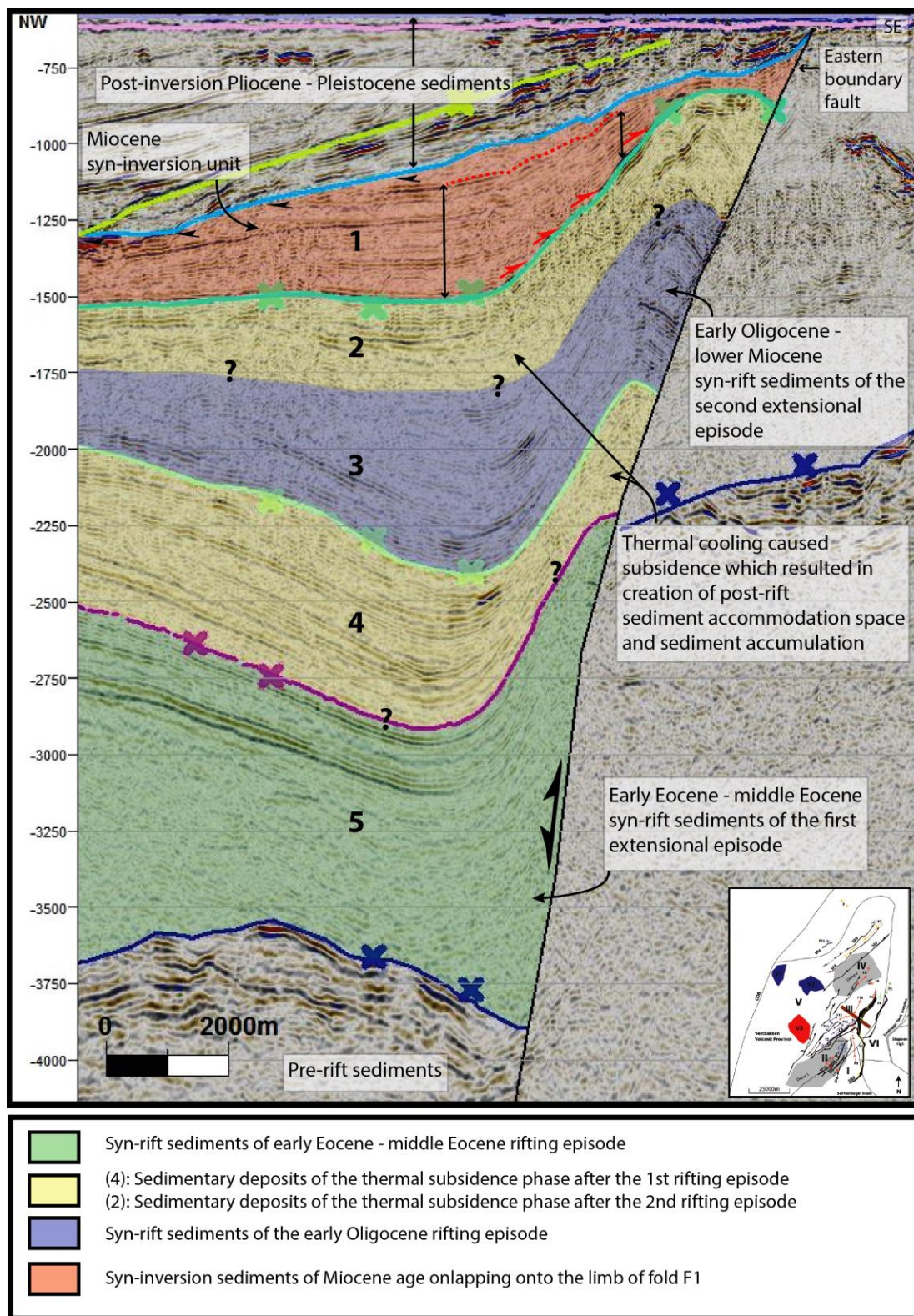
Fig. 5.12: *Interpreted seismic profile of line BV-10-86 showing suggested stratigraphic intervals for the early-Eocene – middle Eocene syn-rift phase, subsequent thermal subsidence phase, early Oligocene syn-rift phase, subsequent thermal subsidence phase, Miocene syn-inversion phase and post-inversion phase. Note onlaps and pinch-out geometry. Question marks indicate that the transition from the syn-rift phase to thermal subsidence phase is not pronounced and cannot easily be determined since the initial configuration is distorted due to contraction. Legend for horizons can be found in Table 5.1. See Fig. 5.1 for location of line and structures. Vertical axis is given in TWT (ms).*

In subarea (III) (**Fig. 5.1**), it is possible that during this period, the EBF was reactivated, but the hanging wall subsidence rate was too low to create a pronounced thickness increase of stratal packages toward the fault plane. It is noteworthy that these two events have generally affected same zones of weakness.
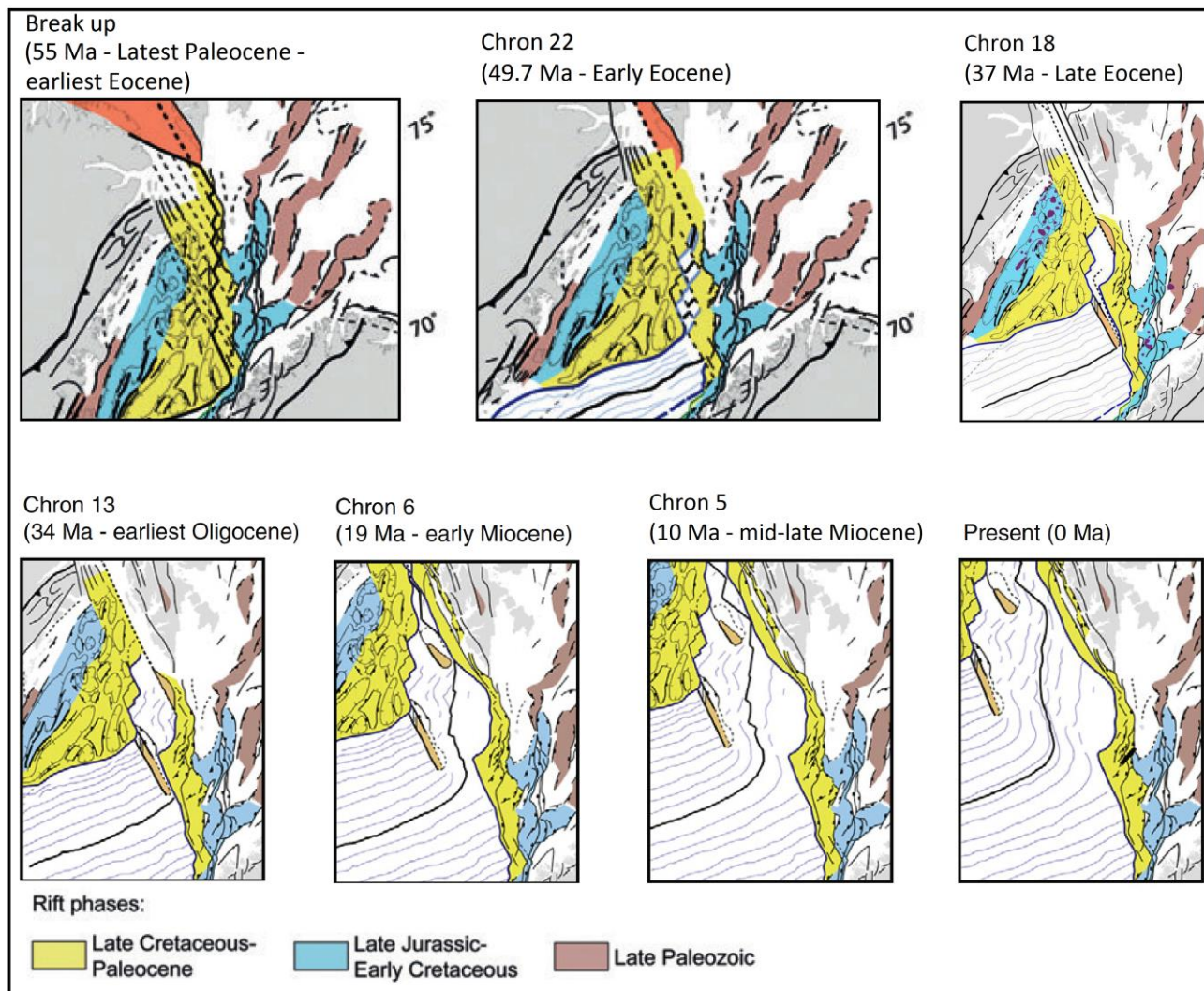
Fig. 5.13: *Plate reconstruction of the western Barents Sea margin from latest Paleocene to Present-day (First two stages modified from Tsikalas et al., 2012 and are based on Faleide et al., 2010, final 5 stages are modified from Faleide et al., 2010).*

It is suggested that the area experienced a phase of post-Oligocene, mainly Pliocene-Pleistocene, uplift which is part of a regional event affecting most of the western Barents Sea (Vågnes et al., 1992; Faleide et al., 1996; Baig et al., 2016). It is well established that a third Pliocene rift event of lower magnitude has reactivated some of the faults in the study area. This event is also related with volcanism as described by Mørk & Duncan (1993) who concluded that there was an event of basaltic volcanism in the Vestbakken Volcanic Province in Late Pliocene time (see also Faleide et al., 1988; Jebsen, 1998). Evidence of this event in the study area is shown in **Fig. 5.4A** and **Fig. 5.16**, showing the central master fault cutting intra lower Miocene – Pliocene strata (upper fault tip at intra upper Pliocene unconformity) with typical drag synclines and nearby fault-related forced

faults. Obviously, this configuration is post-inversion (Miocene) and thus, it can be correlated with the Pliocene extensional phase.

5.2   Growth of folds and timing constraints

Observations discussed in chapter 5.1 showed cogent evidence of inversion and now it is well established that folds and reverse reactivations of normal faults, primarily occurred due to inversion.

There are several methods that can contribute on constraining faulting/folding time and inversion. Some of the most important include the analysis of isochore thickness maps and expansion indices. However, as previously mentioned, Vestbakken Volcanic Province had a complicated and polyphasic evolution and time constraints cannot easily be defined. Erosion removed a valuable stratigraphic interval on the footwall fault block of the EBF (e.g. **Fig. 5.12**) and acted similarly within the basin which shows evidence of several erosional events. Therefore, the use of expansion indices is problematic and difficult to be applied.

Seismic and stratigraphic analysis can provide key observations on timing of inversion. Timing of deformation is described through observations in sub-chapter 4.4.2. This section expands on the discussion with respect to timing of inversion and fold growth. The main logical argument which has been used for determining time constraints is that deformation is younger than the age of the younger layer affected. This argument can be strengthened by observations such as stratal onlaps (red arrows) onto fold limbs and pinch-out geometries. **Fig. 5.12** and **Fig. 5.14A** include these types of observations and illustrate how early to middle Miocene strata onlap onto the east limb of fold F1 (horizon is of intra lower Miocene age). This onlapping pattern is generally evident in subareas (I) (II) and (III), (for subareas see **Fig. 5.1**) and suggests an early to middle or late Miocene phase of shortening. More specifically, inversion may have started in Aquitanian (23-20.4Ma) or in Bardigalian (20.4-16Ma) and it may have lasted until Tortonian (11.6-7.2Ma) or Messinian (7.2-5.3Ma). Therefore, the accumulation of early to middle or late Miocene growth strata represents a syn-inversion stratigraphic unit. The base Pliocene and the intra Pliocene erosional surfaces have truncated and removed large amounts of the Miocene strata (e.g. see extent of time structure map of intra lower Miocene in **Fig. 4.4**) and thus the exact time for the termination of inversion remains controversial. However, a Pliocene extensional event is identified (**Fig. 5.4A** and **Fig. 5.16**), (see Jebsen, 1998; Mørk & Duncan, 1993; Faleide et al., 1988) and thus, contractional phase had logically ceased before the initiation of the extensional phase.

The seismic profile in **Fig. 5.12** illustrates an attempt to visualize the pre-kinematic, syn-kinematic and post-kinematic phases of inversion. In addition, rift episodes and thermal subsidence events are included but are discussed in the previous section. The onlapping configuration shown in **Fig.**

5.5A, **Fig. 5.12** and **Fig. 5.14A** for folds F1 and F2, can be explained when comparing sedimentation rates and fold uplift rates and incorporating regional subsidence
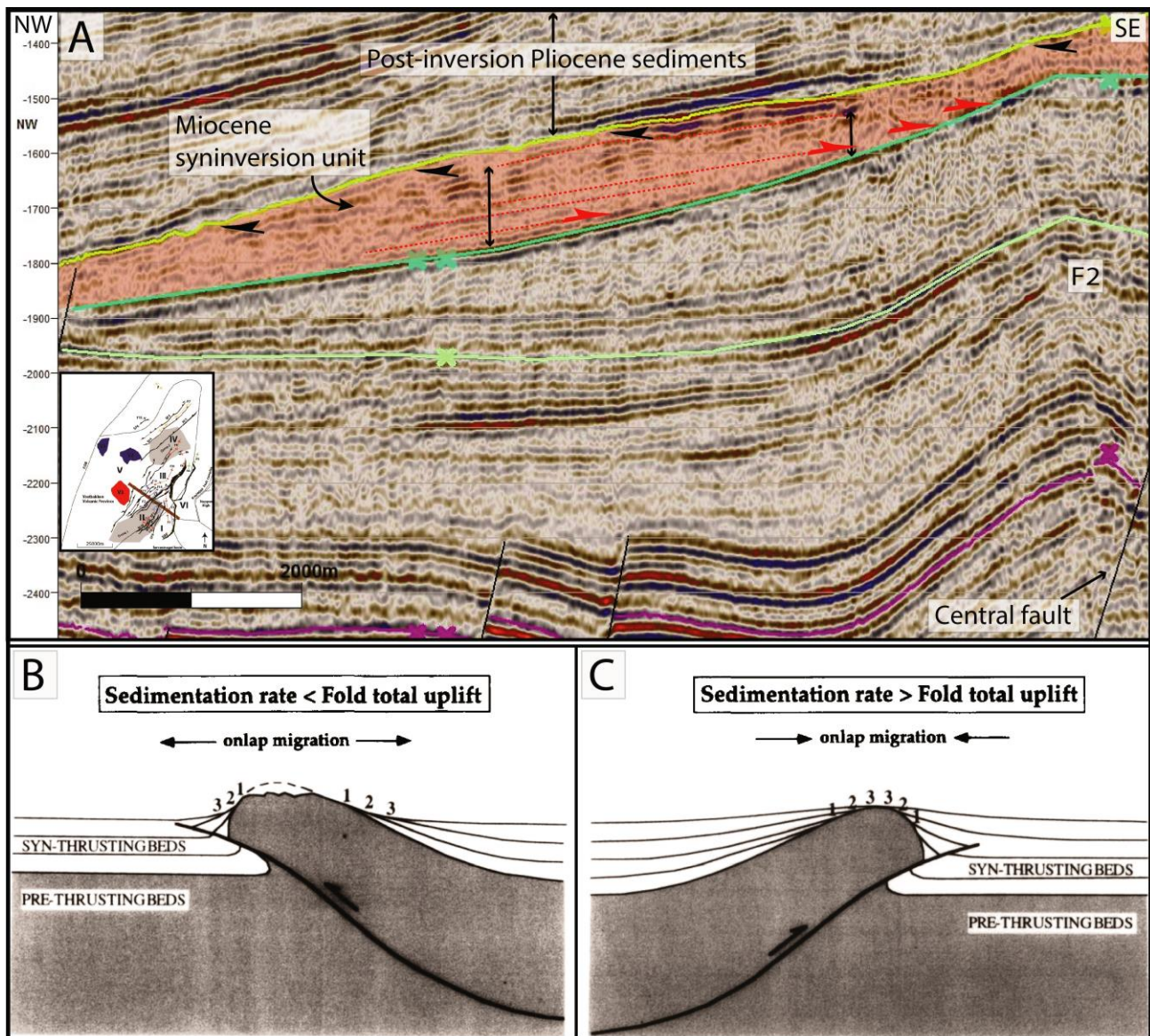
Fig. 5.14: ***(A)*** *Part of the interpreted seismic profile (line GBW-88-032-Y) of* ***Fig. 5.16*** *showing stratal onlapping configuration migrating toward the crest of fold F2 and slight pinch-out geometry adjacent to the central master fault. Red color: syn-inversion unit. See* ***Fig. 5.1*** *for location of line (as* ***Fig. 5.16***) *and structures. Legend for horizons can be found in* ***Table 5.1***. *Vertical axis is given in TWT (ms).* ***(B)*** *When fold uplift rate is greater than the regional subsidence rate, onlaps of syngrowth strata migrate away from the fold crest, and the sedimentation rate is lower than the fold total uplift,* ***(C)*** *on the contrary, onlaps may migrate towards the fold crest when the fold uplift rate is less than the regional subsidence rate, and the sedimentation rate is higher than the fold total uplift (modified from Doglioni & Prosser 1996). Note that eustatic sea level changes can affect the previous configurations.*

and eustatic sea level changes (**Fig. 5.14B** and **Fig. 5.14C**), (see Doglioni & Prosser 1996). Onlaps of the syn-inversion strata seem to migrate towards the fold crest (**Fig. 5.14C** case) indicating that the fold uplift rate is less than the regional subsidence rate (in the case of VVP, subsidence could happen due to thermal cooling, uplift due to later mantle flow that would push upwards the

western shelf of the Barents Sea, see Gac et al., 2016), and the sedimentation rate is higher than the fold total uplift. This of course, implies that eustatic sea level changes allowed or contributed on this configuration. However, it is necessary to analyze the sedimentary evolution of the area as a whole in order to recognize a general trend of onlapping migration and attribute it to fold growth or transgression or to a combination of both. Therefore, this could be part of the proposed future work for the study area.

5.3   Folding mechanisms

Donath and Parker (1964) proposed a classification system of folds based on the mechanisms of their formation. These include: buckling (layer-parallel compression), bending (e.g. from uneven loading) and passive folding (shearing). Bending and buckling are described as active folding (**Fig. 5.15**). It is suggested that the main mechanism which is responsible for the spatial fold distribution in relation with faults within the study area as shown in **Fig. 4.15**, **Fig. 4.16** and **Fig. 4.17**, is buckling. More specifically, an approximately SE-directed contraction, could explain buckling and formation of folds. However, bending due to uneven loading is an important mechanism that could have contributed to a certain degree and in some cases. The flexural response to load (e.g. sedimentary volume or volcanoes in VVP) and its role on folding and doming is a proposed subject for further research within the study area. During buckling of layers with same mechanical properties (e.g. competence), it is known that formation of folds follows a generally harmonic and symmetric shape. Faults act as buttress and accommodate strain and such pre-established structural lineaments affect the overall structural image by concentrating deformation adjacent to faults.
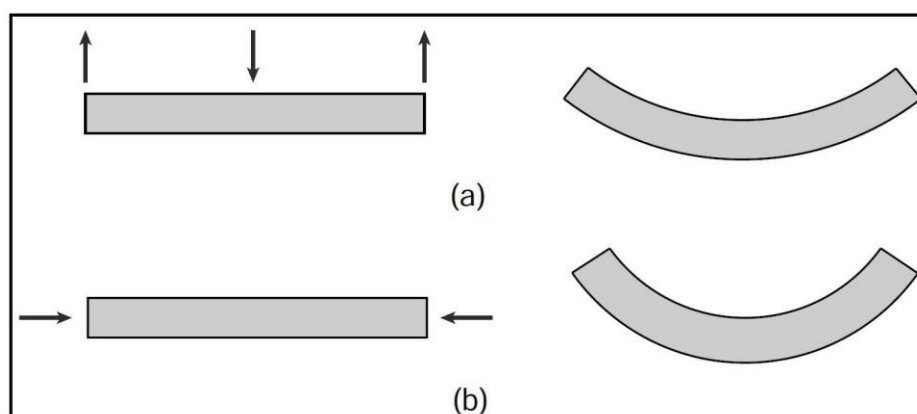
*Fig. 5.15: **(a)** bending and **(b)** buckling of a layer (Van & Marshak 2004).*

In **Fig. 5.16**, seismic profile presents a series of folds together with the two master faults in the study area, and a simplified sketch of a single layer is shown as an extracted isolated line (**Fig. 5.16**A). If faults could be eliminated and neglected, it is suggested that the resulted picture would have a shape similar to the sketch of **Fig. 5.16B** which approaches a symmetric and harmonic shape

indicating that folds were formed due to buckling. Consequently, a logical argument is that faults have played a critical role on the formation and evolution of folds but on the other hand, they have provided cogent evidence for identifying the mechanism responsible for the configuration observed.
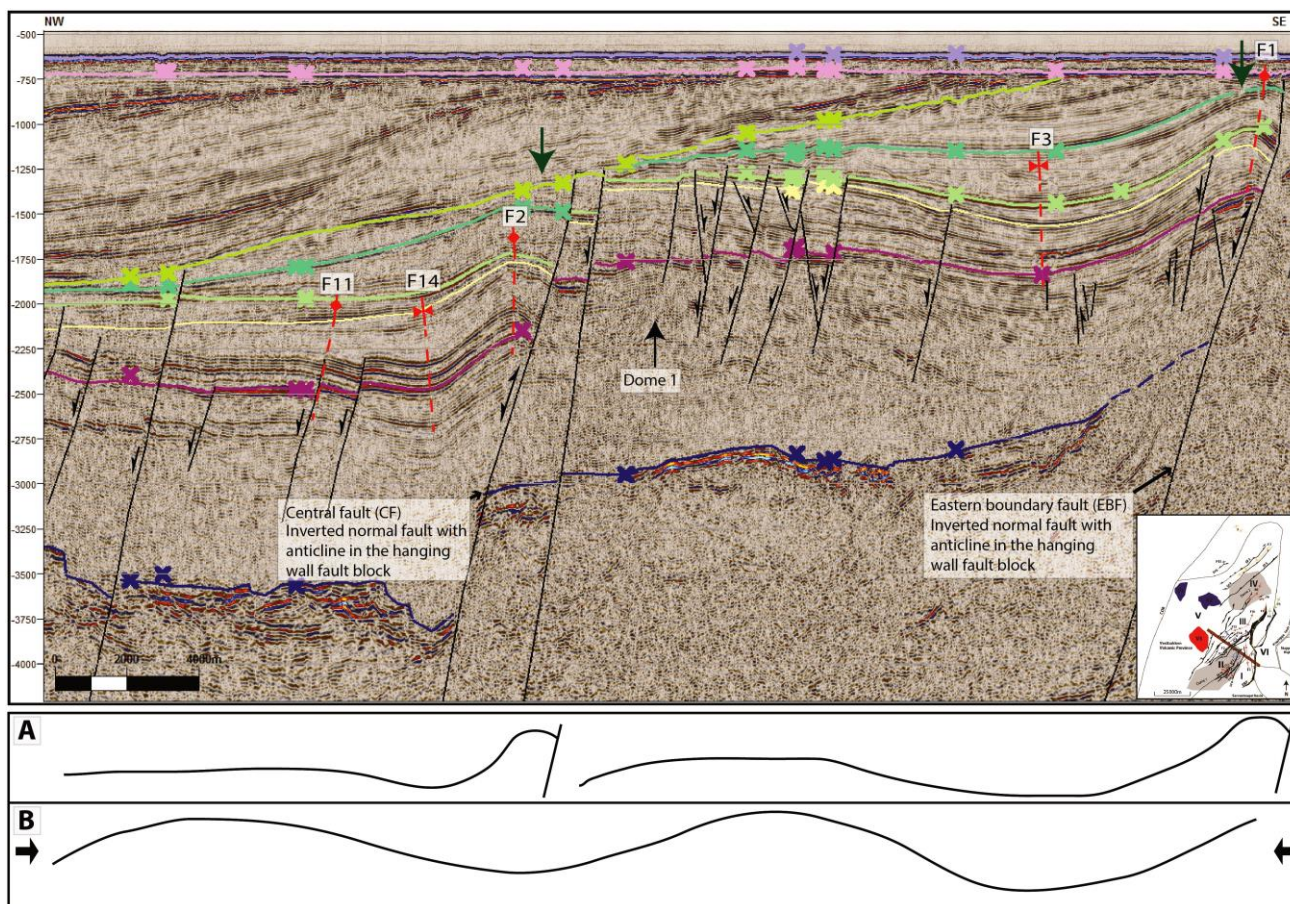
Fig. 5.16: *Interpreted seismic profile of line GBW-88-032-Y showing a series of folds and faults. Note how deformation is focused in the hanging wall fault blocks of the major faults EBF and CF showing higher amount of shortening. Sketch **(A)** illustrates simplification of the present configuration and sketch **(B)** illustrates the same configuration when eliminating and neglecting faults. Note the harmonic and symmetric shape of folding in the second scenario. Legend can be found in **Table 5.1**. See **Fig. 5.1** for location of seismic line, structures and subareas. Vertical axis is given in TWT (ms).*

5.4   Contractional folding in relation to the regional tectonic setting

Buckling is the main folding mechanisms in the study area. The possible driving mechanisms that caused buckling are discussed in this subsection. Contractional structures in the study area are not compatible with the common type of deformation in margins related to gravitational sliding and toe thrusting, thus, other causes must be responsible. Tingay (2009) summarized the main features causing or influencing stress fields within sedimentary basins (**Table 5.2**). It is well known that since Oligocene times, oceanic crust has been generated along the entire Barents Sea margin (**Fig. 5.13**). The Knipovich Ridge is suggested to have started producing ridge push forces in Miocene times

(primary control on stress field), (e.g. Gac et al., 2016). Ridge push is a gravitational force resulting from thermally elevated (expanded lithosphere and asthenosphere) along the mid-ocean ridge. Oceanic crust gradually cools away from the ridge, becomes more dense, and thus, causing gravity to pull the dense lithosphere down the sloping asthenosphere and away from the elevated mid-ocean ridge (e.g. Bott, 1991). A Miocene SE-directed contraction is suggested to be related with ridge push and has affected the Vestbakken Volcanic Province, Sørvestnaget Basins and Bjørnøyrenna Fault Complex (see Gabrielsen et al., 1997; Gac et al., 2016; Lundin and Doré, 2002).

Feature	Examples	Effect	Scale
Plate Boundary Forces	Mid-ocean ridges, continental collision zones, subduction zones	'Primary' control on stress field	Plate to regional: 100s-1000s of km
Major intraplate Forces	Surface loads, isostatic compensation, continent-ocean transition, deglaciation	'Secondary' control on stress field	Regional: 100s of km
Detachment zones	Evaporites, overpressured shales, low angle faults.	Mechanically detach overlying sediments from primary/secondary ('basement') stress field	Basin to local scale: 10s-100s of km
Basin Geometry	Tertiary deltas,	Regional control on stress field, particularly in detached basins	Basin scale (100s of km)
Major Topography (Mountain Belts)	Foreland basins, back-arc basins, intermontaine basins	Gravitational forces exerted due to weight of thickened lithosphere	Basin scale (100s of km)
Geological Structures	Faults, fractures, diapirs, folds	Rotation of stress field due to mechanical contrasts between units	Local (meters to a few kms)
	Active faults	Temporal change in stress associated with seismic cycle	Local to regional depending on scale of fault activity: 1 to 100s km
Local Topography	Mountains, valleys	Rotation of principal stresses due to Earth's surface being a free surface	Shallow regions only: near surface, within approximately one 'wavelength' of topography

Table 5.2: Summary of the main features causing or influencing stress fields in sedimentary basins and the approximate scale at which they affect the stress field (Tingay 2009).

Previous studies have addressed the tectonic importance of ridge-push on the formation of contractional structures at the Norwegian continental shelf emphasizing its contribution during Neogene (e.g. Vågnes et al., 1998). This statement is in agreement with observations of this study in the VVP. Furthermore, studies on neotectonic stress orientations in the Northern Norway have shown that the mean orientation of the maximum horizontal stress axis is NW-SE which is consistent with the North Atlantic ridge-push forces (e.g. Pascal et al., 2005, 2006, 2010; Pascal & Gabrielsen, 2001). Therefore, gravitational ridge-push is expressed as a constantly increasing over time force that constructively contributes on contractional deformation along the margin. Note that the role of the morphology of the Knipovich Ridge (**Fig. 5.17A**) has not been studied in this

work but could influence the stress field and the distribution of the amount of ridge push (e.g. Doré and Lundin, 1996). Similar contractional structures of mainly of Miocene age are reported along the east Greenland margin (e.g. Price, 1997; Lundin and Doré, 2002; Tsikalas et al., 2012) where ridge push is suggested to be the main mechanism for their formation (see **Fig. 5.17A**). However, it is controversial to suggest ridge-push alone as a mechanism for the amount of deformation observed in the VVP since the amount of shortening is relatively higher than that observed in the east Greenland. Therefore, it is likely that other important events have additionally influenced the evolution of the Vestbakken Volcanic Province during the Miocene.

Breivik et al. (2008), showed how Neogene intraplate magmatism relates to the spreading ridge-mantle plume interaction in the region north of the Aegir Ridge (**Fig. 5.17A**). They also discussed the relationship of this model with observed Miocene oceanic basement uplift and concluded that there was a rapid phase of uplift that occurred in response to crustal thickening caused by magmatic addition to the older oceanic crust. Other seamounts in the area are also explained similarly. This process responsible for oceanic intraplate deformation cannot be neglected when studying mid-Cenozoic deformation even on the Norwegian Continental Shelf as it is directly related to mantle dynamics, and hence, can influence its evolution.

Rickers et al. (2013) constrained temperature anomalies in the NE Atlantic Ocean and on the Barents Shelf. The model shown in **Fig. 5.17A** shows shear-wave velocity variations with respect to a standard velocity model where lower velocities (represented with red color) are usually linked to hotter mantle. This image reflects the present day configuration but can be connected to recent events during Cenozoic such Neogene uplift. They concluded that, on the one hand, velocity perturbations are strongest closer to hotspots (one beneath Iceland and one beneath the northern part of the Kolbeinsey Ridge close to Jan Mayen) and along the Mid-Atlantic Ridge but, on the other hand, a low-velocity layer extends beneath the oceanic lithosphere and, locally also beneath the continental lithosphere. A closer look of the panel in **Fig. 5.17B** in correlation with the tectonic setting of **Fig. 5.17A**, the position of mid-Cenozoic contractional structures and position of stars indicating uplift together with added observations of this study (black rectangles in **Fig. 5.17**) shows that the Vestbakken Volcanic Province has probably been affected by this configuration that is able to explain thinning of the continental lithosphere with reduced lithospheric strength prone to deformation and Neogene uplift in this region. It is notable how lithospheric thinned areas with high temperature anomalies beneath the lithosphere match the areas that record compressional deformation and uplift. It indicates that mantle flow patterns have affected the evolution of the North Atlantic region more that probably initially thought.

Similarly to what discussed in the previous paragraph, Gac et al. (2016) suggested that hot mantle flow eroded the base of the western Barents Sea lithosphere and hence, contributing on lithosphere thinning. This resulted in a configuration prone to deformation and uplift that was later amplified by Pliocene glacial-related erosion and uplift. Also, they suggested that horizontal stresses produced by ridge-push and gravitational forces by the elevated Iceland margin were

higher than needed to cause the deformation observed along the margin of the Vestbakken Volcanic Province. As pre-mentioned this force was established during Miocene as a result of the development of the Knipovich Ridge, and only from that period and on could be considered as a force able to cause compressional deformation in western Barents Sea. Doré et al. (2008) suggested that the total gravitational force caused by the elevated region around Iceland is adequate to cause the formation of Cenozoic compressional domes as observed along the Norwegian margin.

Timing of inversion and folding in the Vestbakken Volcanic Province was found herein to have occurred in the Miocene (Ch. 5.2) which fits in time with when ridge-push stresses, gravitational stresses by the elevated Iceland margin, plume-enhance spreading and the impact of the lithospheric mantle flow on lithospheric strength are proposed to have been initiated. Furthermore, contraction is shown to be roughly SE-directed (transverse to the dominant strike of faults and fold axes which is NE-SW), further supporting ridge push stresses sourced from the Knipovich Ridge as a driving mechanism. However, as previously discussed, ridge push cannot alone explain the amount of shortening observed within the VVP, and hence, it is suggested that it was accompanied by the mechanisms also related to mantle dynamics (plume-enhanced spreading and increased lithospheric mantle flow).
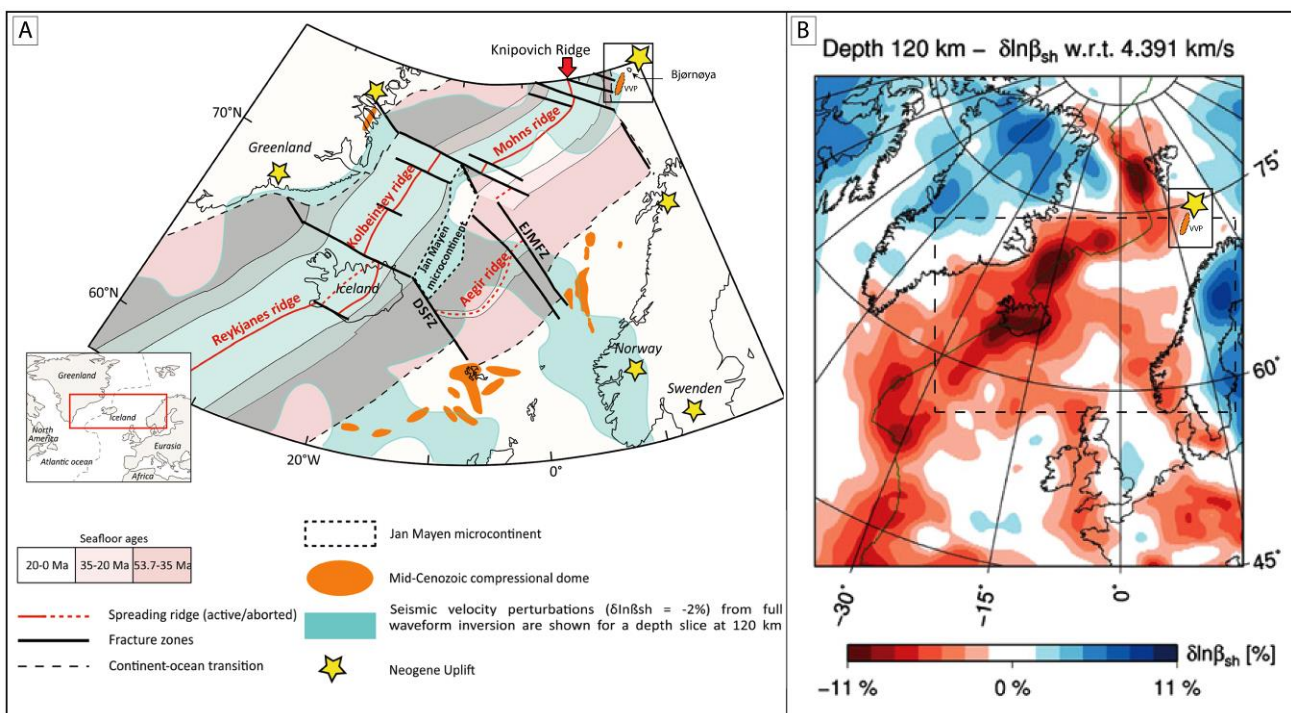
Fig. 5.17: ***(A)*** *Tectonic setting of the North Atlantic region (modified from Koptev et al., 2017 after Lundin and Doré 2002).* ***(B)*** *Horizontal depth slice through the βsh-component of model NA-IP, at depth 120 km. Seismic velocity perturbations are with respect to the reference velocity indicated in the panel (modified from Rickers et al., 2013). Black rectangles are modified parts, and were added to indicate that mid-Cenozoic compressional deformation is observed in the Vestbakken Volcanic Province and Neogene uplift has also been recorded in the form of domal and anticlinal features as well as regionally (e.g. Doré et al., 1999).*

5.5   An ongoing present day example of similar system in the Gulf of California

The architecture of the Gulf of California displays a well-developed transtensional plate margin linked to the rupture of Baja California from the southwestern North America (Aragón-Arreola and Martín-Barajas 2007). The present day configuration of this setting is illustrated in **Fig. 5.18A**. This modern day example is found of particular interest since it resembles the configuration of plate reconstruction suggested for the Vestbakken Volcanic Province during middle to late Eocene within a dextral shear system (**Fig. 5.18B**).

The main difference between the two systems is that the Gulf of California is dominated by a transtensional regime (Aragón-Arreola and Martín-Barajas 2007) in contrast with the Vestbakken Volcanic Province which has probably evolved in a more extensional rather than transtensional regime due to the nature of an east-stepping bend. However, the motion and position of the continental sliver (Greenland Ridge) should have been of great importance throughout the evolution of the study area causing early transtensional movements in the VVP. Also, note that some structuring has probably occurred earlier than the stage shown in **Fig. 5.18B**, during the late Paleocene – early Eocene phase of extension through the Knølegga Fault Complex to the east, thus, predating the setting on which this discussion focuses and follows in the next paragraphs.
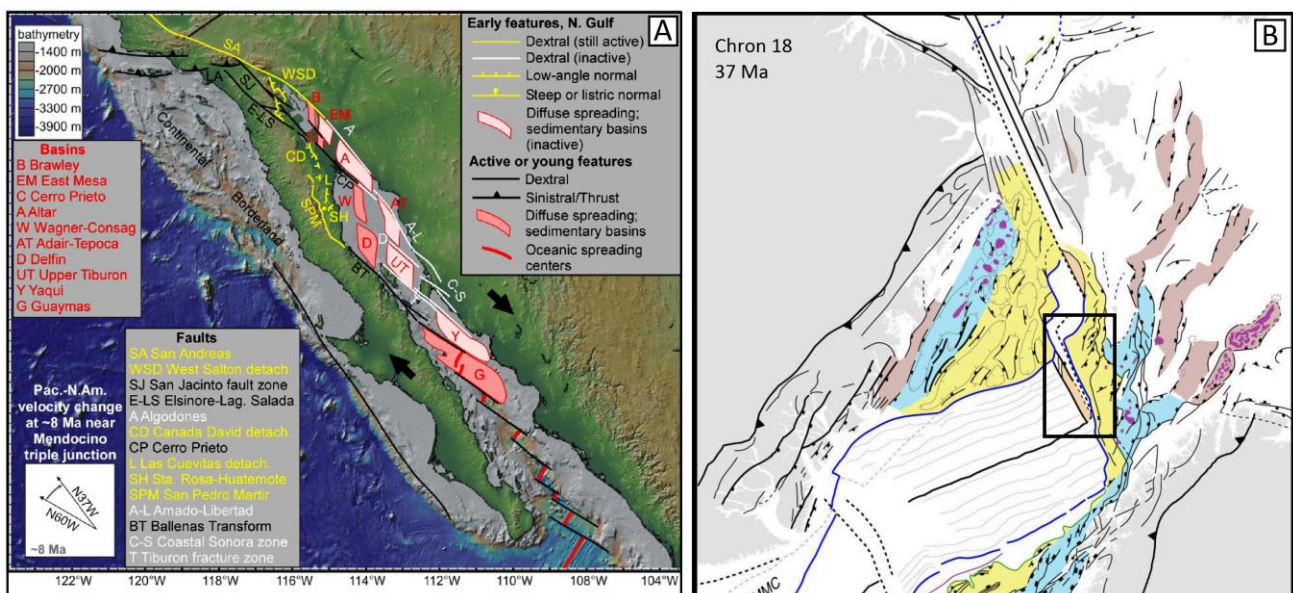
*Fig. 5.18: (A) Current tectonic setting in the Gulf of California emphasizing the eastern tectonically inactive margin and the western tectonically active margin together with the oceanic spreading centers to the southeast (modified from Wijk et al., 2017), (B) Plate reconstruction of late Eocene (Chron. 18). Note the position of continental sliver (Greenland Ridge) located exactly to west of VVP within the black rectangle. See legend in **Fig. 5.13** and entire Cenozoic plate reconstruction (modified from Faleide et al., 2010). The area marked with black rectangle can be compared with (A) as similar tectonic environments.*

Some of the main structural characteristics of the development of the Gulf of California include:

- Early development of basins to the eastern side due to focused transtensional activity and subsequent abandonment (**Fig. 5.18A**) when the locus of transtension shifted to its present location due to westward migration of strain (Wijk et al., 2017)
- Separation of the older system and its associated basins with the new active western margin and related basins by a wide basement high (e.g. anticline in **Fig. 5.19A**), (Aragón-Arreola and Martín-Barajas, 2007; Wijk et al., 2017).
- Formation of Volcanic knolls at the western part of the Gulf

Note that geometric differences between pull-apart basins are inherited from the initial geometry of the strike-slip fault step-over, which results from the forming phase of the strike-slip fault system (Wijk et al., 2017). In addition, Wijk et al. (2017) in their models for the Gulf of California, suggested that larger length-to-width ratios with overlapping faults are least likely to form basin-crossing faults, and pull-apart basins with similar geometry are prone to progress to continental rupture. This is evident at the SE part of the Gulf as shown in **Fig. 5.18A**.

It is suggested that the structural imprint observed today in the Vestbakken Volcanic Province exhibits great similarities to the Gulf of California (**Fig. 5.19**):

- The example of a general northwestward migration of fault activity together with depocenters and abandonment of sub-basins (multi-stage development of pull-apart basins) fits in very well in the study area. This can even be extended partly to the northern part of the Sørvestsnaget Basin (with respect to basin abandonment) and further east to the Knølegga Fault Complex (with respect to tectonic activity). As discussed in chapter 4 and 5, subarea (I) (**Fig. 5.19B**) could be the example of the partial abandonment of a sub-basin and subarea (III) could represent the new more recent tectonically active area.
- The broad anticlinal dome 1 in the study area (**Fig. 5.19B**) can be correlated with the anticlinal high in the central part of the northern area in the Gulf of California (**Fig. 5.19A**). This domal structure separates an older inactive sub-basin from new active sub-basins to the NW marked as active depocenters. Similarly, in the study area (**Fig. 5.19B**), subareas (I) and (III) are separated by dome 1.
- Position of volcanoes in the Vestbakken Volcanic Province is similar to the position of volcanic knolls in the Gulf of California. These are generally located to the western margin/part at the transition from shear to rift segments.
- In a regional context, as shown in **Fig. 5.18A**, the Gulf of California is dominated by transtension, with local extension and pull-apart basins at its central parts while the NW part is subjected to transpression. This configuration is quite similar to the western Barents Sea margin with the Senja Fracture Zone (transtension), northern part of Sørvestnaget Basin and the Vestbakken Volcanic Province (transtension-extension, pull-apart basins) and the northern Hornsund Fault Zone (transpression) defining similar margin segments.

In addition, it is notable that the scale of this comparison is very similar (see **Fig. 5.19**). Furthermore, the evolution of VVP and the continued structuring of the area was probably a result of the interaction between the area and the continental sliver now known as the (East) Greenland Ridge (Døssing et al., 2016), (**Fig. 5.18B**). There is evidence which suggests their connection in the past (e.g. Døssing et al., 2016, 2008; Faleide et al., 1993; Tsikalas et al., 2012). The phase of gradual separation and rupture initiated in early Eocene along the Senja Fracture Zone in a transtensional regime and lasted until late Eocene-Earliest Oligocene when extensional tectonics prevailed (Døssing et al., 2008) and the ridge subsided due to the change in relative plate motion (**Fig. 5.13**) when Greenland (and North America) moved in a more westerly direction with respect to Eurasia (e.g. Faleide et al., 1993; Doré et al., 1997; Engen et al., 2008; Faleide et al., 2010).
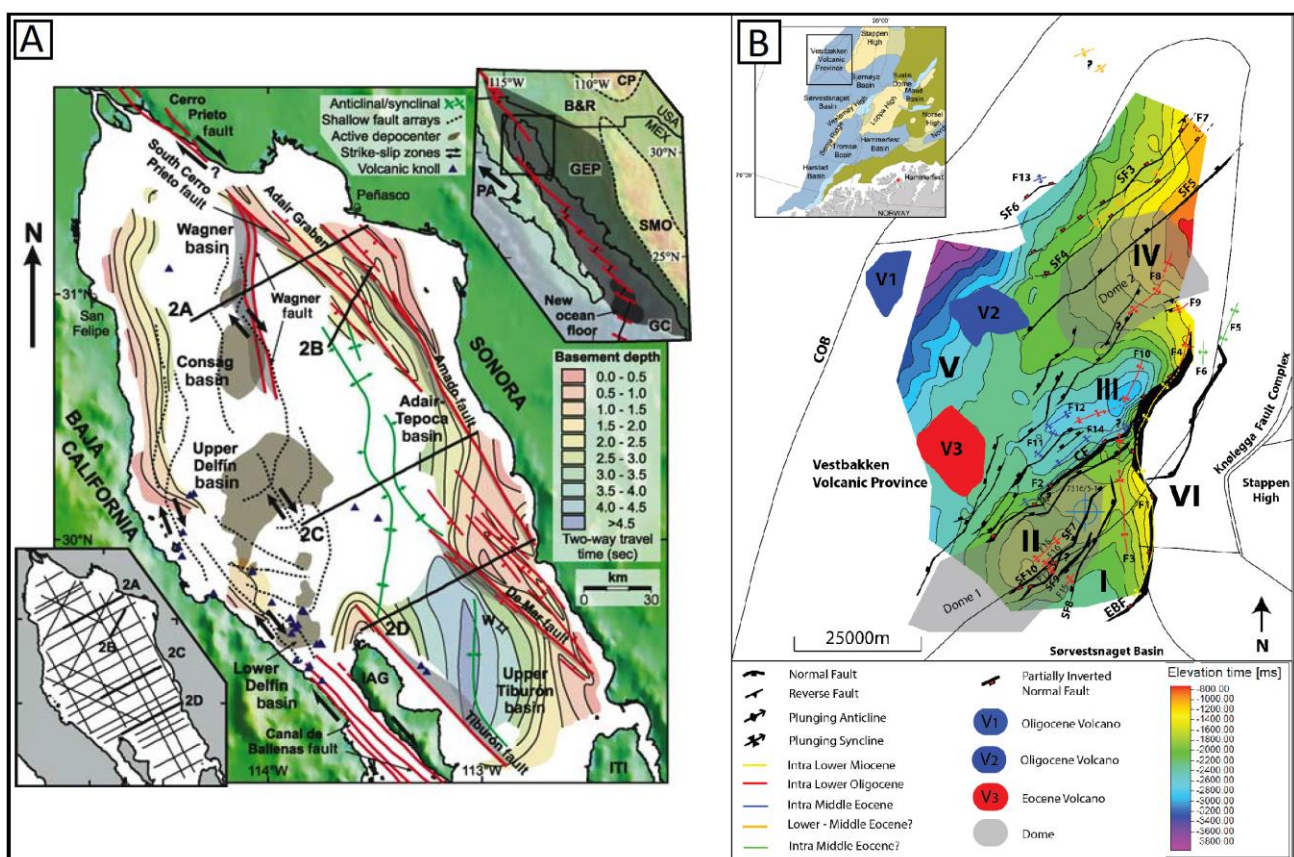
***Fig. 5.19**: **(A)** Structural map of Northern Gulf of California (modified from Aragón-Arreola and Martín-Barajas 2007) Note the eastern tectonically inactive margin and western active modern rift; **(B)** Structural contour map of the study area within the Vestbakken Volcanic Province. Fault interpretations are displayed at intra middle Eocene level (as heave). Fold axes are mapped at various stratigraphic levels as shown in the legend. Inset (upper left corner) shows the location of the study area (modified from Henriksen et al., 2011). COB: Continent-Ocean boundary. EBF: eastern boundary fault, CF: central fault. All fault and fold abbreviations are shown in the list of abbreviations of **Table 4.1**. All subareas are described in chapter 4.1 and are shown with their corresponding Latin numbers I, II, III, IV, V and VI.*

Chapter 6

6   Conclusions

- The geological structures in the Vestbakken Volcanic Province are described on the basis of detailed seismic interpretation of 2D seismic reflection data and the structural analysis is accompanied by structural maps, time maps and special maps which focus on the geometric and spatial relations among faults and folds. The stratigraphic interval of interest spans from early Eocene to base Pliocene.

- The area comprises distinct structural subareas and has been divided into 6 tectonically homogenous subareas. A NNE-SSE half-graben developed in the southern part of the study area and is bounded from the central NE-SW striking half-graben by a wide domal structure that strikes NE-SW. In the northern parts of the area a second domal structure developed in a NE-SW orientation. The uplifted footwall fault block of the eastern boundary fault is also defined as a subarea. The west part of the basin is generally characterized by a gently dipping slope which is only disturbed by the appearance of 3 volcanoes.

- Cenozoic tectonic activity is concentrated at the east part of the Vestbakken Volcanic Province.

- Structuring of the area occurred after the cessation of early Eocene volcanism which resulted in an extensive cover of volcanic flows in the entire area.

- The study reveals the existence of two partially inverted master faults, several branch faults with anastomosing character and many isolated secondary faults, a few reverse faults and thrust faults and 18 folds. The dominant strike of structural features in the Vestbakken Volcanic Province is NE-SW. Exceptions include the N-S striking eastern boundary fault which defines the boundary between Vestbakken Volcanic Province and Stappen High to the east. Faults primarily dip towards NW. Structural analysis of faults revealed chiefly planar fault plane geometries that locally are interpreted to be slightly modified through later deformation. The eastern boundary fault is locally observed as listric and locally with vertical segmentation. Lateral segmentation is locally observed in the southwestern extension of the central fault. Secondary normal faults seem to develop mostly at the central and southern part of the study area and display an anastomosing character. They affect strata of early Eocene to intra lower Miocene age and are decoupled from the basement. They exhibit a general NE-SW to NNE-SSW strike and NW to NNW dip direction. They all display planar fault plane geometry.

- Three extensional events have been identified: (i) a late Paleocene-early Eocene event which is related to the continental break-up in the Norwegian-Greenland Sea, (ii) an early Oligocene event attributed to the plate reorganization (34 Ma) affecting mainly NW-SE striking faults and (iii) an extensional Pliocene event.

- There are several contractional structures mapped in the study area and two main structural styles of folds have been recognized. The first includes upright to steeply inclined close to open anticlines that are typically present in the hanging wall of master faults and have wavelengths in

the order of 2.5 to 4.5 kilometers, and amplitudes of several hundred meters. Most commonly, they appear with snakehead (head on) geometries and are interpreted as buckle folds. The second style includes upright or steeply inclined gentle to open synclines that are interpreted as partly inverted hanging wall synclinal depocentres with wavelengths in the order of 5 to 7 kilometers and amplitudes of several tens of meters to several hundred meters.

- Synclines generally display lower amounts of shortening compared to anticlines.
- Folds are principally observed to be fault-related, where regionally expressed anticlines are developed in the upper stratigraphic sections, in the hanging wall fault blocks of pre-existing extensional master faults, typically affecting middle Eocene – lower Miocene strata
- Deformation is found to be controlled by the geometry of the faults which act as buttresses accommodating shortening. Folds are mainly interpreted as buckle folds. Fault-bend folding and fault propagation folding are observed locally.
- Onlap configuration and pinch-out geometries reveal that the phase of tectonic inversion (which caused folding, reverse faulting and reverse reactivation of extensional faults) commenced in early Miocene times under a SE-directed contractional regime prior to the onset of Pliocene. The event is suggested to be primarily related to the development of the Knipovich Ridge in the NW which caused SE-directed stress through ridge-push. A SE-directed tectonic transport direction is consistent with geometric observations such as slight steeper forelimbs compared to backlimbs, axial plane inclinations, direction of fault plane flexural rotation, thrust faults that ramp-up to the SE and forethrusting.
- Other processes that may have been involved include: (i) lithospheric thinning due to mantle flows that would reduce lithospheric strength, (ii) gravitational stresses by the elevated Iceland margin and (iii) plume-enhanced spreading.

7   References

Anell, Ingrid, Jan Inge Faleide, and Alvar Braathen. 2016. "Regional tectono-sedimentary development of the highs and basins of the northwestern Barents Shelf." *Norsk Geologisk Tidsskrift* 96 (1):27–41. https://doi.org/10.17850/njg96-1-04.

Aragón-Arreola, Manuel, and Arturo Martin-Barajas. 2007. "Westward migration of extension in the northern Gulf of California, Mexico." *Geology* 35 (6):571–74. https://doi.org/10.1130/G23360A.1.

Baig, Irfan, Jan Inge Faleide, Jens Jahren, and Nazmul Haque Mondol. 2016. "Cenozoic exhumation on the southwestern Barents Shelf: Estimates and uncertainties constrained from compaction and thermal maturity analyses." *Marine and Petroleum Geology* 73. Elsevier Ltd:105–30. https://doi.org/10.1016/j.marpetgeo.2016.02.024.

Blaich, O. A., F. Tsikalas, and J. I. Faleide. 2017. "New insights into the tectono-stratigraphic evolution of the southern Stappen High and its transition to Bjørnøya Basin, SW Barents Sea." *Marine and Petroleum Geology* 85. Elsevier Ltd:89–105. https://doi.org/10.1016/j.marpetgeo.2017.04.015.

Bott, M. H.P. 1991. "Ridge push and associated plate interior stress in normal and hot spot regions." *Tectonophysics* 200 (1–3):17–32. https://doi.org/10.1016/0040-1951(91)90003-B.

Brandes, Christian, and David C. Tanner. 2014. "Fault-related Folding: A review of kinematic models and their application." *Earth-Science Reviews* 138. Elsevier B.V.:352–70. https://doi.org/10.1016/j.earscirev.2014.06.008.

Breivik, Asbjørn Johan, Jan Inge Faleide, and Rolf Mjelde. 2008. "Neogene magmatism northeast of the Aegir and Kolbeinsey Ridges, NE Atlantic: Spreading ridge-mantle plume interaction?" *Geochemistry, Geophysics, Geosystems* 9 (2). https://doi.org/10.1029/2007GC001750.

Cooper, M.A., Williams, G.D. et al. 1989. Inversion tectonics—a discussion. In: Cooper, M.A. & Williams, G.D. (eds) Inversion Tectonics. Geological Society, London, Special Publications, 44, 335–347, http://doi.org/10.1144/GSL.SP.1989.044.01.18

Cooper, M.A. & Williams, G.D. (eds) 1989. Inversion Tectonics. Geological Society, London, Special Publications, 44, http://doi.org/10.1144/GSL.SP.1989.044.01.25

Cooper, Mark, and Marian J. Warren. 2010. "The geometric characteristics, genesis and petroleum significance of inversion structures." *Geological Society, London, Special Publications* 335 (1):827–46. https://doi.org/10.1144/SP335.33.

Coward, Mike P. 1996. "Balancing sections through inverted basins." *Geological Society, London, Special Publications* 99 (1):51–77. https://doi.org/10.1144/GSL.SP.1996.099.01.06.

Dalland, A., Worsley, D. & Ofstad, K. (eds) 1988. A Lithostratigraphical Scheme for the Mesozoic and Cenozoic Succession Offshore Mid-and Northern Norway. Norwegian Petroleum Directorate, Bulletins, 4, 1–65.

Dallmann, W. K. (ed.) 1999. Lithostratigraphic lexicon of Svalbard: Upper Paleozoic to Quaternary bedrock. Review and recommendation for nomenclature use. Norwegian Polar Institute, Tromsø.

Dewey, J.F., 1989. Kinematics and dynamics of basin inversion. Geol. Soc. Lond. Spec. Publ. 44 352–352.

Doglioni, Carlo, and Giacomo Prosser. 1997. "Fold uplift versus regional subsidence and sedimentation rate." *Marine and Petroleum Geology* 14 (2):179–90. https://doi.org/10.1016/S0264-8172(96)00065-7.

Donath F.A. Parker R.B., 1964. Folds and folding: Geological Society of America Bulletin , v. 75, p. 45–62, doi:10.1130/0016-7606 (1964)75[45:FAF]2.0.CO;2

Doré, A. G., and E. R. Lundin. 1996. "Cenozoic compressional structures on the NE Atlantic Margin; nature, origin and potential significance for hydrocarbon exploration." *Petroleum Geoscience* 2 (4):299–311. https://doi.org/10.1144/petgeo.2.4.299.

Doré, A.G., Lundin, E.R., Fichler, C., Olesen, O., 1997. Patterns of basement structure and reactivation along the NE Atlantic margin. J. Geol. Soc. Lond. 154, 85–92.

Doré, A G, E R Lundin, L N Jensen, O Birkeland, P E Eliassen, and C Fichler. 1999. "Principal tectonic events in the evolution of the northwest European Atlantic Margin." *Petroleum Geology Conference Proceedings* 5 (0):41–61. https://doi.org/10.1144/0050041.

Doré, A. G., E. R. Lundin, N. J. Kusznir, and C. Pascal. 2008. "Potential mechanisms for the genesis of Cenozoic domal structures on the NE Atlantic Margin: pros, cons and some new ideas." *Geological Society, London, Special Publications* 306 (1):1–26. https://doi.org/10.1144/SP306.1.

Døssing, Arne, Peter Japsen, Anthony B. Watts, Tove Nielsen, Wilfried Jokat, Hans Thybo, and Trine Dahl-Jensen. 2016. "Miocene uplift of the NE Greenland Margin linked to plate tectonics: Seismic evidence from the Greenland Fracture Zone, NE Atlantic." *Tectonics* 35 (2):257–82. https://doi.org/10.1002/2015TC004079.

Døssing, Arne, T. Dahl-Jensen, H. Thybo, R. Mjelde, and Y. Nishimura. 2008. "East Greenland Ridge in the North Atlantic Ocean: An integrated geophysical study of a continental sliver in a boundary transform fault setting." *Journal of Geophysical Research: Solid Earth* 113 (10):1–33. https://doi.org/10.1029/2007JB005536.

Eidvin, T.E., Goll, R.M., Grogan, P., Smelror, M. & Ulleberg, K. 1998: The Pleistocene to Middle Eocene stratigraphy and geological evolution of the western Barents Sea continental margin at well site 7316/5-1 (Bjørnøya West area). *Norsk Geologisk Tidskrift 78,* 99 - 123.

Engen, Øyvind, Jan Inge Faleide, and Toril Karlberg Dyreng. 2008. "Opening of the Fram Strait gateway: A review of plate tectonic constraints." *Tectonophysics* 450 (1–4):51–69. https://doi.org/10.1016/j.tecto.2008.01.00.

Faleide, J I, A M Myhre, and O Eldholm. 1988. "Early Tertiary volcanism at the Western Barents Sea Margin.; Early Tertiary volcanism and the opening of the NE Atlantic." *Geological Society Special Publications* 39 (39):135–46.

Faleide, J. I., Gudlaugsson, S.T., Eldholm, O., Myhre, A.M., and Jackson, H.R., 1991, Deep seismic transects across the western Barents Sea continental margin: Tectonophysics, v. 189, pp. 73–89.

Faleide, Jan I., Erling Vågnes, and Steinar T. Gudlaugsson. 1993. "Late Mesozoic-Cenozoic evolution of the South-Western Barents Sea in a regional Rift-Shear Tectonic Setting." *Marine and Petroleum Geology* 10 (3):186–214. https://doi.org/10.1016/0264-8172(93)90104-Z.

Faleide, Jan Inge, Anders Solheim, Anne Fiedler, Berit O. Hjelstuen, Espen S. Andersen, and Kris Vanneste. 1996. "Late Cenozoic evolution of the Western Barents Sea-Svalbard continental Margin." *Global and Planetary Change* 12 (1–4):53–74. https://doi.org/10.1016/0921-8181(95)00012-7.

Faleide, J.I., Tsikalas, F., Eldholm, O., 2001. Regional rift-shear tectonic setting and Late Cretaceous-early Tertiary events linking the Lofoten-Vesteralen and SW Barents Sea margins (NE Atlantic). In: Roth, S., Ruggeberg, A. (Eds.), 2001 MARGINS Meeting, Schriftenreihe der Deutschen Geologischen Gesellschaft, vol. 14. 56–57.

Faleide, J I, Filippos Tsikalas, Rolf Mjelde, Jonas Wilson, and Olav Eldholm. 2008. "Structure and evolution of the continental margin off Norway and the Barents Sea." *Episodes* 31 (March):82–91.

Faleide, J.I., Bjørlykke, K., Gabrielsen, R.H.O., 2010. Chapter 22: Geology of the Norwegian Continental Shelf. In: Bjørlykke, K. (Ed.), Petroleum Geoscience: From Sedimentary Environments to Rock Physics. Springer-Verlag Berlin Heidelberg, pp. 467–499.

Ferrill, D.A., Morris, A.P. & McGinnis, R.N. 2012. Extensional fault-propagation folding in mechanically layered rocks: the case against the frictional drag mechanism. Tectonophysics, 576–577, 78–85.

Gabrielsen, R. H. 1984. "Long-lived fault zones and their influence on the tectonic development of the southwestern Barents Sea." *Journal of the Geological Society* 141 (4):651–62. https://doi.org/10.1144/gsjgs.141.4.0651.

Gabrielsen, R.H., Faerseth, R.B. & Jensen, L.N. 1990. Structural elements of the Norwegian continental shelf, Part. 1. The Barents Sea Region. Norwegian Petroleum Directorate, Stavanger.

Gabrielsen, R.H., Grunnaleite, I. & Rasmussen, E. 1997. Cretaceous and Tertiary inversion in the Bjørnøyrenna Fault Complex, south-western Barents Sea. Marine and Petroleum Geology, 14, 165–178.

Gac, Sébastien, Peter Klitzke, Alexander Minakov, Jan Inge Faleide, and Magdalena Scheck-Wenderoth. 2016. "Lithospheric strength and elastic thickness of the Barents Sea and Kara Sea region." *Tectonophysics* 691. Elsevier B.V.:120–32. https://doi.org/10.1016/j.tecto.2016.04.028.

Goudswaard, W., Jenyon, M.K. (Eds.), 1988. Seismic atlas of structural and stratigraphic features. European Association of Exploration Geophysicists. CIP-Gegevens Koninklijke Bibliotheek, Den Haag, p. D1.

Gradstein, F. M., Anthonissen, E., Brunstad, H., Charnock, M., Hammer, Ø., Hellem, T., & Lervik, K. S. (2010). Norwegian Offshore Stratigraphic Lexicon (NORLEX). Newsletters on Stratigraphy, 44(1), 73–86. https://doi.org/10.1127/0078-0421/2010/0005.

Grasemann, Bernhard, Steve Martel, and Cees Passchier. 2005. "Reverse and normal drag along a fault." *Journal of Structural Geology* 27 (6):999–1010. https://doi.org/10.1016/j.jsg.2005.04.006.

Grunnaleite, I., W. Fjeldskaar, J. Wilson, J. I. Faleide, and J. Zweigel. 2009. "Effect of local variations of vertical and horizontal stresses on the Cenozoic structuring of the mid-Norwegian shelf." Tectonophysics 470 (3–4). Elsevier B.V.:267–83. https://doi.org/10.1016/j.tecto.2009.01.005.

Harland, W. B. 1969. Contribution of Spitsbergen to understanding of tectonic evolution of North Atlantic region. In: North Atlantic; Geology and Continental Drift (Ed. M. Kay), Am. Assoc. Petrol. Geol. Mem. No. 12, pp. 817-851

Henriksen, E., A. E. Ryseth, G. B. Larssen, T. Heide, K. Ronning, K. Sollid, and A. V. Stoupakova. 2011. "Chapter 10 Tectonostratigraphy of the greater Barents Sea: implications for petroleum systems." *Geological Society, London, Memoirs* 35 (1):163–95. https://doi.org/10.1144/M35.10.

Homberg, C., J. Schnyder, V. Roche, V. Leonardi, and M. Benzaggagh. 2017. "The brittle and ductile components of displacement along fault zones." *Geological Society, London, Special Publications* 439 (1):395–412. https://doi.org/10.1144/SP439.21.

Indrevær, Kjetil, Roy H. Gabrielsen, and Jan Inge Faleide. 2017. "Early Cretaceous synrift uplift and tectonic inversion in the Loppa High area, southwestern Barents Sea, Norwegian shelf." *Journal of the Geological Society* 174 (2):242–54. https://doi.org/10.1144/jgs2016-066.

Jackson, C. A.L., S. T. Chua, R. E. Bell, and C. Magee. 2013. "Structural style and early stage growth of inversion structures: 3D seismic insights from the Egersund Basin, Offshore Norway." *Journal of Structural Geology* 46. Elsevier Ltd:167–85. https://doi.org/10.1016/j.jsg.2012.09.005.

Jebsen, C., 1998. Kenozoisk utvikling av Vestbakkvulkanittprovinsen på den vestlige Barentshavsmarginen. Cand. Scient (Doctoral dissertation, Thesis, University of Oslo, Norway).

Jebsen, C. and Faleide, 1998. Tertiary rifting and magmatism at the western Barents Sea margin (Vestbakken volcanic province): III international conference on Arctic margins, ICAM III; abstracts; plenary lectures, talks and posters, pp. 92.

Kristensen, Thomas B., Atle Rotevatn, Maria Marvik, Gijs A. Henstra, Robert L. Gawthorpe, and Rodmar Ravnås. 2018. "Structural evolution of sheared margin basins: the role of strain partitioning. Sørvestsnaget Basin, Norwegian Barents Sea." *Basin Research* 30 (2):279–301. https://doi.org/10.1111/bre.12253.

Larssen, G. B., Elvebakk, G. et al. 2005. Upper Palaeozoic lithostratigraphy of the southern part of the Norwegian Barents Sea. Norges Geologiske Undersøkelser Bulletin, 444, 3–43.

Leever, Karen A., Roy H. Gabrielsen, Jan Inge Faleide, and Alvar Braathen. 2011. "A transpressional origin for the West Spitsbergen fold-and-thrust belt: Insight from analog modeling." *Tectonics* 30 (2). https://doi.org/10.1029/2010TC002753.

Lundin, E., Doré, A.G., 2002. Mid-Cenozoic post-breakup deformation in the 'passive' margins bordering the Norwegian–Greenland Sea. Marine and Petroleum Geology 19, 79–93.

Mørk, M. B.E., and R. A. Duncan. 1993. "Late Pliocene basaltic volcanism on the western Barents Shelf margin: Implications from petrology and ^{40}Ar-^{39}Ar dating of volcaniclastic debris from a shallow drill core." *Norsk Geologisk Tidsskrift* 73 (4): 209–25.

Nøttvedt, A., Berglund, L. T., Rasmussen, E. & Steel, R. 1988. Some aspects of Tertiary tectonics and sedimentation along the western Barents Shelf. In: Morton, A. C. & Parsons, L. M. (eds) Early Tertiary Volcanism and the opening of the North Atlantic. Geological Society, London, Special Publications, 39, 421–425.

Natural history Museum - Oslo. *Norwegian Stratigraphic Lexicon* . n.d. http://nhm2.uio.no/norges/litho/Barents_Chart.html (last accessed May 27, 2018).

NPD*.: Norwegian petroleum Directorate. factpages [Online].* n.d. http://factpages.npd.no/ReportServer?/FactPages/PageView/strat_Litho_level1_group_formation&rs:Command=Render&rc:Toolbar=false&rc:Parameters=f&NpdId=113&IpAddress=37.191.222.162&CultureCode=en (last accessed May 27th, 2018).

NPD*.: Norwegian petroleum Directorate. factpages [Online].* n.d. http://factpages.npd.no/ReportServer?/FactPages/PageView/strat_Litho_level1_group_formation&rs:Command=Render&rc:Toolbar=false&rc:Parameters=f&NpdId=154&IpAddress=37.191.222.162&CultureCode=en (last accessed May 27th, 2018).

NPD*.: Norwegian petroleum Directorate. factpages [Online].* n.d. http://factpages.npd.no/ReportServer?/FactPages/PageView/strat_Litho_level1_group_formation&rs:Command=Render&rc:Toolbar=false&rc:Parameters=f&NpdId=122&IpAddress=37.191.222.162&CultureCode=en (last accessed May 27th, 2018).

Ogg, James G., G.M. Ogg, and Felix M. Gradstein. 2016. "A Concise Geologic Time Scale," no. June:240.

Pascal, C., and R. H. Gabrielsen. 2001. "Numerical modeling of Cenozoic stress patterns in the mid-Norwegian margin and the northern North Sea." Tectonics 20 (4):585–99. https://doi.org/10.1029/2001TC900007.

Pascal, Christophe, David Roberts, and Roy H. Gabrielsen. 2005. "Quantification of neotectonic stress orientations and magnitudes from field observations in Finnmark, northern Norway." Journal of Structural Geology 27 (5):859–70. https://doi.org/10.1016/j.jsg.2005.01.011.

Pascal, C., Roberts, D. & Gabrielsen, R.H. 2006. Present-day stress orientations in Norway as deduced from stress-release features. In: Lu, M., Li, C.C., Kjørholt, H. & Dahle, H. (eds) In-situ rock stress: measurement, interpretation and application. Taylor & Francis, London, 209–213.

Pascal, C., D. Roberts, and R. H. Gabrielsen. 2010. "Tectonic significance of present-day stress relief phenomena in formerly glaciated regions." *Journal of the Geological Society* 167 (2):363–71. https://doi.org/10.1144/0016-76492009-136.

Price, S., J. Brodie, a. Whitham, and R.a.Y. Kent. 1997. "Mid-Tertiary rifting and magmatism in the Traill Ø region, East Greenland." *Journal of the Geological Society* 154 (3):419–34. https://doi.org/10.1144/gsjgs.154.3.0419.

Rasmussen, E., Skott, P.H. & Larsen, K-B. 1995: Hydrocarbon potential of the Bjørnøya West Province, western Barents Sea Margin. In: Hanslien, S. (ed), *Petroleum Exploration and Exploitation in Norway.* Norwegian Petroleum Society Special Publication 4, 277 - 286. Elsevier, Amsterdam.

Richardsen, G., E. Henriksen, and T. O. Vorren. 1991. "Evolution of the Cenozoic sedimentary wedge during rifting and seafloor spreading west of the Stappen High, western Barents Sea." *Marine Geology* 101 (1–4):11–30. https://doi.org/10.1016/0025-3227(91)90060-H.

Rickers, Florian, Andreas Fichtner, and Jeannot Trampert. 2013. "The Iceland-Jan Mayen plume system and its impact on mantle dynamics in the North Atlantic Region: Evidence from full-waveform inversion." *Earth and Planetary Science Letters* 367. Elsevier:39–51. https://doi.org/10.1016/j.epsl.2013.02.022.

Ryseth, A, J H Augustson, M Charnock, O Haugerud, S M Knutsen, P S Midboe, J G Opsal, and G Sundsbo. 2003. "Cenozoic stratigraphy and evolution of the Sørvestsnaget Basin, southwestern Barents Sea." *Norwegian Journal of Geology* 83 (2):107–30.

Sattarzadeh, Y., J. W. Cosgrove, and C. Vita-Finzi. 2002. "The geometry of structures in the Zagros cover rocks and its neotectonic implications." *Geological Society, London, Special Publications* 195 (1):205–17. https://doi.org/10.1144/GSL.SP.2002.195.01.11.

Schlische, R. W. 1995. "Geometry and Origin of Fault-Related Folds in Extensional Settings." *American Association of Petroleum Geologists Bulletin* 79 (11):1661–78. https://doi.org/10.1306/7834DE4A-1721-11D7-8645000102C1865D.

Skogseid, Jakob, Sverre Planke, Jan Inge Faleide, Tom Pedersen, Olav Eldholm, and Flemming Neverdal. 2000. NE Atlantic continental rifting and volcanic margin formation. *Geological Society, London, Special Publications*. Vol. 167. https://doi.org/10.1144/GSL.SP.2000.167.01.12.

Song, T., 1997. Inversion styles in the Songliao basin (northeast China) and estimation of the degree of inversion. Tectonophysics 283, 173e188.

Tingay, M. 2009. "State and Origin of Present-Day Stress Fields in Sedimentary Basins." *ASEG Extended Abstracts* 2009 (1):1. https://doi.org/10.1071/ASEG2009ab037.

Tsikalas, Filippos, Jan Inge Faleide, Olav Eldholm, and Olav Antonio Blaich. 2012. The NE Atlantic conjugate margins. *Regional Geology and Tectonics*. https://doi.org/10.1016/B978-0-444-56357-6.00004-4.

Turner, Jonathan P., and Gareth A. Williams. 2004. "Sedimentary basin inversion and intra-plate shortening." *Earth-Science Reviews* 65 (3–4):277–304. https://doi.org/10.1016/j.earscirev.2003.10.002.

ULIANA, M. A., ARTEAGA, M. E, LEGARRETA, L., CERDAN, J. J. & PERONI, G. O. 1995. Inversion structures and hydrocarbon occurrence in Argentina. In: BUCHANAN, J. G. & BUCHANAN, P. G. (eds) Basin Inversion. Geological Society, London, Special Publications, 88, 211–233.

Vågnes, E., Faleide, J. I. and Gudlaugsson, S. T. 1992. Glacial erosion and tectonic uplift of the Barents Sea. Norsk Gee/. Tidsskr. 72, 333-338.

Vågnes, E., R. H. Gabrielsen, and P. Haremo. 1998. "Late Cretaceous-Cenozoic intraplate contractional deformation at the Norwegian continental shelf: timing, magnitude and regional implications." Tectonophysics 300 (1–4):29–46. https://doi.org/10.1016/S0040-1951(98)00232-7

Van Der Pluijm, B.A. and Marshak, S. (2004) Earth Structure: An Introduction to Structural Geology and Tectonics. 2nd Edition, WW Norton, New York.

Wijk, J. van, G. Axen, and R. Abera. 2017. "Initiation, evolution and extinction of pull-apart basins: Implications for opening of the Gulf of California." *Tectonophysics* 719–720. Elsevier B.V.:37–50. https://doi.org/10.1016/j.tecto.2017.04.019.

Williams, G.D., Powell, C.M., Cooper, M.A., 1989. Geometry and kinematics of inversion tectonics. In: Cooper, M.A., Williams, G.D. (Eds.), Inversion Tectonics. Geological Society Special Publication, vol. 44, pp. 3 –15.

Withjack, Martha Oliver, Mark S. Baum, and Roy W. Schlische. 2010. "Influence of preexisting fault fabric on inversion-related deformation: A case study of the inverted Fundy rift basin, southeastern Canada." *Tectonics* 29 (6):1–22. https://doi.org/10.1029/2010TC002744.

Worsley, David. 2008. "The Post-Caledonian development of Svalbard and the western Barents Sea." *Polar Research* 27 (3):298–317. https://doi.org/10.1111/j.1751-8369.2008.00085.x.

Ziegler, P.A., 1988. Evolution of the Arctic-North Atlantic and the Western Tethys, Memoir, vol. 43. American Association of Petroleum Geologists.

https://engineering.purdue.edu/stratigraphy (last accessed 27th May, 2018)

https://www.software.slb.com/products/petrel (last accessed 27th May, 2018)